12-1993

The geology of the Tuff of Bridge Spring: Southern Nevada and northwestern Arizona

Shirley Ann Morikawa
University of Nevada, Las Vegas

The Geology of the Tuff of Bridge Spring: Southern Nevada and Northwestern Arizona

by

Shirley Ann Morikawa

A thesis submitted in partial fulfillment
of the requirements for the degree of

Master of Science
in
Geology

Geoscience Department
University of Nevada, Las Vegas
December, 1993

The thesis of Shirley Ann Morikawa for the degree of Master of Science in Geology is approved.

[redacted]

Chairperson, Eugene I. Smith, Ph.D.

[redacted]

Examining Committee Member, Wanda J. Taylor, Ph.D.

[redacted]

Examining Committee Member, Ernest M. Duebendorfer, Ph.D.

[redacted]

Graduate Faculty Representative, Donna E.Weistrop, Ph.D.

Dean of the Graduate College, Ronald W. Smith, Ph.D.

University of Nevada, Las Vegas
December, 1993

Abstract

The Tuff of Bridge Spring (TBS) is a regionally-widespread, andesite to rhyolite (59.50 to 74.91 wt. %) ash-flow tuff of mid-Miocene age (ca. 15.2 Ma) that is exposed in the northern Colorado River extensional corridor of southern Nevada and northwestern Arizona. Determination of the areal distribution, geochronology, lithology, geochemistry, and internal stratigraphy of the TBS is important for its establishment as a reliable stratigraphic reference horizon for tectonic reconstructions of the extensional corridor during the middle Miocene. Based on reoccurring patterns of major and trace element variation, the TBS is divided into constant Cr/variable SiO_2 and variable Cr/variable SiO_2 chemical members. Reconciliation of chemical member assignments and regional stratigraphic relationships allows the division of the TBS into three stratigraphic members. The regionally-extensive nature of a Zr/Ti vs. Ba chemical horizon in the TBS suggests that its chemical signature is magmatic in origin.

The presence of linear isotopic arrays of Nd/Rb/Pb plots, regionally-consistent geochemical trends, and disequilibrium textures in feldspars in the TBS suggests it was formed by magma mixing processes which involved the injection of mafic magma into a normally-zoned felsic magma chamber. The Nd/Rb/Pb isotopic signature of the Tuff of Bridge Spring suggests that the TBS may be cogenetic with either the Aztec Wash pluton, Nevada or the Mt. Perkins pluton, Arizona. Comparison of the isotopic signatures of the TBS with tuffs collected from Salt Spring Wash, Arizona, and the Lucy Gray Range, Nevada suggests that these tuffs are not cogenetic with the TBS. Incremental release $^{40}Ar/^{39}Ar$ analysis of the tuff of Dolan Springs (16.09 ±0.15 Ma) suggests it was derived from a different source than the TBS.

Contents

Abstract iii
Figures vi
Tables viii
Acknowledgments ix
Introduction 1
The Tuff of Bridge Spring: A Brief Description 3
Regional Setting: The Northern Colorado River Extensional Corridor 5
History of Extension 5
Regional Volcanic/Plutonic Stratigraphy 6
Instrumental Techniques 12
Analytical Techniques 12
Whole Rock Vs. Pumice Sampling 14
Analytical Data 20
Major and Trace Element Geochemistry 20
Tuff of Bridge Spring Geochemistry 21
Other Ash-flow Tuffs 24
Petrologic Descriptions 25
Regional Correlation 61
Isotopic Correlation of the Tuff of Bridge Spring 61
Interstate-15 63
Other Ash-flow Tuffs 64
Salt Spring Wash and Lucy Gray Range 64
Dolan Springs 64
Origin of the Tuff of Bridge Spring Data Array 65
Lithic Contamination 66
Patsy Mine Volcanics 66
Alkali Olivine Basalts 68
Precambrian Basement 69
Mixing Trend 70
The Role of Contaminants in the Genesis of the Salt Spring Wash and Lucy Gray Range Tuffs 70

Internal Stratigraphy 80
Introduction 80
Eruptive Units 82
Chemical Criteria 82
Field Evidence 83
Chemical Members of the Tuff of Bridge Spring 86
Regional Members of the Tuff of Bridge Spring 88
Fine Scale Chemical Variation 89
Magma Chamber Processes 91
Location of Source 109
Introduction 109
Radiogenic Isotopes 111
Geochronology 112
Discrepancies in Tuff of Bridge Spring Geochronology 113
Comparative Geochronology 114
Geochemistry 114
Chemical path correlation 115
Field and Petrologic Studies 117
Field Indicators 118
Location of Pluton 119
Magmatic Mixing Textures 119
The Dolan Springs Volcanic Section 120
Summary and Conclusion 121
Summary and Conclusion 127
Future Work 131
References Cited 132

Appendix A: Major and Trace Element Analyses 139
Appendix B: Thin Section Point Counts 145
Part I: Whole Rock Modal Analyses 145
Part II: Phenocryst Modal Analyses 152
Appendix C: Statigraphic Section Descriptions 156

Figures

Figure 1. Map showing locations of mountain ranges of the northern Colorado River extensional corridor referred to in the text. 8
Figure 2. Map showing known exposures (in black) of the Tuff of Bridge Spring..... 9
Figure 3. Generalized geologic map of the northern Colorado River extensional corridor and adjacent regions (from Faulds, 1989)..... 10
Figure 4. Location map of plutons and volcanic complexes of the northern Colorado River extensional corridor..... 11
Figure 5. Plot of xenolith abundance vs. element concentration for the Eldorado Mountains section..... 19
Figure 6. Map showing locations of sections sampled for geochemistry and petrology. 28
Figure 7. Plot of Na2O vs. K2O. The field of unmetasomatized rocks shown from Carmichael et al. (1974)..... 29
Figure 8. Harker variation plots of Tuff of Bridge Spring sections: major element oxides and trace elements vs. SiO2..... 31
Figure 9. Plots of relative stratigraphic position vs. element concentration of Tuff of Bridge Spring sections. 40
Figure 10. Harker variation plots of Tuff of Bridge Spring sections and three non-correlative tuffs: major element oxides and trace elements vs. SiO2..... 56
Figure 11: Plot of Nd vs. 87Sr/86Sr of the Tuff of Bridge Spring and three non-correlative tuffs. Sample numbers shown..... 73
Figure 12. Plot of 87Sr/86Sr vs. SiO2 of the Tuff of Bridge Spring and three non-correlative tuffs shown with sample numbers..... 74
Figure 13. 40Ar/39Ar incremental release age analysis (biotite) of the Dolan Springs Tuff..... 75
Figure 14. Generation of a hypothetical isotope array by xenolith contamination. See text for explanation..... 76
Figure 15. Plot of Nd vs. 87Sr/86Sr for the Tuff of Bridge Spring, Patsy Mine Volcanics, and Petroglyph Wash Basalt..... 77

Figure 16. Appproximate geographic distribution of Early Proterozoic Nd and Pb provinces in the southwestern United States shown with the distribution area of the Tuff of Bridge Spring. 78
Figure 17. Pb isotope plots of a representative Tuff of Bridge Spring sample with samples of Mojave and Arizona Early Proterozoic crustal provinces rocks. 79
Figure 18. Diagram showing different types of chemical breaks. 94
Figure 19. Plot of relative position vs. element concentration for the Eldorado Mountains section showing chemical breaks. 95
Figure 20. Division of Tuff of Bridge Spring stratigraphic sections into eruptive units 100
Figure 21. Plot of Cr vs. SiO2 showing division of the Tuff of Bridge Spring into constant Cr and variable Cr members. 101
Figure 22. Plots of Cr vs. Sr, and Y vs. Zr, and Ti/Sr vs. FeO. 102
Figure 23. Plot of Ti/Sr vs FeO. 103
Figure 24. Plot of Zr/Ti vs. Ba showing division of the Tuff of Bridge Spring into variable Zr/Ti, constant Ba group (constant Cr member), and variable Zr/Ti, variable Ba group (variable Cr member). 104
Figure 25. Regional members of the Tuff of Bridge Spring. See text for explanation. 105
Figure 26. Distribution of the regional members of the Tuff of Bridge Spring. 106
Figure 27. Compilation of plots of sections with variable Zr/Ti, constant Ba showing chemical paths and inflection points. 107
Figure 28. Harker variation plots of the Eldorado Mountains section showing cyclical variation. 108
Figure 29. Plot of Nd vs. 87Sr/86Sr for the Tuff of Bridge Spring and selected plutons and volcanic suites of the northern Colorado River extensional corridor. 123
Figure 30. Plot of 87Sr/86Sr vs. 206Pb/204Pb for the Tuff of Bridge Spring and selected volcanic complexes and plutons of the northern Colorado River extensional corridor. 124
Figure 31. Hypothetical Zr/Ti vs. Ba chemical path diagram 126

Tables

Table 1: Calibration standards for the Rigaku X-Ray Fluorescence Spectrometer, University of Nevada, Las Vegas. 16
Table 2: Precision for the Rigaku 3030 X-Ray Fluorescence Spectrometer, University of Nevada, Las Vegas. 17
Table 3: Accuracy for the Rigaku 3030 X-Ray Fluorescence Spectrometer, University of Nevada, Las Vegas. 18
Table 4: Regional major and trace element variation of the Tuff of Bridge Spring. 30
Table 5: Major and trace element variation of sections compared to a base composition averaged from Highland Spring, Eldorado Mountains, Sheep Mountain, and Interstate 15 sections. 50
Table 6: Nd, Rb, and Pb isotope analyses. 72
Table 7: Geochronology of the Tuff of Bridge Spring. 125

Acknowledgments

Financial support for this thesis was provided by the Center for Volcanic and Tectonic Studies (CVTS) at UNLV, and by research grants from the Geological Society of America and the Graduate Student Association of UNLV.

I would like to thank the members of my graduate committee: Dr. Gene Smith (a most patient and generous advisor), Dr. Wanda Taylor, Dr. Ernie Duebendorfer, and Dr. Donna Weistrop for their guidance and support. I would like to acknowledge the following individuals for contributions of data that were incorporated into this thesis: Dr. Jim Faulds (University of Iowa) for Tuff of Bridge Spring $^{40}Ar/^{39}Ar$ geochronology, Hayden Bridwell (UNLV) for Interstate 15 thin sections, Dr. Jim Mills (CVTS) for Tuff of Hoover Dam isotope data, Dr. Rod Metcalf (UNLV) for Mt. Perkins pluton isotope data, and Claudia Falkner and Dr. Calvin Miller (Vanderbilt University) for Aztec Wash pluton isotope data and geochronology. Isotope analyses were completed by Dr. Doug Walker (University of Kansas), Dr. Tim Bradshaw (CVTS), and Dr. Mark Martin (CVTS). Dr. Dan Lux (University of Maine) ran the tuff of Dolan Springs $^{40}Ar/^{39}Ar$ analysis.

For logistical support, my thanks goes to the UNLV geoscience staff: Margaret Kaufman, Vicki DeWitt, Daryl Depry, and Sarah Crooks, and to Gina Jaramillo (Motor Pool), Barbara Hogue (UNLV Graduate College), Yagang Wang (CVTS), and Kathy Morgan (UNLV Operations and Maintenance).

I would especially like to express my gratitude to my parents- Don and Harlene Morikawa, my sister Sandy, and brother Steve for their support and interest in my studies.

And finally, my personal thanks to all the good people- students, faculty, and

staff- I've come to know during my stay at UNLV, especially: Joe Blaylock (for encouragement and much appreciated reality adjustments), Jan Lamb, Clint Christensen, John Schmeltzer, and Gary Gin.

Introduction

The Tuff of Bridge Spring is a regionally-extensive, andesitic to rhyolitic ash-flow tuff (57 to 75 wt. % SiO_2) that crops out in the Lake Mead region of the southern Basin and Range province, Clark County, Nevada and Mohave County, Arizona (Fig. 1). Eruption of the Tuff of Bridge Spring was coeval with intense crustal extension in the structurally-complex northern Colorado River extensional corridor of southern Nevada and northwestern Arizona. The timing of the emplacement of the Tuff of Bridge Spring, its widespread distribution, and distinctive lithology makes it a key stratigraphic reference horizon on which correlations of Miocene-aged stratigraphic units and tectonic reconstructions in the northern Colorado River extensional corridor are based (Anderson, 1971; Anderson et al., 1972; Smith, 1982; Davis, 1984; Schmidt, 1987; Faulds, 1989; Cascadden, 1991; and Bridwell, 1991). The complex nature of these stratigraphic correlations and tectonic reconstructions require that correlation and identification of the Tuff of Bridge Spring are based on reliable parameters. It is the purpose of this study to determine the areal distribution, geochronology, lithology, geochemistry, internal stratigraphy, and locate the source of the Tuff of Bridge Spring in order to establish the unit as a reliable stratigraphic marker.

This thesis utilizes Nd, Sr, and Pb isotopes as the primary criteria on which regional correlation of sections is based. Major and trace element geochemistry, field studies, and $^{40}Ar/^{39}Ar$ geochronology was used to confirm isotope-based correlations. This body of evidence suggests that stratigraphic sections in the Eldorado Mountains, McCullough Range, Highland Spring Range, Interstate 15 (near Sloan, Nevada), and Sheep Mountain in Nevada, and the Black Mountains, Temple Bar, White Hills in Arizona are correlative to the Tuff of Bridge Spring (Fig. 1).

The Tuff of Bridge Spring is divided into two chemical members on the basis of the occurrence of two distinct patterns of major and trace element variation. The presence of these two regionally-persistent chemical groups directly reflects chemical processes and zonations within the source chamber at the time of eruption of the Tuff of Bridge Spring. The chemical group concept not only forms the foundation for furthur division of the Tuff into three regional stratigraphic members, but also has important implications for the petrogenesis of the Tuff of Bridge Spring.

Lastly, this thesis compares the isotopic signature of the Tuff of Bridge Spring with available isotopic analyses of several plutons of the northern Colorado River extensional corridor to tentatively suggest that the source of the Tuff of Bridge Spring is either the Aztec Wash pluton, Nevada, or the Mt. Perkins pluton, Arizona.

Although not directly related to the Tuff of Bridge Spring, an important finding in this thesis is the identification of proximal-type pyroclastic deposits in the volcanic complex at Dolan Springs, Arizona. The occurrence of these deposits are suggestive of the presence of a caldera somewhere in the immediate area. Similarities of isotopic signature of the Dolan Springs tuff and the Tuff of Bridge Spring, and the overlap in ages of the Dolan Springs tuff and the Mt. Perkins pluton has interesting implications for the existence of regionally-extensive magmatic systems and the possible correlation of the Dolan Springs tuff to the Mt. Perkins pluton.

Organization of this thesis is built around three main topics: (1) regional correlation; (2) determination of internal stratigraphy; and (3) location of the source of the Tuff of Bridge Spring. For each topic, only those aspects of isotopic, major/trace geochemistry, field studies, petrologic studies, geochronology, and introductory material (e.g., previous work) which can be utilized to synthesize an interpretation and conclusion are presented. This requires that introductory material, geochemistry, descriptive volcanology, and interpretation are spread throughout the thesis, unlike the

format of a more "traditional" thesis in which such information is usually presented in separate/isolated sections. Repetition of data or discussion is avoided wherever possible by the use of cross references. Most of the supporting data and section descriptions are included in appendices. Summary figures and tables are included at the end of each section to clarify discussions.

The Tuff of Bridge Spring: A Brief Description

The first description of the Tuff of Bridge Spring was made by Longwell (1963) in a study of the regional geology of the Lake Mead/Davis Dam area of Nevada and Arizona. Ash-flow tuffs exposed in this area were originally correlated to the Golden Door Volcanics of Arizona, but were later given the informal name Tuff of Bridge Spring when Anderson (1971) demonstrated that the type section of the Golden Door Volcanics correlated with the Middle Member of the regionally-extensive Patsy Mine Volcanics. The designation Golden Door Volcanics was formally abandoned in 1971 (Anderson, 1971).

The type section of the Tuff of Bridge Spring is Bridge Spring (Anderson, 1971), which is located approximately 2.5 km north-northeast of Nelson, Nevada, in the Eldorado Mountains. The name Bridge Spring refers to a small spring that occurs near a natural rock arch that formed in variably welded exposures of the Tuff of Bridge Spring.

Based upon the occurrence of stratigraphic sections examined in this study, the Tuff of Bridge Spring extends discontinuously over an area of approximately 4300 km^2 from latitude 36° 00' N (Temple Bar) to latitude 35° 35' N (Highland Spring Range), and from longitude 115° 15' W (Interstate 15 section) to longitude 114° 22' W (Temple

Bar). The present overall distribution pattern of the Tuff of Bridge Spring is elongated east to west (Fig. 2).

The Tuff of Bridge Spring is mid-Miocene in age and is one of two regionally extensive lithostratigraphic units that crop out in this region; the other unit is the 18.5 Ma Peach Springs Tuff (Young and Brennan, 1989). Other ash-flow tuffs of similar age are exposed in the northern Colorado River extensional corridor (e.g., the tuff of Hoover Dam) (Mills, 1985), but have limited distributions. While the absolute age of the Tuff of Bridge Spring has not been unequivocally resolved by radiometric analysis (see later discussion of geochronology), a date of 15.23 ± 0.14 Ma ($^{40}Ar/^{39}Ar$ on sanidine, Bridwell, 1991) is accepted in this study as being representative of the true age of the Tuff of Bridge Spring.

The topographic expression of the Tuff of Bridge Spring varies with the degree of welding. Densely-welded outcrops form prominent ledges or ridges, and moderately- to poorly- welded intervals form slopes. Tuff affected by vapor phase mineralization has a characteristic pale lilac-gray weathered color that is associated with low, rounded outcrops that are platy to cavernous. Color of the weathered Tuff of Bridge Spring varies from black, dark brown, to reddish brown in densely welded intervals. Poorly welded intervals are light colored. The Tuff of Bridge Spring contains between 7.8 (Black Mountains) and 46.4 (Temple Bar) modal percent phenocrysts of sanidine, plagioclase, biotite, clinopyroxene, sphene, opaque iron oxide (undifferentiated), ± zircon, ± apatite, and ± hornblende (rare). The Tuff of Bridge Spring also contains pumice (usually in the form of fiamme), and lithic clasts of mafic composition (basalt to basaltic andesite).

Regional Setting: The Northern Colorado River Extensional Corridor

History of Extension

The northern Colorado River extensional corridor of the southern Basin and Range province is a 50 to100 km wide structural terrane that was subjected to severe extensional tectonism during the mid-Tertiary (approximately 18-4.7 Ma) (Anderson et al., 1972; Duebendorfer and Smith, 1991; Faulds et al., 1992;) (Fig. 3). The extensional corridor is bounded to the north by the Lake Mead fault zone (Lake Mead shear zone) and the Las Vegas Valley shear zone, to the east by the stable Colorado Plateau, and to the west by the Spring Range. The rocks of the northern Colorado extensional corridor consist of Tertiary volcanic and sedimentary rocks that were deposited directly upon Proterozoic crystalline basement. Thick accumulations of Paleozoic and Mesozoic rocks lie to north, east, and west of the extensional corridor, but are absent in the corridor itself (Anderson et. al., 1972). Bisecting the northern Colorado River extensional corridor in the southern Eldorado Mountains, Nevada and the central Black Mountains, Arizona, is an east-west trending, five to ten kilometer wide, 40 km long accomodation zone which separates a northern extensional domain of east-tilted fault blocks from a southern domain of west-tilted fault blocks (Faulds, 1989).

The intense nature of mid-Miocene extensional deformation in the northern Colorado River extensional corridor is reflected by estimates of 300 to 400% total extension of the Las Vegas region during the Neogene (Wernicke et al., 1988), 100% extension of the Eldorado Mountains (Anderson, 1971), and up to 65 km of west-directed, strike-slip fault displacement of the Frenchman Mountain block (Anderson, 1973; Rowland et al., 1990). Anderson (1971) was the first to suggest that large

magnitude extension was accommodated by low-angle detachment faults. Later work in the Lake Mead area suggested that synchronous movement on regional detachment structures (the Saddle Island detachment fault) and strike-slip structures (the Lake Mead fault zone and the Las Vegas Valley Shear Zone) accommodated extension from 13 to 9 Ma. (Smith, 1982; Choukroune and Smith, 1985; Duebendorfer and Wallin, 1991). From 9 to 4.7 Ma, extension was accommodated by high angle normal faulting.

Regional Volcanic/Plutonic Stratigraphy

The Miocene volcanic stratigraphy of the Lake Mead area consists of (in order of decreasing age): (1) the 18.5 Ma Peach Springs Tuff- a regionally extensive, rhyolitic ash-flow tuff (Young and Brennan, 1989); (2) andesites, basalts, basaltic andesites, and rhyolites of the Patsy Mine Volcanics (18.3 to 15.2 Ma) (Anderson, 1971; Anderson et al., 1972); (3) the ca. 15.2 Ma Tuff of Bridge Spring (Bridwell, 1991); and (4) rhyolite, andesites, and basalts of the approximately 15 to 12 Ma Mt. Davis Volcanics (Anderson, 1971; Anderson et al., 1972; Darval, 1991).

A number of localized Neogene volcanic complexes occur in the Lake Mead region. These include the Eldorado Mountains stratovolcano, Nevada (Anderson, 1971); the Hoover Dam volcanic center, Nevada and Arizona (Mills, 1985); the River Mountains volcanic complex, Nevada which is the coeval volcanic cover of the Wilson Ridge pluton of Arizona (Smith et al., 1982; Weber and Smith, 1987); the McCullough Pass caldera (Schmidt, 1987), Sloan Sag (Bridwell, 1991), and the Henderson volcanic complex, Nevada (Tuma-Switzer and Smith, 1993); and the Dolan Springs volcanic complex, Arizona (this study) (Fig. 4).

Miocene-aged plutons exposed in the northern Colorado River extensional corridor include the Nelson/Aztec Wash pluton (15.12 ± 0.6 Ma) (Calvin Miller,

personal communication to Smith, 1993) which crops out in the Eldorado Mountains, Nevada, the 15.96 ± 0.04 Ma Mt. Perkins pluton and the Wilson Ridge pluton (13.5 ± 0.4 Ma) in the Black Mountains, Arizona (Faulds, personal communication to Smith, 1993; and Larsen and Smith, 1990), and the Boulder City pluton, Arizona (13.8 ± 0.6 Ma) (Anderson et al., 1972) (Fig. 4).

The topographic surface upon which the Tuff of Bridge Spring was erupted consisted of paleohills formed by a series of stratovolcanoes and associated dome fields, and paleovalleys containing regionally-extensive mafic flows (Anderson, 1971). In the McCullough Range, a structural buttress of Precambrian basement rock formed a major topographic barrier to the flow of the Tuff of Bridge Spring (Schmidt, 1987).

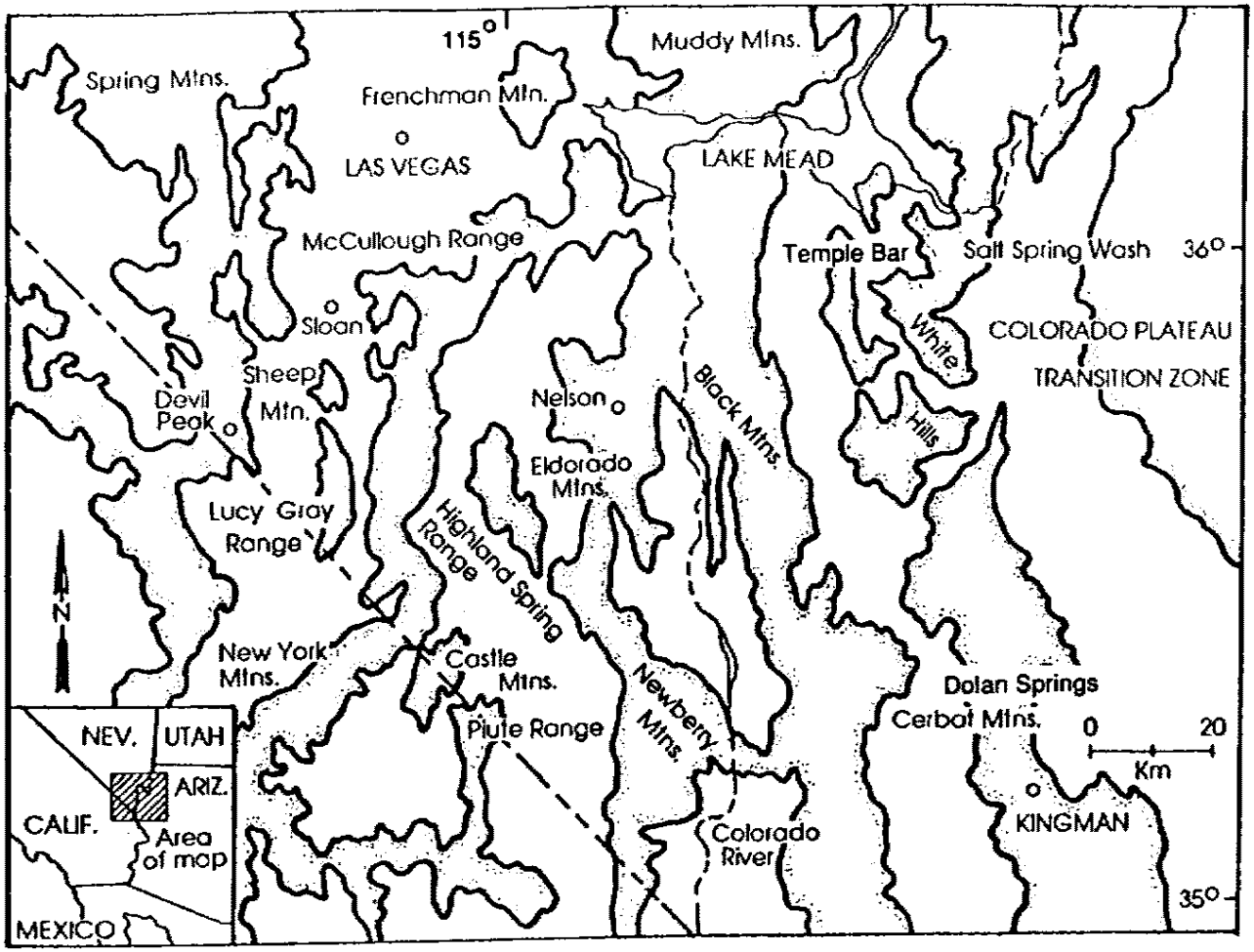

Figure 1. Map showing locations of mountain ranges of the northern Colorado River extensional corridor referred to in the text.

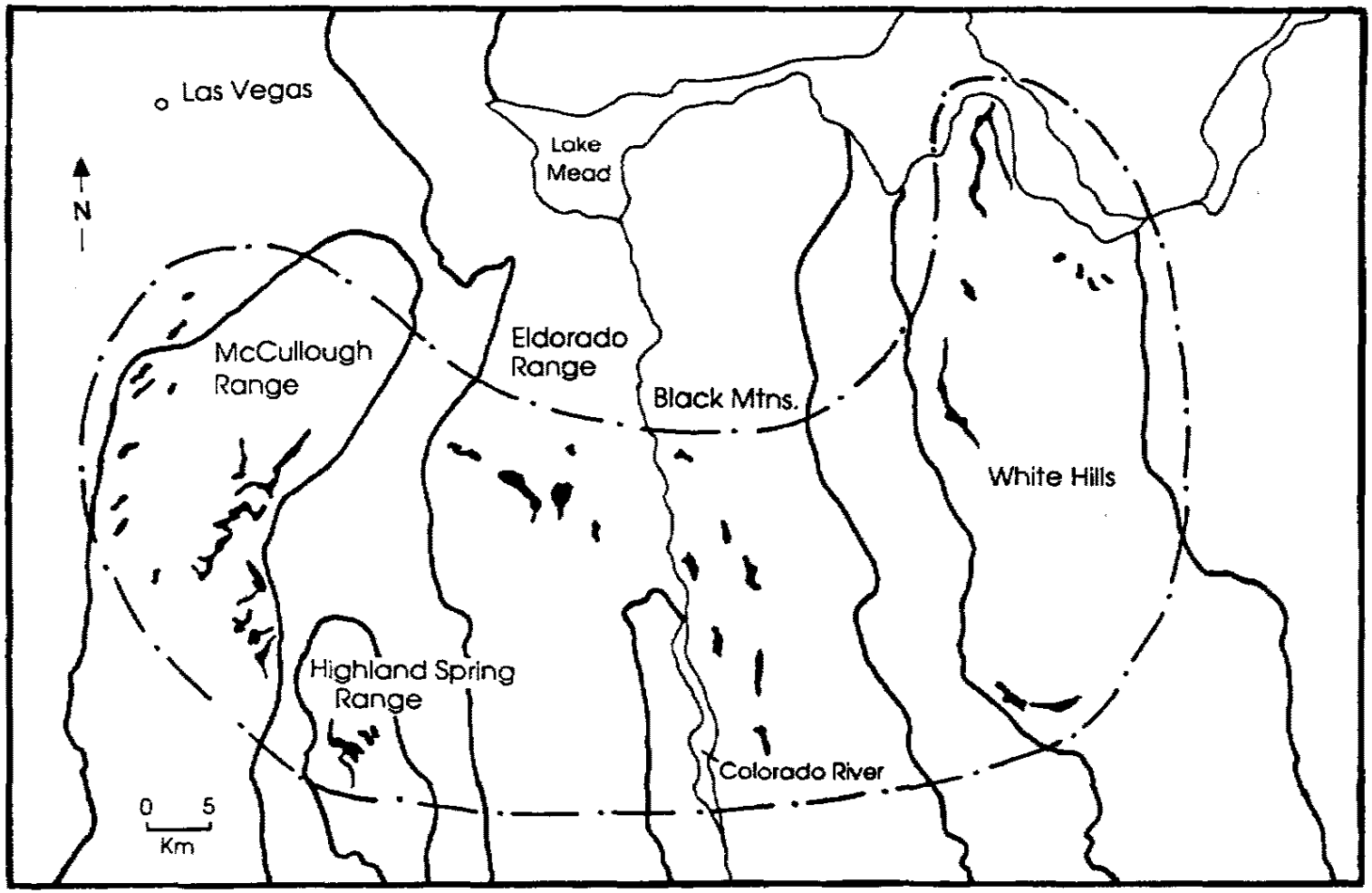

Figure 2. Map showing known exposures (in black) of the Tuff of Bridge Spring. Area of distribution is enclosed by dashed/dotted line. Modified from Cascadden (1991).

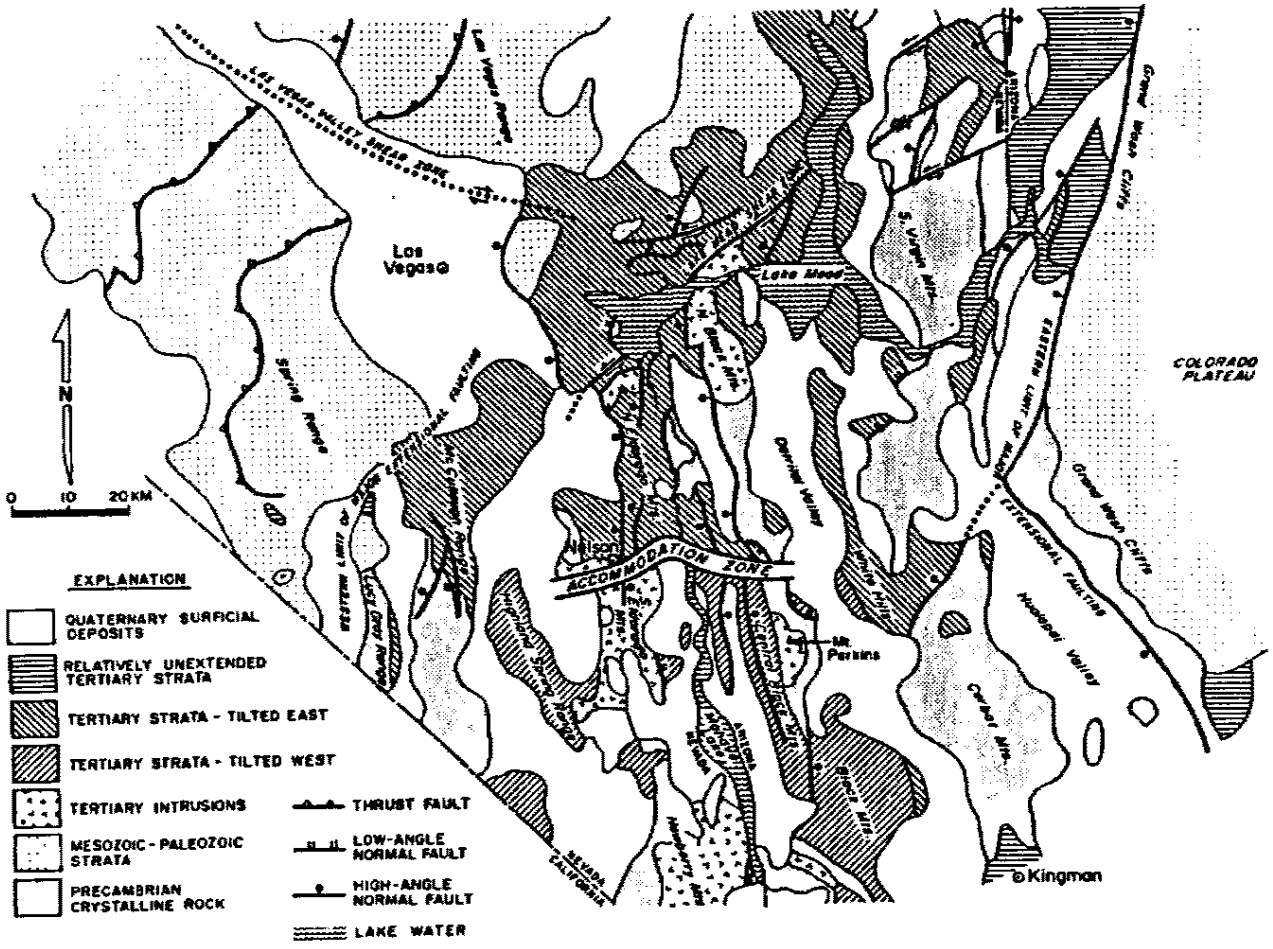

Figure 3. Generalized geologic map of the northern Colorado River extensional corridor and adjacent regions (from Faulds, 1989).

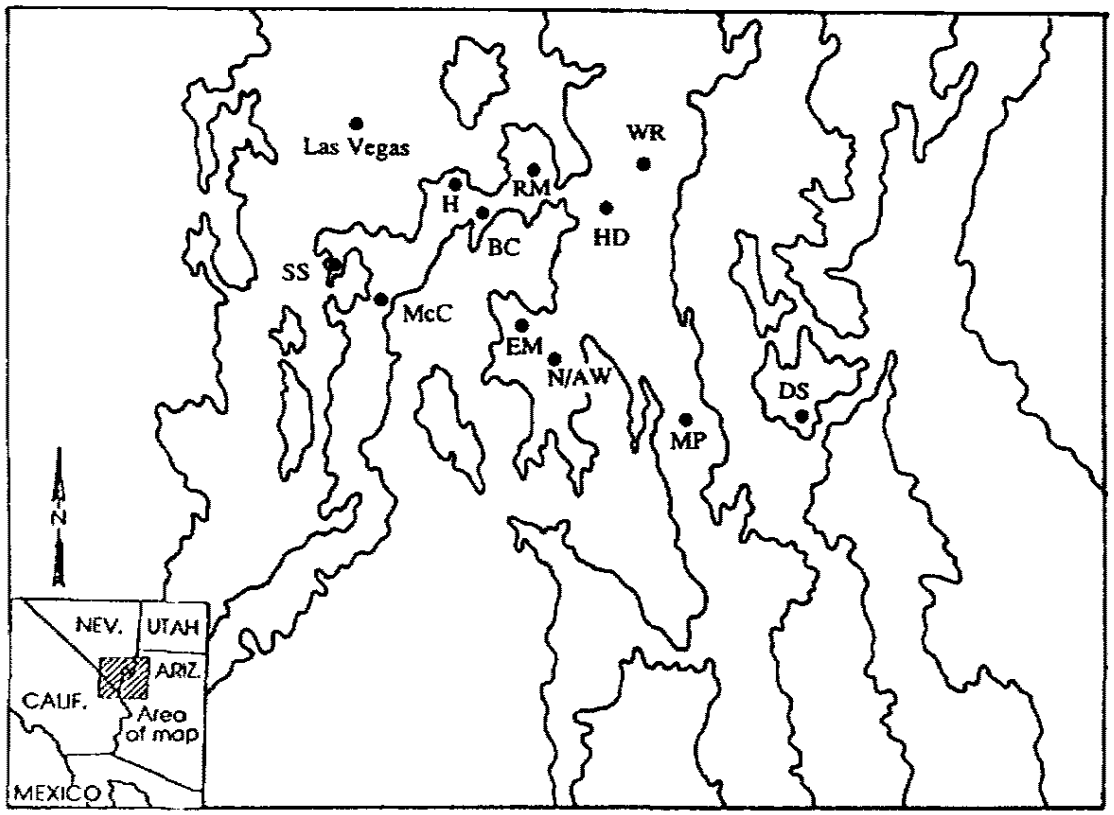

Figure 4. Location map of plutons and volcanic complexes of the northern Colorado River extensional corridor. EM = Eldorado Mountains stratovolcano; HD = Hoover Dam volcanic center; RM = River Mountains volcanic complex; McC = McCullough Pass caldera; SS = Sloan Sag volcanic center; H = Henderson volcanic complex; DS = Dolan Springs volcanic complex. N/AW = Nelson/Aztec Wash pluton; MP = Mt. Perkins pluton; BC = Boulder City pluton; WR = Wilson Ridge pluton.

Instrumental Techniques

Analytical Techniques

Fifty-seven samples were collected and analyzed for major and trace elements. Radiogenic isotope analyses (Sm/Nd, Rb/Sr, and Pb systems) were completed on fourteen samples. Geochemistry was completed almost exclusively on whole rock samples. Samples were selected on the basis of distinctive changes in tuff lithology. Approximately 1-1.5 kg of fresh, unweathered sample were collected for each analysis. Xenoliths larger than 0.7 cm were removed by hand from samples prior to pulverizing. Samples were initially pulverized to <100 mesh in a Dyna Mill Supercollider air suspended impact attrition mill. A geochemical split (approximately 300 ml in volume) was separated from each pulverized sample and powdered to <200 mesh using a Pulverisette automated agate mortar and pestle. The standard practice of leaching powdered rock samples in dilute HCl solution to remove carbonate contaminates was found to significantly affect retention of major and trace elements. For this reason, dilute HCl leaching was not employed in this study for preparation of samples for major and trace element analysis (unpublished study, Morikawa, 1992). Radiogenic isotope compositions of rock samples are presumably not affected by dilute acid leaching. Consequently, this method was used to treat samples submitted for isotope analyses.

Samples were processed into fused glass disks for major element analysis by heating 1.0 g sample, 9.0 g lithium tetraborate, and 0.16 g ammonium nitrate at 1100°C in gold-platinum crucibles and pouring the resultant melt into heated Au-Pt molds (Noorish and Hutton, 1969; Mills, 1991). Samples for trace element analysis were prepared by mixing 2.5 g sample with 0.5 g methyl cellulose, enclosing this mixture with a rim and backing of additional methyl cellulose, and compressing to 10,000 psi in

a Buehler specimen mount press to form a disk (Hutchison, 1974). All samples and reagents were weighed to ± 0.0005 g. All prepared samples were stored in dessicators prior to analysis.

X-ray fluorescence analysis of major and trace elements were completed using the Rigaku 3030 X-ray Spectrometer at the University of Nevada, Las Vegas. Calibration of this spectrometer was based on the internal standards listed in Table 1. The analytical uncertainty and accuracy for major and trace elements are given in Tables 2 and 3. Comparison of the average of several analyses of a commercially prepared analytical standard (AGV-1) to the published values is given in Table 3.

Loss on Ignition (LOI) was determined for two samples from each location sampled for this study (Appendix A). Each sample (approximately 2 to 4 g) was initially weighed, heated in ceramic crucibles to 1000°C for 2 hours, cooled in the oven gradually to 300°C, and cooled completely to room temperature under dessication. Comparison of heated sample weight to initial (wet) weight was used to calculate % weight loss (LOI).

Isotopes were analyzed using the VG Sector 54 mass spectrometer at the University of Kansas, Lawrence. A thorough discussion of isotope analytical methods is presented by Feuerbach et al., (in press).

An incremental release $^{40}Ar/^{39}Ar$ analysis of sanidine and biotite separated from pumice collected from an ash-flow tuff that crops out in Dolan Spring, Arizona was completed at the University of Maine, Orono. Approximately 8 pounds of pumice were collected, trimmed of any weathered rind, crushed in the attrition mill described previously, and sieved into five fractions (600, 250, 180, 125, and 90 μm) using a Rotap automated shaker. Initial separation of biotite (180 μm fraction) and feldspar was done using the Frantz magnetic separator. Final separation of biotite was done by hand using the paper shaking technique (Taylor, personal communication, 1993), and

hand-picking under a binocular microscope. Final separation of feldspar (125 μm fraction) was done using heavy liquids (sodium metatungstate and bromoform), and hand picking.

Whole Rock Vs. Pumice Sampling

The primary magmatic compositions of ash-flow tuffs can be modified by eruptive and/or flow-induced mechanical fractionation processes as well as by entrainment of xenolithic/xenocrystic contaminants during emplacement (Hildreth and Mahood, 1985) (Valentine et al., 1992). Because of these factors, the original magmatic chemical signatures of ash-flow tuffs are more likely to be preserved by cognate pumice than by whole rock ash-flow tuffs. Pumice represents essentially a magmatic "grab-sample" unaltered by syn- and post-eruptive fractionation processes. Therefore, pumice is the material of choice for regional correlation of ash-flow tuffs that are based specifically upon geochemical signatures.

Pumice in the Tuff of Bridge Spring generally occurs as fiamme that cannot be easily separated from rock matrix and is rarely suitable for collection for geochemical analysis. The Tuff of Bridge Spring does, however, exhibit several characteristics that allow sampling of whole rock in lieu of pumice to obtain meaningful chemical analyses. (1) The Tuff of Bridge Spring contains low modal abundances of xenoliths (average= 6.1%). Xenoliths are consistently mafic (basaltic to basaltic andesite) in composition. (2) Thin section studies indicate that the majority of phenocrysts present in the Tuff of Bridge Spring are primary (i.e., are not xenocrystic). (3) Geochemical data (see internal stratigraphy section) demonstrate the presence of relatively simple magmatic zonation, the regional preservation of extremely fine-scale chemical partitioning in the Tuff of Bridge Spring, and a non-correspondence of modal lithic abundances to the

concentration of those elements normally present in mafic rocks (e.g., Cr, Mg, etc.) (Fig. 5). These regionally-distributed chemical patterns indicate that syn- and/or post-eruption chemical fractionation/contamination did not significantly alter the original magmatic composition of the Tuff of Bridge Spring. The presence of regionally-distributed chemical patterns suggests that xenoliths did not significantly skew the geochemical signature of the Tuff of Bridge Spring other than by imparting a minimal and constant background "static" that is persistent over its entire range of composition. These observations support the use of whole rock samples for determination of the geochemistry of the Tuff of Bridge Spring.

Table 1: Calibration standards for the Rigaku 3030 X-ray Fluorescence Spectrometer, University of Nevada, Las Vegas. All standards are United States Geological Standards unless otherwise noted.

Trace Elements	Major Elements
G-2	SCO-1
W-2	STM-1
BIR-1	GSP-1
RGM-1	GSP-1
QLO-1	DNC-1
BHVO-1	RGM-1
PCC-1	BHVO-1
GSP-1	PCC-1
AGV-1	AGV-1
DNC-1	QLO-1
	AL-1*

* French Standard

Table 2: Precision for the Rigaku 3030 X-ray Fluorescence Spectrometer, University of Nevada, Las Vegas using U.S.G.S. Standard AGV-1 as reference.

Element	Mean Relative Error (%)	Element	Mean Relative Error (%)
SiO_2	3.00	Nb	10.00
Al_2O_3	7.00	Ni	>20
TiO_2	2.00	Rb	2.00
FeO (total)	3.00	Sr	2.00
CaO	2.00	Th	12.00
K_2O	2.00	Y	2.00
MnO	10.0	Zr	5.00
P_2O_5	10.00	Ba	10.00
Na_2O	6.00		
MgO	2.00		

Table 3: Accuracy for the Rigaku 3030 X-Ray Fluorescence Spectrometer, University of Nevada, Las Vegas. Accuracy determined by analyzing U.S.G.S. standards AGV-1, BIR-1, and BHVO-1. Results for 10 replicate analyses of AGV-1 are given below.

Element	Published concentration of AGV-1	Mean of 10 replicate analyses of AGV-1
Cr	10.1	11.0
Ni	16	15.91
Rb	67.3	65.22
Sr	662	657
Th	6.5	6.1
Y	20	21.41
Zr	227	239
Ba	1226	1271
Nb	15	14.24

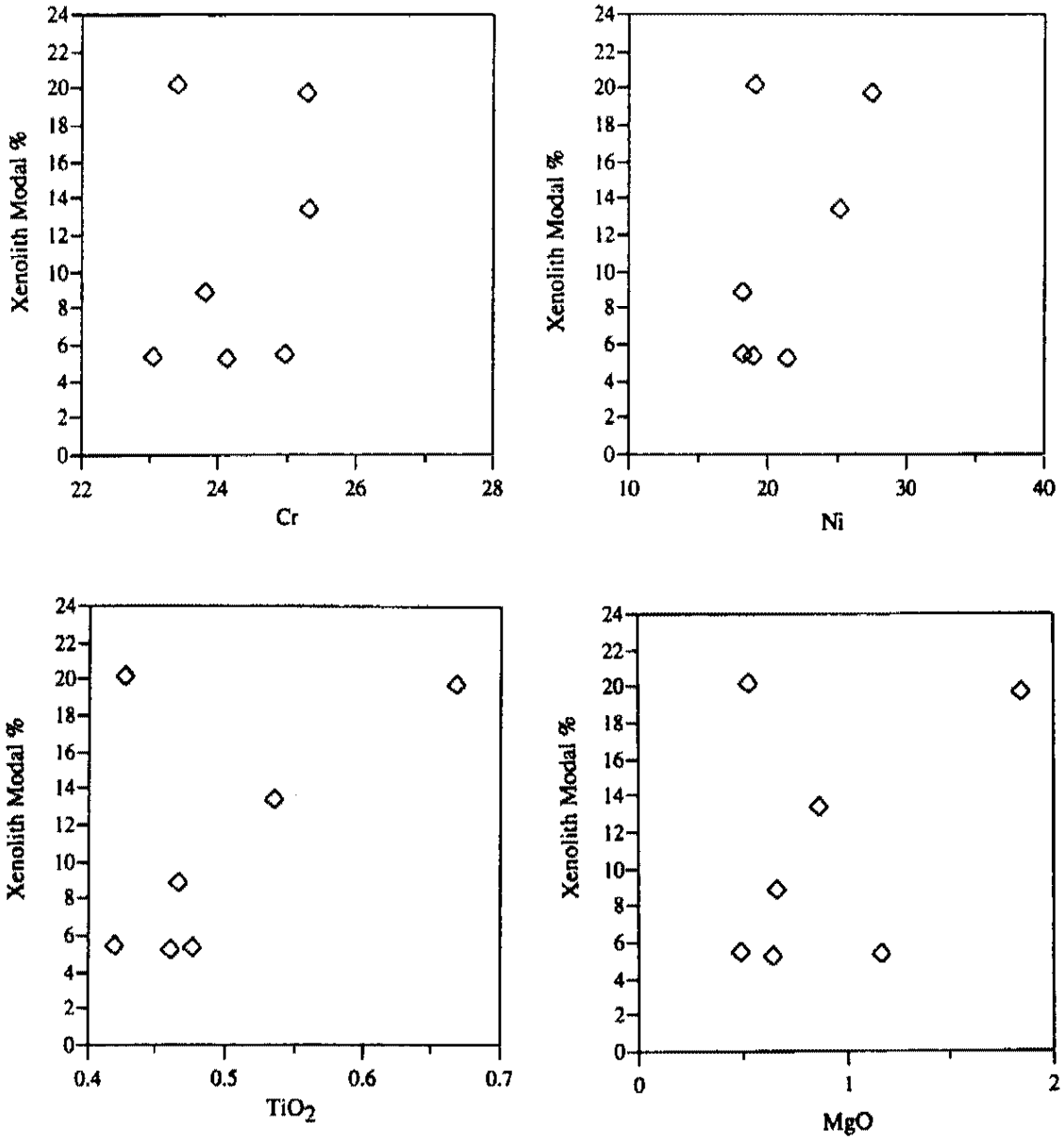

Figure 5. Plot of xenolith abundance vs. element concentration for the Eldorado Mountains section. Oxides in wt. % and trace elements in ppm in this and all subsequent plots.

Analytical Data

Presented below are summaries of major/trace element geochemical data and thin section petrology for the Tuff of Bridge Spring. Major and trace element analyses are given in Appendix A. Major element oxide values used in plots presented in the text have been normalized to 100 wt. %. LOI values were excluded from these calculations. Major element concentrations are reported in wt. % and trace element concentrations are reported in ppm. Thin section point counts (whole rock) and normalized phenocryst modes are given in Appendix B. 500 points were counted in each thin section. Presentation of isotopic analyses is deferred to the discussion of regional correlation. Detailed stratigraphic section descriptions are given in Appendix C.

Major and Trace Element Geochemistry

Fifty-seven samples for major and trace element analysis were collected from eleven sections scattered across the northern Colorado River extensional corridor (Fig. 6: location map of samples). Major and trace element analyses of these samples are given in Appendix A.

K-metasomatism of volcanic rocks is common in many locations in the extensional corridor (Smith et al., 1990). In order to determine whether metasomatism has significantly affected Tuff of Bridge Spring samples, Tuff of Bridge Spring data are plotted on a Na_2O versus K_2O plot from Smith et al., (1990) which includes the field of unmetasomatized intermediate and felsic rocks as defined by Carmichael et al. (1974) (Fig. 7). This plot indicates that 47 % of the analyses have not been metasomatized. With the exception of the analyses of the Temple Bar ash-flow tuff,

the remaining data points fall very close to the field of unmetasomatized rocks. Also, 70 % of the LOI values determined for twenty Tuff of Bridge Spring samples have values under 2 %, which suggests that they have not been altered. Since most incompatible trace element concentrations are not appreciably affected by metasomatism (Smith et al., 1990), and since negative correlation of K and Na concentrations in some northern Colorado River extensional corridor rocks (Wilson Ridge pluton) suggests the presence of closed system/equilibrium conditions (Smith et al., 1990), it is assumed that metasomatism did not significantly affect the chemistry of samples collected for this study and, consequently, that the analyses are representative of ash-flow tuff compositions present at the time of their eruption.

Tuff of Bridge Spring Geochemistry

The following description of geochemistry focuses on those stratigraphic sections that are isotopically equivalent to the Tuff of Bridge Spring (see regional correlation section). Discussion of the geochemistry of those sections that are isotopically different from the Tuff of Bridge Spring (Lucy Gray and Salt Spring Wash) or are not equivalent in age to the Tuff of Bridge Spring (Dolan Springs) will be deferred to the end of this discussion. Interpretation of geochemistry will be presented in later sections.

The Tuff of Bridge Spring continuously ranges in composition from andesite (White Hills: 59.50 % SiO_2) to rhyolite (Black Mountains: SiO_2 = 74.91 % SiO2), and has an average composition of dacite (67 % SiO_2) (Table 4). There is a rough trend of decreasing silica in a northeastward direction across the distribution area of the Tuff of Bridge Spring. In the southwest portion of the Tuff of Bridge Spring distribution area, the Black Mountains, Highland Spring Range, and Sheep Mountain are rhyolitic in

composition. Sections in the middle of the distribution area, which includes the Eldorado Mountains, McCullough Range, and Interstate 15 sections, range in composition from dacite to rhyolite. The Temple Bar section is dacitic in composition, and the White Hills section in the northeastern corner of the Tuff of Bridge Spring distribution area ranges from andesite to dacite. The greatest variation of SiO_2 within a single section is found in the McCullough Range (8.6 wt. % SiO_2). The smallest variation in found in the Sheep Mountain section (0.46 wt. % SiO_2).

Harker variation plots (Fig. 8) show a general trend of decreasing Al, Ti, Fe, Mg, Ba, Zr, and Sr with increasing silica, and increasing Th and Nb with increasing silica. Other general observations of Tuff of Bridge Spring chemistry include (1) unusually high concentrations of Cr (approximately 150 ppm in the Sheep Mountain section); (2) very low K (5.7 wt. % in the basal Sheep Mountain section); and (3) anomalously large ranges of Rb (40 to 300 ppm), Ba (100 to >1500 ppm), Sr (50 to >1500 ppm), and Na (0.2 to 4 wt. %).

Since the large variation of silica in each Tuff of Bridge Spring section tends to obscure distinct element groupings in conventional Harker variation plots, comparisons of general patterns of geochemical trends and detection of any departures from these patterns were found to be more clearly discerned by the use of relative stratigraphic position vs. elemental oxide plots (Fig. 9). These plots use the convention in which larger numerical values are assigned to stratigraphic intervals which occur higher in the section and smaller numerical values are assigned to intervals lying in lower positions in the section. (N.B.- correlation of intervals having the same relative stratigraphic position value is <u>not</u> inferred between different sections; e.g., position 5.5 in one section is not equivalent to position 5.5 in another section).

Relative stratigraphic position vs. elemental oxide plots (Fig. 9) show that the chemistry of the Tuff of Bridge Spring (1) varies widely over its range; (2) can vary

considerably within each stratigraphic section; and (3) the geochemical trends of the Eldorado Mountains, Highland Spring Range, Interstate 15, and Sheep Mountain sections are relatively invariable for most major and trace elements (with the exceptions of Ca, Cr, Ni, and Th) and form a chemical group that can be used to create a baseline reference against which any deviations exhibited by the other Tuff of Bridge Spring sections can be compared with and quantified (Table 5).

The following is a short summary of deviations from the invariable Tuff of Bridge Spring group described above. Important variations from the baseline reference chemistry include (Fig. 9 and Table 5):

(1) The lower part of the Temple Bar section (intervals 4-8) is enriched in K by approximately 4.4 wt. %.

(2) The Temple Bar and Black Mountains sections have slightly lower Mn concentrations (0.02 wt. % Mn).

(3) The Interstate 15, Temple Bar, and Sheep Mountain sections show highly variable (a minimum of 23 ppm) enrichment of Cr.

(4) The lower Temple Bar section (intervals 5-8) is significantly enriched in Rb (100 ppm).

(5) The McCullough Range and White Hills sections are enriched in Sr (a minimum of 170 ppm).

(6) Intervals 6-7.5 of the McCullough Range section are significantly enriched in Zr (210 ppm).

(7) The McCullough Range is enriched in Ba by a minimum of 320 ppm and contains a Ba spike at stratigraphic intervals 6-7.5. This spike corresponds to the peak observed for Zr at the same stratigraphic positions. The Temple Bar and White Hills sections also show enrichment in Ba (870 ppm).

(8) The McCullough Range, White Hills, and Black Mountains sections show much greater variability of Y than the rest of the sections.

(9) The basal interval of the McCullough Range section consistently shows significant variation for Si, Al, K, Mg, Na, Rb, Zr, and Sr as compared to the upper part of the section. In the Eldorado Mountains, large variation of Ca, Na, Rb, Y, Na and Mg occurs in the three stratigraphically lowest-lying intervals. In the Temple Bar section, deviation of Ti, Ca, K, Mg, Rb, Y, Fe, and Mn occurs in the stratigraphically uppermost interval.

(10) The McCullough Range section shows a significant enrichment in Fe, Si, Al, Ti, Ca, Zr, Ba, Y, and Nb at position 8.

Other Ash-flow Tuffs

Based on isotopic analyses (see regional correlation section), the Salt Spring Wash, Lucy Gray, and Dolan Springs sections are not equivalent to the Tuff of Bridge Spring. These tuffs are rhyolitic in composition (Tuff of Dolan Springs: 73.7-75.6 wt. % SiO_2; Salt Spring Wash: 70.1-73.9 wt. % SiO_2; and Lucy Gray Range: 72.4-72.9 wt. % SiO_2) (Appendix A). The maximum SiO_2 value of Tuff of Dolan Springs exceeds that of the highest value of the Tuff of Bridge Spring (Black Mountains section: 74.91 %). Harker variation plots for these sections compared with the Tuff of Bridge Spring (Fig. 10) show:

(1) The Dolan Springs section is noticeably depleted in Al, Ti, Fe, and Mn, and is significantly depleted in Nb (5.3 ppm), Th (8.5 ppm), Y (2.2 ppm), and Zr (139.7 ppm) with respect to the Tuff of Bridge Spring.

(2) The Lucy Gray Range section exhibits depletion in Fe, Ca, Ba, Mg, Ti, and Sr, and is enriched in Y with respect to the Tuff of Bridge Spring.

(3) The lowest value of the Salt Spring Wash section for Zr, Y, Th Ca, Nb,and Al falls below the lowest value for these elements for the Tuff of Bridge Spring.

Petrologic Descriptions

The Tuff of Bridge Spring contains from 7.8 % to 46.4 % phenocrysts (Black Mountains and Temple Bar sections, respectively) and from 0 % to 25.4 % lithic fragments (maximum from the Black Mountains section) (Appendix B). The matrix of the Tuff of Bridge Spring is moderately devitrified, which is reflected by the presence of fine- to coarse-grained crystallization textures. Another common matrix texture is an axiolitically-devitrified matrix in which the faint outlines of glass shards in the matrix are still discernable. Unaltered glass shards are rare in the Tuff of Bridge Spring with the exceptions of the Sheep Mountain and Interstate 15 sections. Spherulitic devitrification is also rare in the Tuff of Bridge Spring. Spherulites in the Highland Spring Range section are anomalously large (< 7 cm in diameter).

Pumice is rare in the Tuff of Bridge Spring and generally occurs as moderately-compressed, subangular fragments that are less than one millimeter wide. Preservation of larger pumice fragments is rare, and is limited to occurrences in the basal intervals of the Sheep Mountain and Interstate 15 sections. Pumice from these sections range in size from <3 mm to 8 cm.

Eutaxitic textures are common in the Tuff of Bridge Spring. Fiamme vary from <1.0 cm to over 9 cm (Eldorado Mountains section). Banded fiamme can sometimes be observed in the Eldorado Mountains section.

The majority of Tuff of Bridge Spring sections are either unaltered or are weakly-altered by secondary carbonate. Temple Bar samples are heavily contaminated with secondary carbonate. Alteration of feldspar phenocrysts in Temple Bar samples

makes the discrimination of sanidine from plagioclase difficult, requiring the use of the "undifferentiated feldspar" nomenclature used in the Appendix B.

Lithic fragments in the Tuff of Bridge Spring consist of basalt to basaltic andesite. Basalts commonly contain plagioclase phenocrysts. Basaltic andesite lithic fragments contain phenocrysts of plagioclase, clinopyroxene, and opaque iron oxide (undifferentiated).

Phenocrysts in the Tuff of Bridge Spring include, in decreasing order of abundance: sanidine, plagioclase, biotite, clinopyroxene, opaque iron oxide (undifferentiated), sphene, ± zircon, and ± apatite (Appendix B). Primary quartz is not present in the Tuff of Bridge Spring. Trace amounts of hornblende, which is rare and possibly xenocrystic, is present in the McCullough Range and White Hills sections. Plagioclase ranges from An_{11} (Black Mountains section) to An_{36} (Eldorado Mountains section) (Table 6). Feldspar phenocrysts commonly display disequilibrium textures which include resorbed margins in sanidine phenocrysts, sieve textures in plagioclase and sanidine, and mantling of plagioclase phenocrysts by sanidine.

Glomerocrysts are ubiquitous in the Tuff of Bridge Spring, and occur as: (1) monomineralic clusters of plagioclase, sanidine, or sphene, and (2) polymineralic clusters that commonly occur in the following combinations: (*i*) clinopyroxene + sphene + Fe-oxide opaque ± plagioclase ± biotite ± zircon ± apatite; (*ii*) sphene + Fe-oxide opaque + zircon ± apatite ± biotite; and (*iii*) plagioclase + biotite + sphene ± zircon ± sanidine. Glomerocrysts generally occur as aggregations of five or fewer crystals, and are < 0.8 mm in width.

Two small (< 0.3 mm in length) mafic enclaves were observed in thin sections of the Tuff of Bridge Spring. These consist of the following samples. (1) Sample 92-E3-10 (Eldorado Mountains section): this oblate-shaped enclave (length ≅ 2 mm) consists of a core of blebby biotite, opaque iron oxide, and plagioclase feldspar which is

enclosed in a microcrystalline matrix of unknown composition. This core is enclosed within a rim of subhedral to anhedral plagioclase feldspar. (2) Sample Mc 69 (Interstate 15 section): this enclave, found in a thin section that was previously described by Bridwell (1991), is approximately 3 mm long and consists of an irregularly fractured core of orange, microcrystalline unknown mineral that is enclosed in successive, concentric rims of (*i*) anhedral, opaque iron oxide enclosed in black, microcrystalline matrix, (*ii*) anhedral clinopyroxene, and (*iii*) euhedral to subhedral biotite (listed in order of occurrence from enclave core to rim).

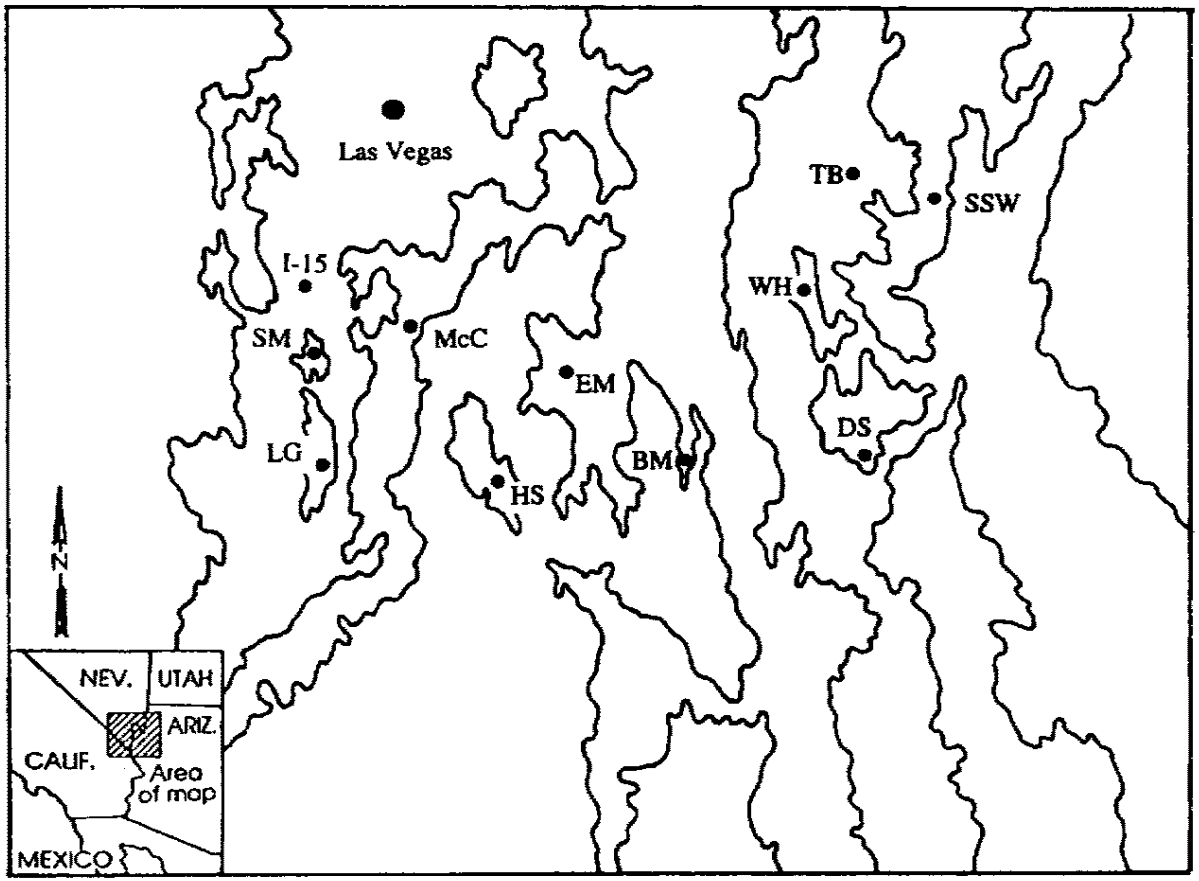

Figure 6. Map showing locations of sections sampled for geochemistry and petrology. LG = Lucy Gray Range; SM = Sheep Mountain; I-15 = Interstate 15; EM = Eldorado Mountains; McC = McCullough Range; HS = Highland Spring Range; BM = Black Mountains; TB = Temple Bar; WH = White Hills; DS = Dolan Springs; SSW = Salt Spring Wash.

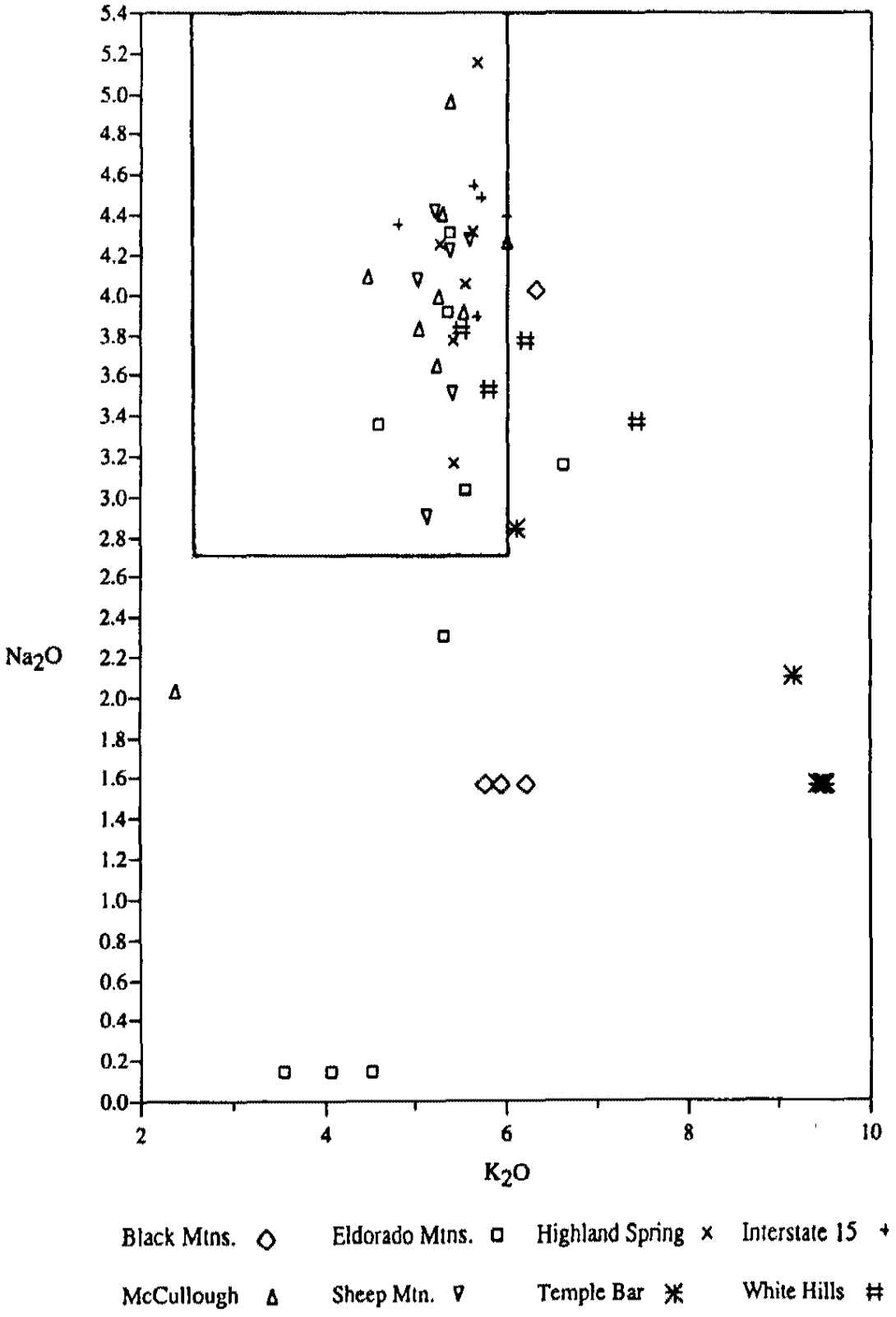

Figure 7. Plot of Na_2O vs. K_2O. The field of unmetasomatized rocks from Carmichael et al. (1974). Samples falling within the field are interpreted to be either unaffected or marginally affected by metasomatization.

Table 4: Regional Major and Trace Element Variation: Tuff of Bridge Spring.
Major element oxides in wt.% and trace elements in ppm.

	Minimum	Maximum	Range	Section Containing Minimum Value	Section Containing Maximum Value	Section Containing Least Variation	Range of Variation	Section Containing Greatest Variation	Range of Variation
SiO2	57.47	74.91	17.44	White Hills	Black Mountains	Highland Spring	1.88	McCullough Range	8.6
Al2O3	12.52	17.38	4.86	Black Mountain	White Hills	Highland Spring	0.32	McCullough Range	4.12
TiO2	0.26	0.70	0.43	Black Mountain	White Hills	Sheep Mountain	0.05	Eldorado Mountains	0.25
Fe2O3	1.69	3.85	2.46	Black Mountain	White Hills	Sheep Mountain	0.26	Eldorado Mountains	1.31
CaO	0.79	5.25	4.45	Temple Bar	White Hills	I-15	0.64	Black Mountains	3.19
K20	2.62	9.88	7.26	Temple Bar	Temple Bar	Black Mountains	0.26	McCullough Range	3.64
MnO	0.03	0.10	0.07	Temple Bar	White Hills	Highland Spring	0	Temple Bar	0.04
P2O5	0.00	0.25	0.25	Sheep Mtn./Highland Spring	White Hills	I-15	0.05	White Hills	0.15
Na2O	0.14	5.00	4.85	Eldorado Mtns.	Highland Spring	White Hills	0.04	Eldorado Mountains	4.25
MgO	0.14	2.13	1.99	Black Mountains	McCullough Range	Black Mountains	0.19	Eldorado Mountains	1.34
Cr	2.2	111.6	109.5	Black Mountains	Sheep Mountain	Eldorado Mountains	3.7	Sheep Mountain	92.9
Nb	24.0	51.9	27.9	McCullough Range	Highland Spring	Sheep Mountain	2.6	Highland Spring	15.4
Ni	8.2	30.4	22.2	Black Mountains	Eldorado Mountains	White Hills	2.1	Sheep Mountain	15.1
Rb	36	314	278	McCullough Range	Temple Bar	Sheep Mountain	19	McCullough Range	144
Sr	49	1083	1034	Black Mountains	McCullough Range	Sheep Mountain	39	McCullough Range	753
Th	16.7	44.6	27.9	White Hills	Highland Spring	Sheep Mountain	5.5	Highland Spring	15.4
Y	22.9	31.0	8.1	McCullough Range	Eldorado Mountains	Sheep Mountain	1	McCullough Range	5.1
Zr	261	638	377	Black Mountains	McCullough Range	White Hills	15	McCullough Range	337
Ba	63	1753	1690	Sheep Mountain	McCullough Range	Sheep Mountain	20	McCullough Range	1223

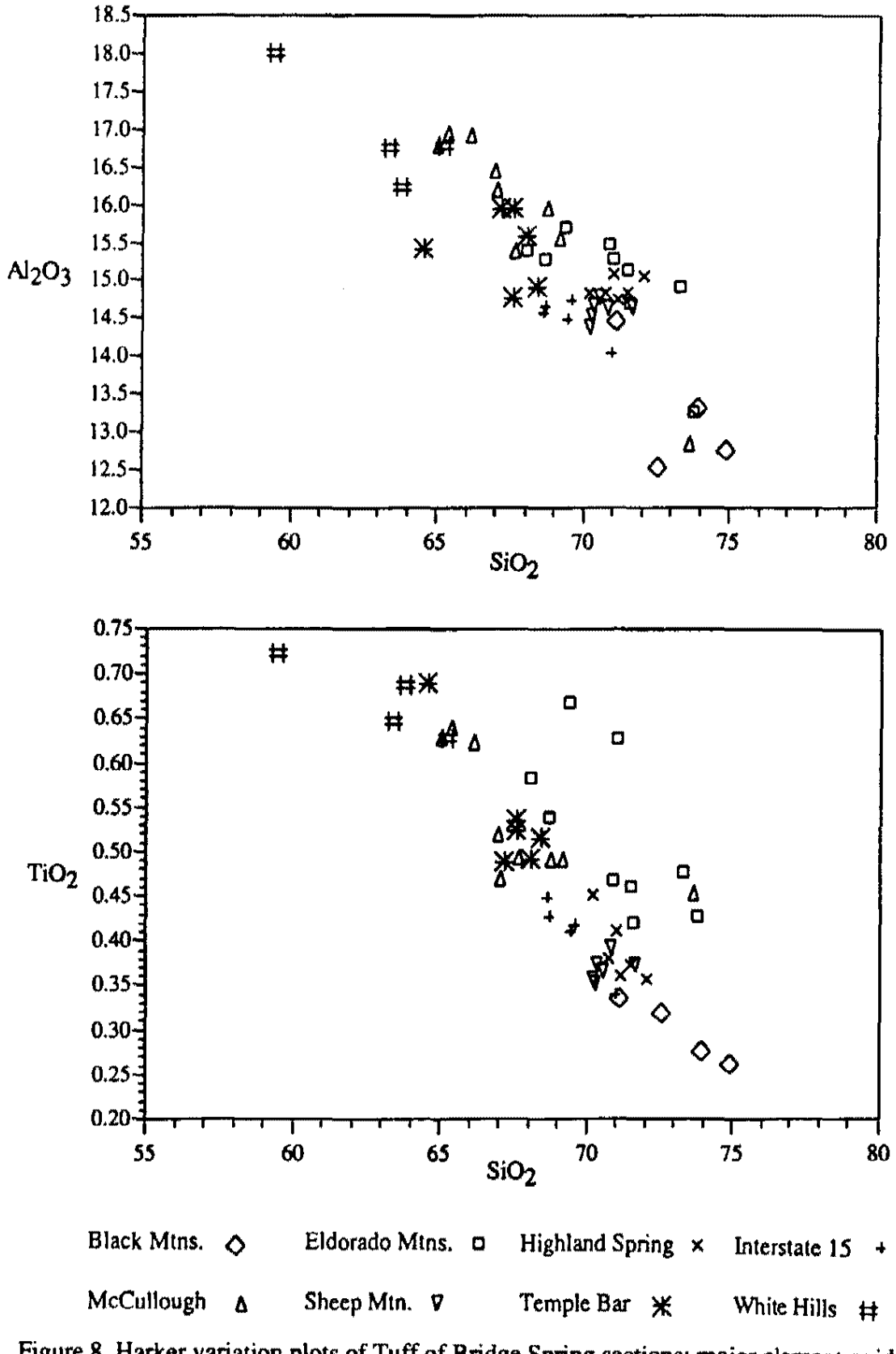

Figure 8. Harker variation plots of Tuff of Bridge Spring sections: major element oxides and trace elements vs. SiO_2.

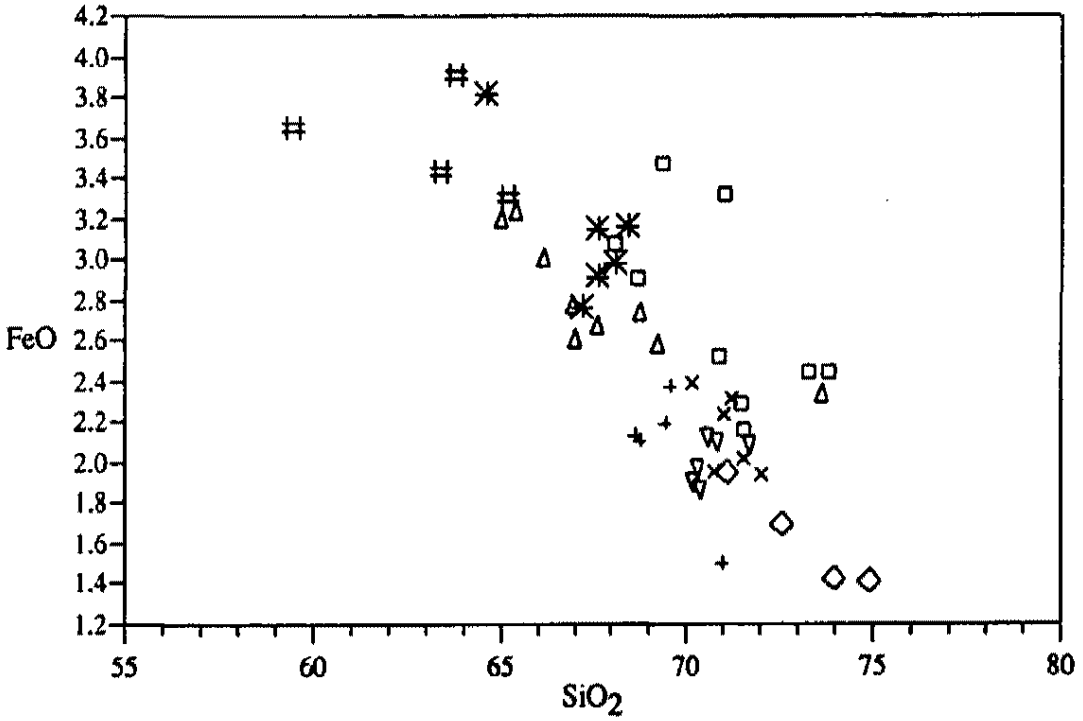

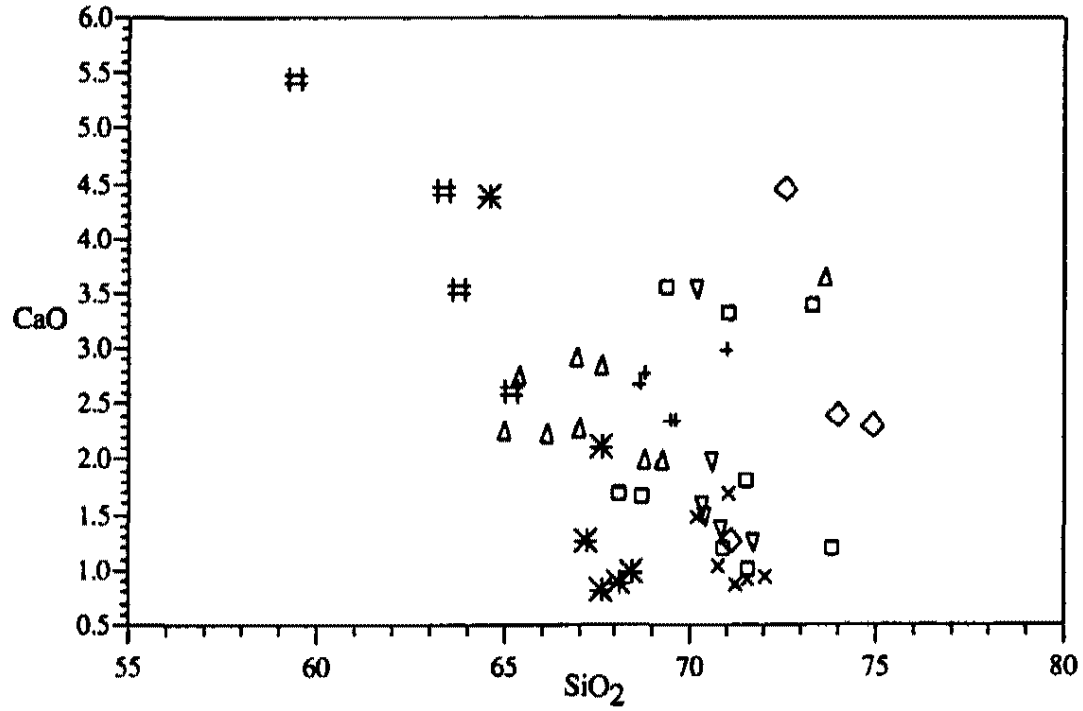

Black Mtns. ◇ Eldorado Mtns. □ Highland Spring × Interstate 15 +

McCullough △ Sheep Mtn. ▽ Temple Bar ✳ White Hills #

Figure 8, continued.

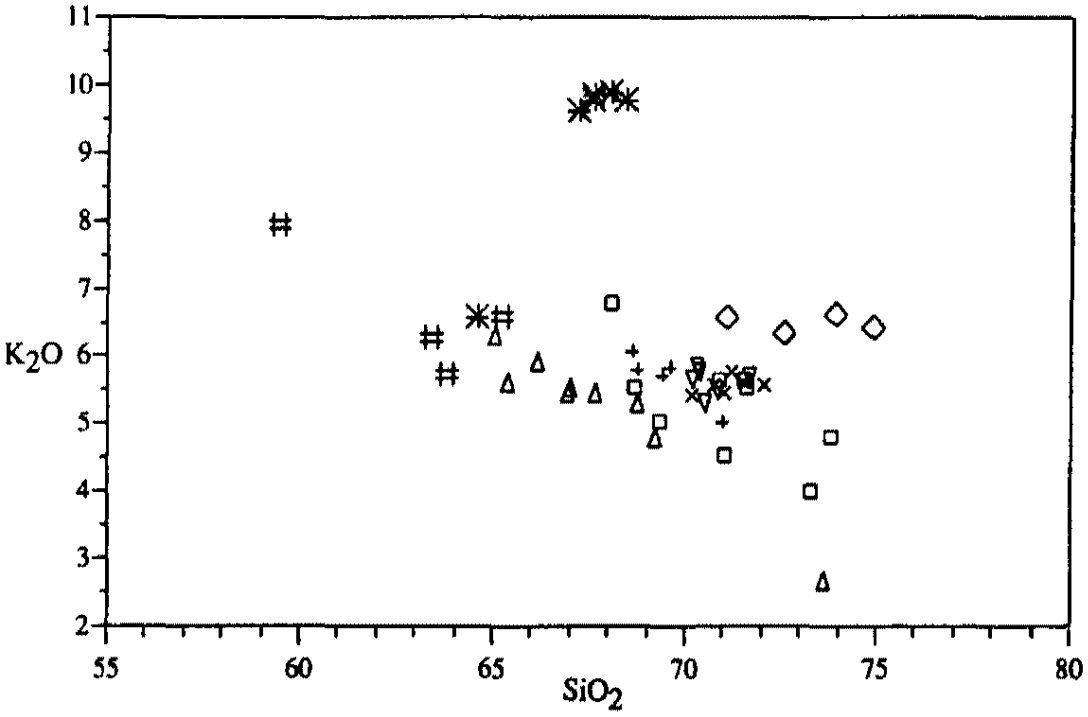

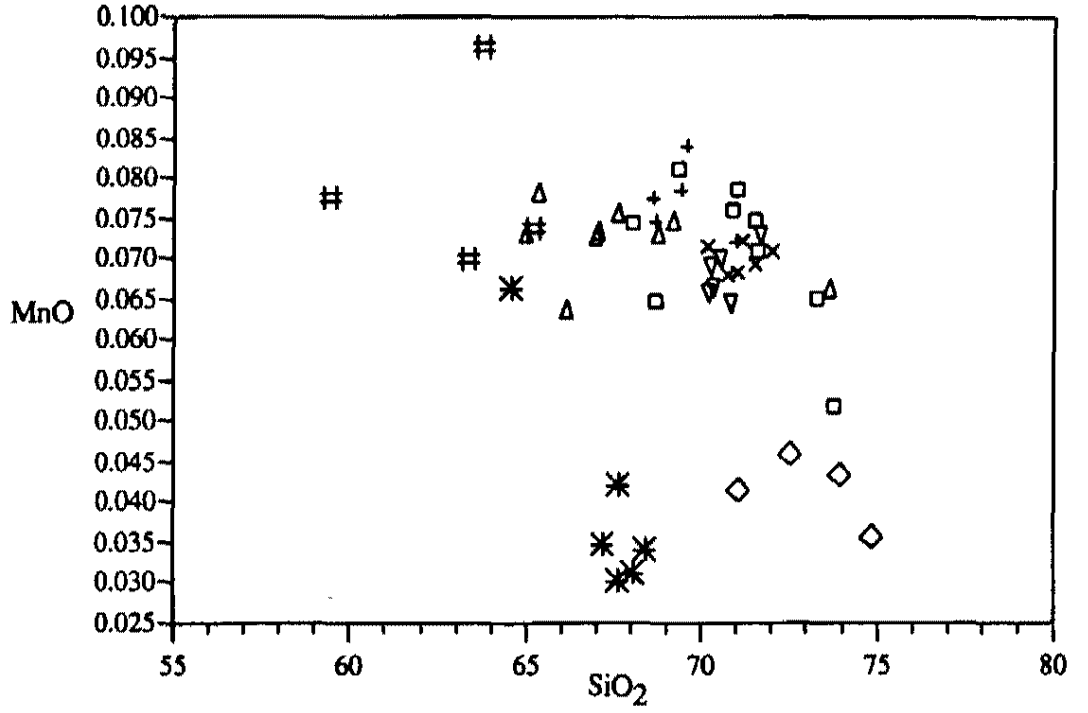

Black Mtns. ◇ Eldorado Mtns. □ Highland Spring × Interstate 15 +

McCullough △ Sheep Mtn. ▽ Temple Bar ✳ White Hills #

Figure 8, continued.

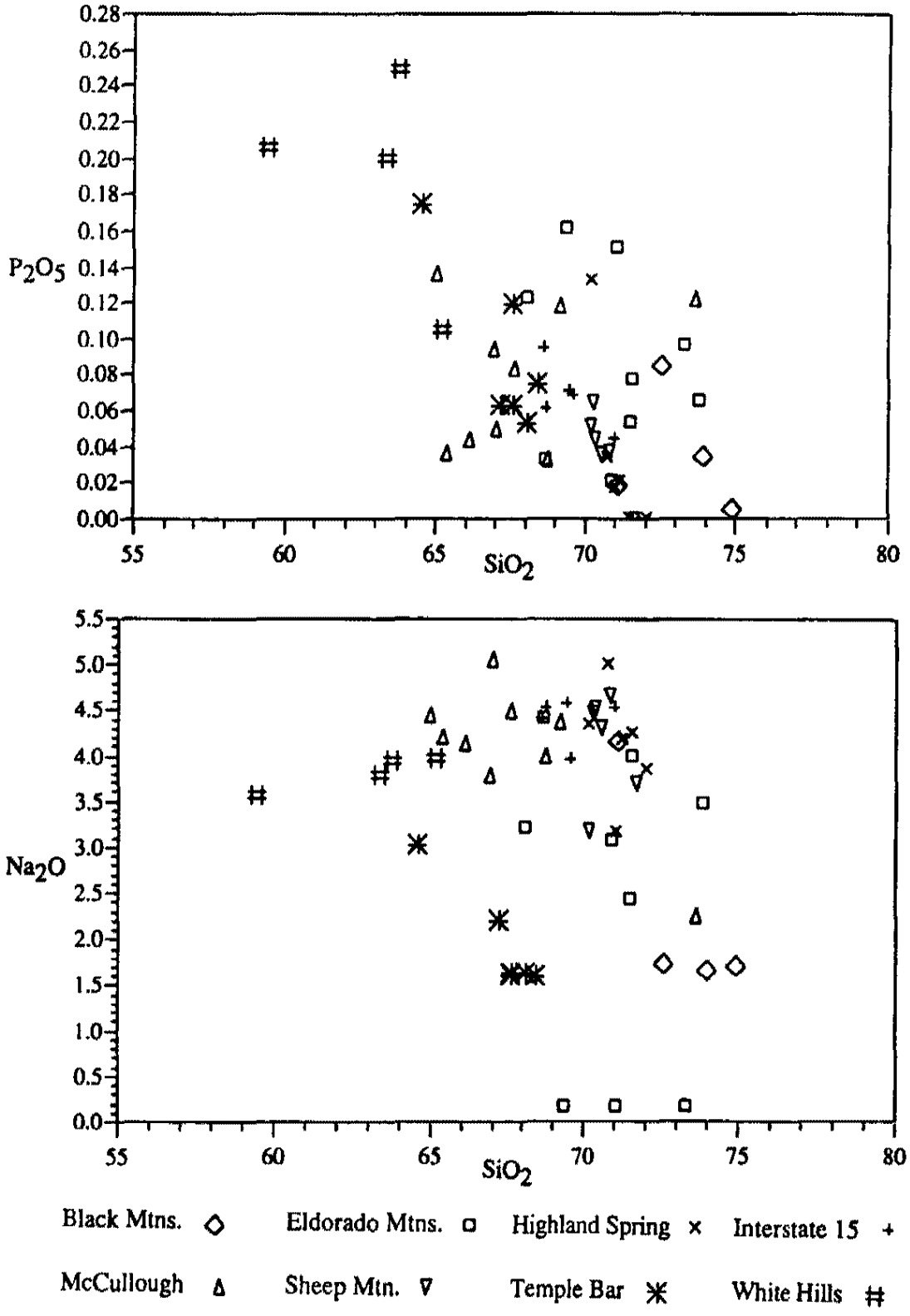

Figure 8, continued.

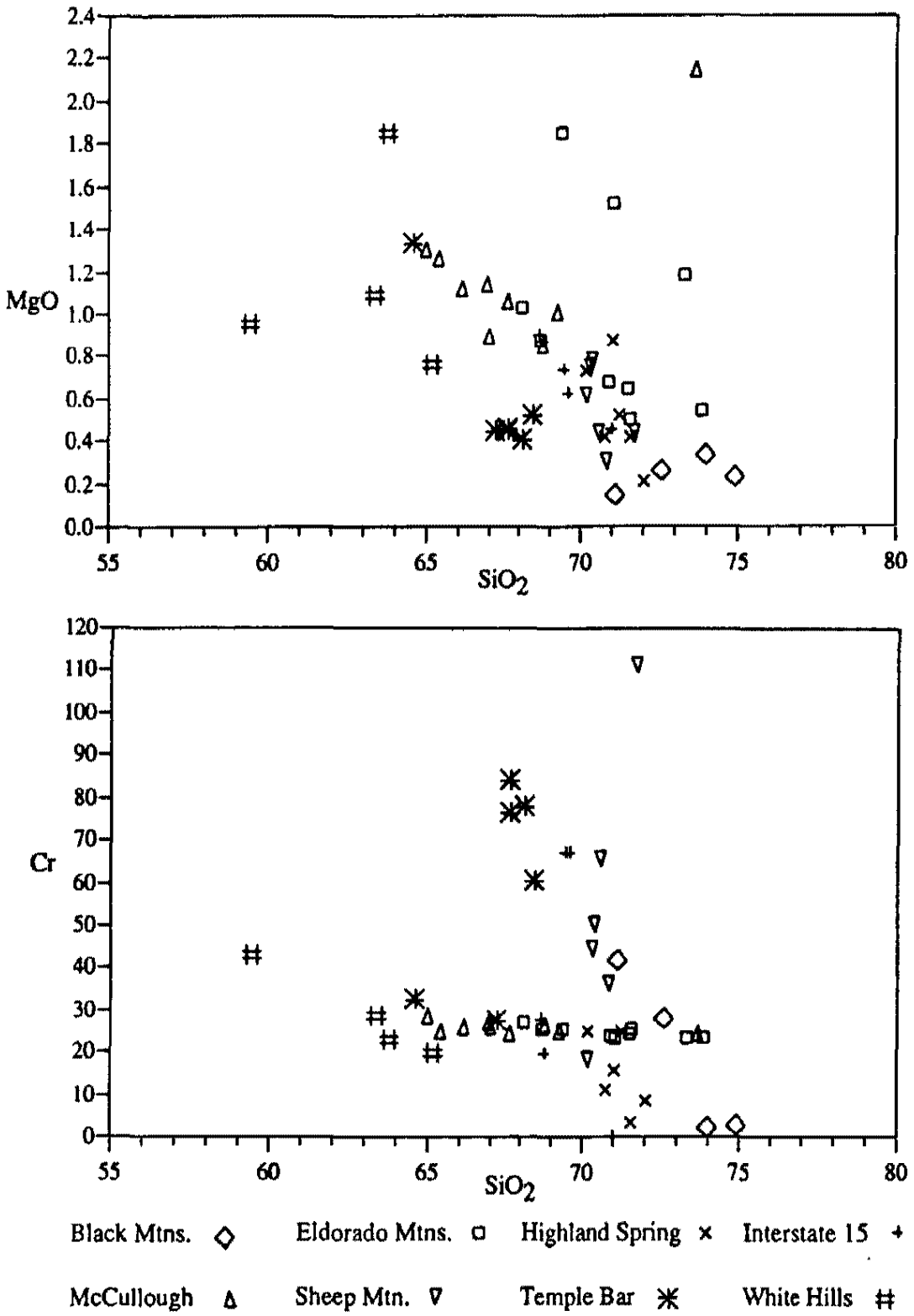

Figure 8, continued.

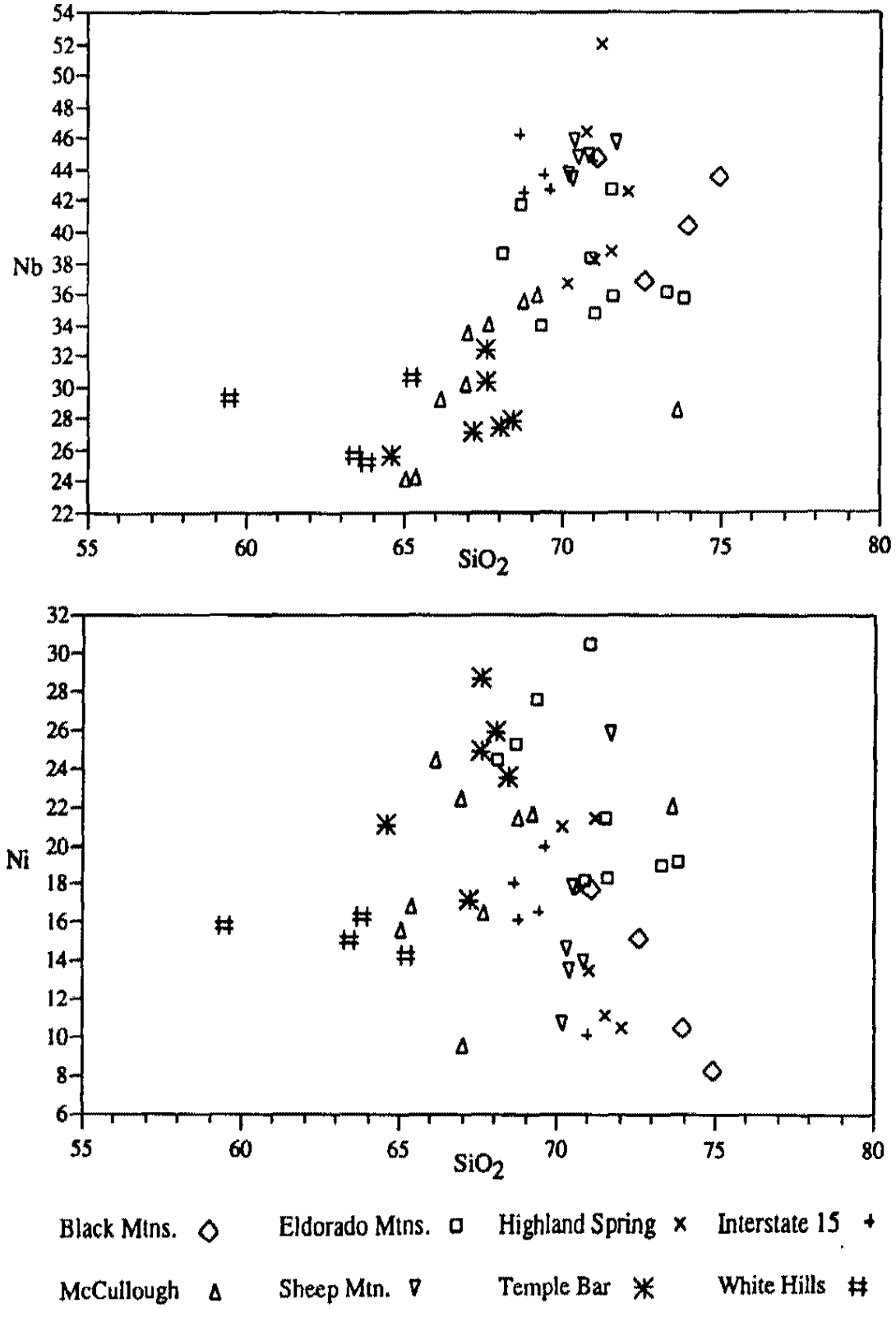

Figure 8, continued.

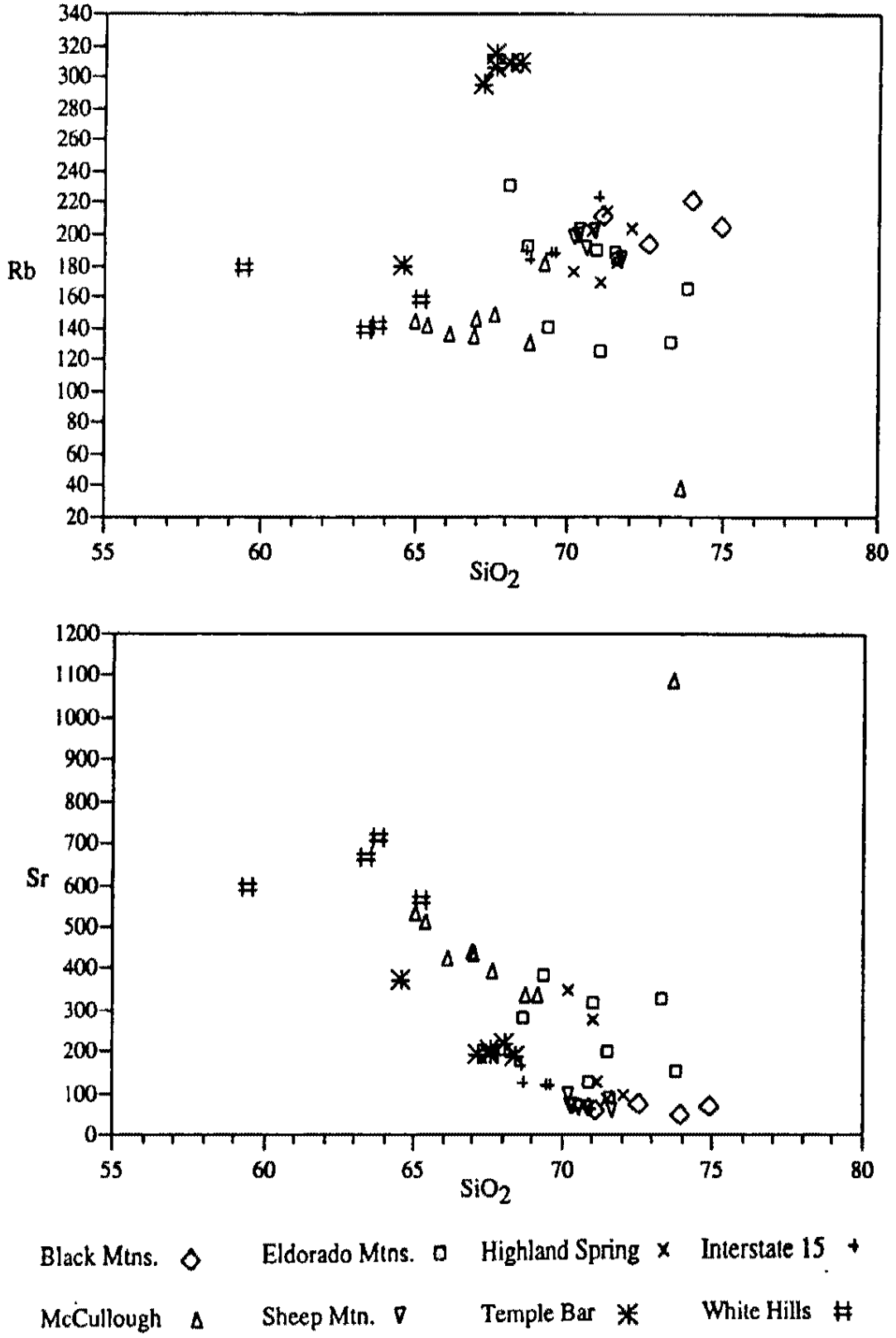

Figure 8, continued.

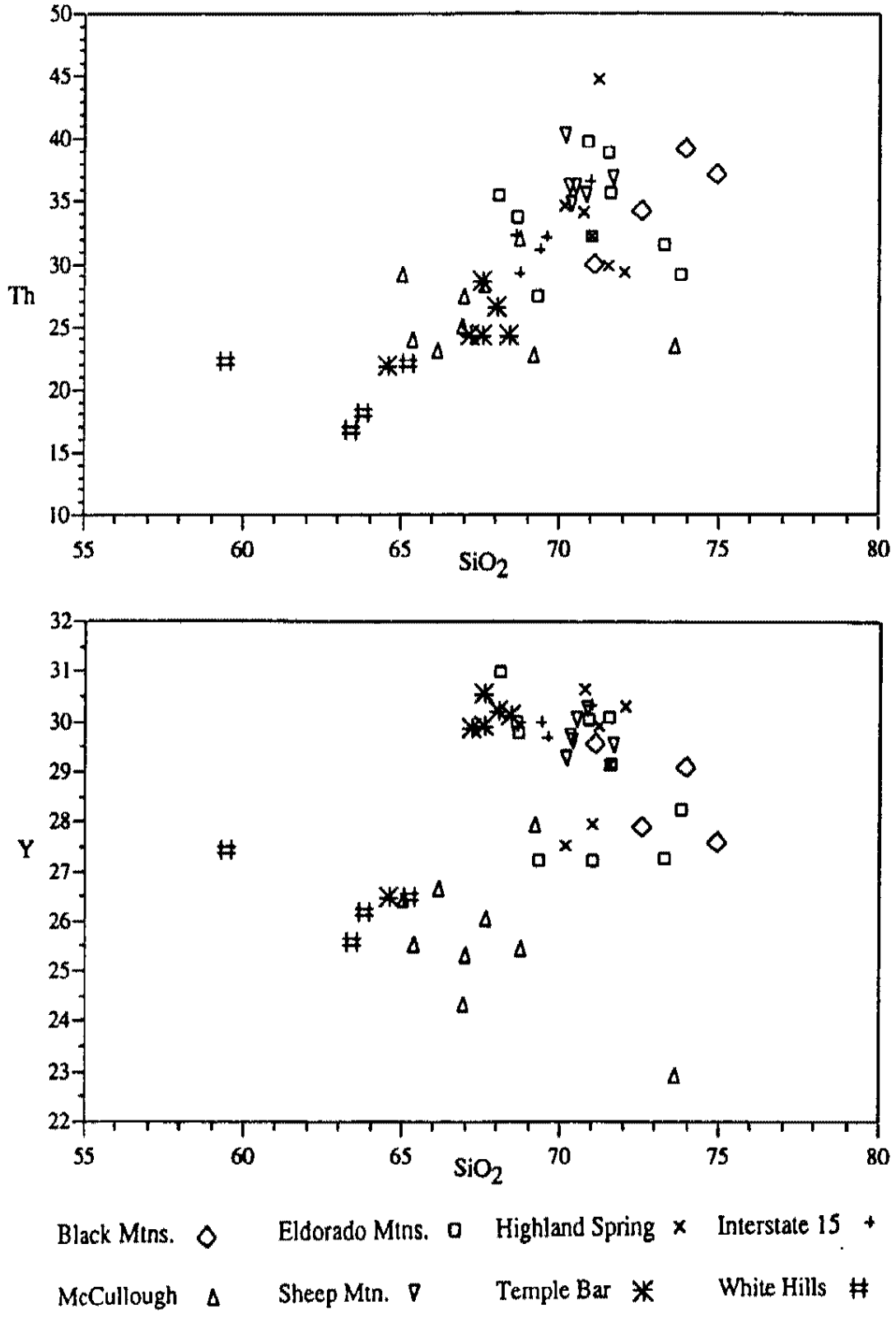

Figure 8, continued.

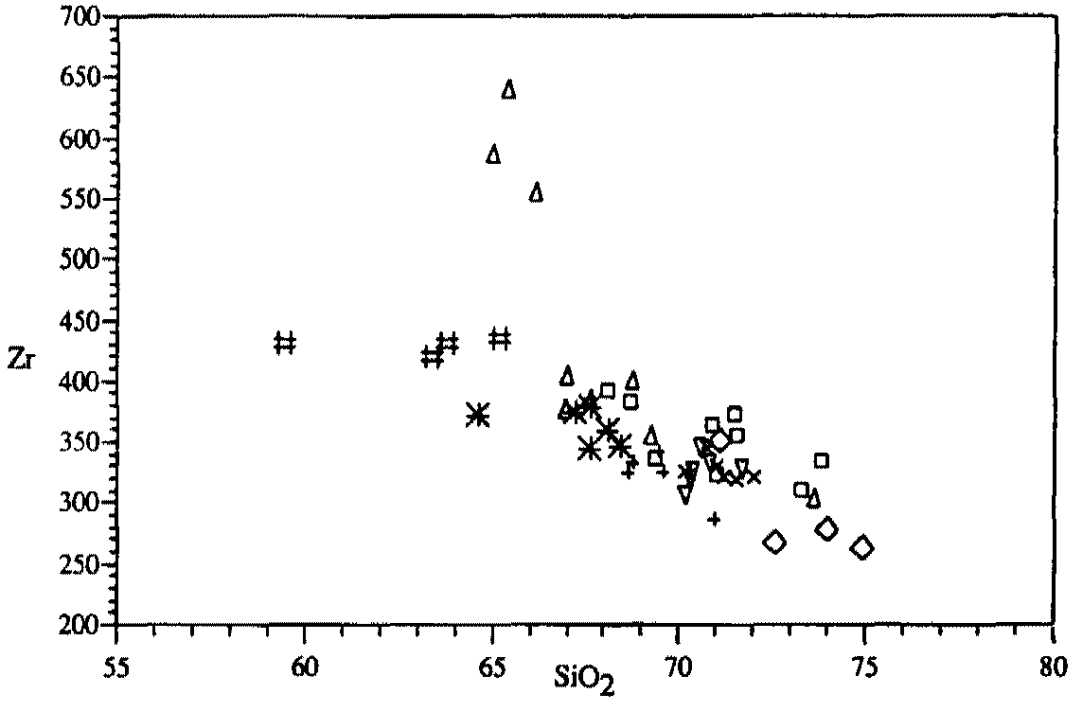

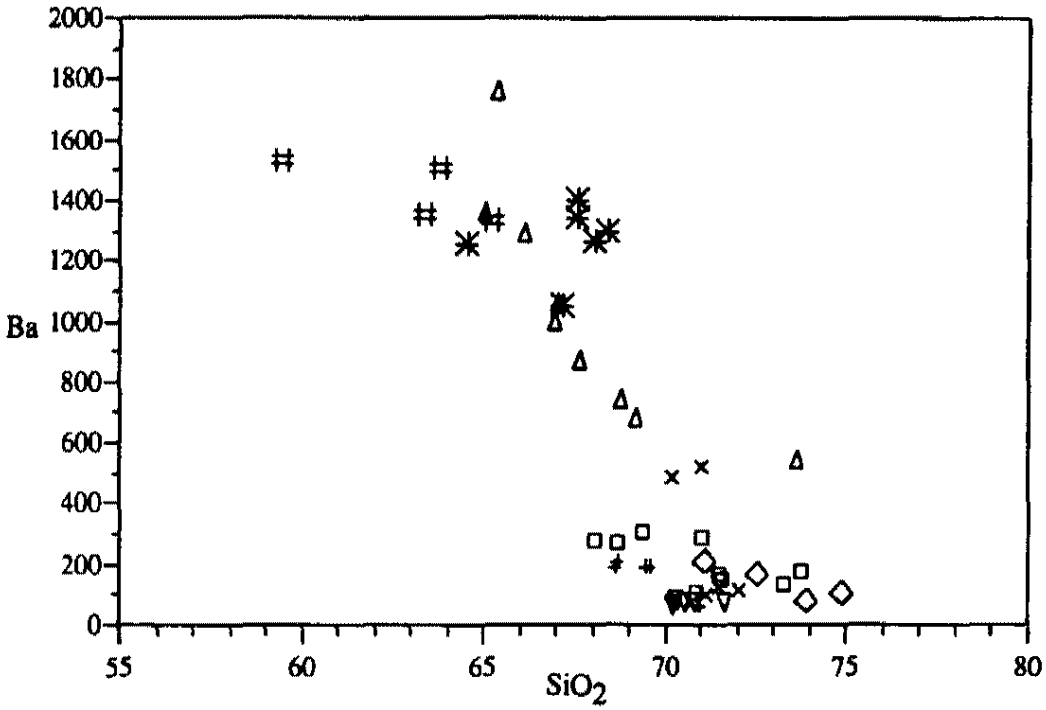

Black Mtns. ◇ Eldorado Mtns. □ Highland Spring × Interstate 15 +

McCullough △ Sheep Mtn. ▽ Temple Bar ✳ White Hills #

Figure 8, continued.

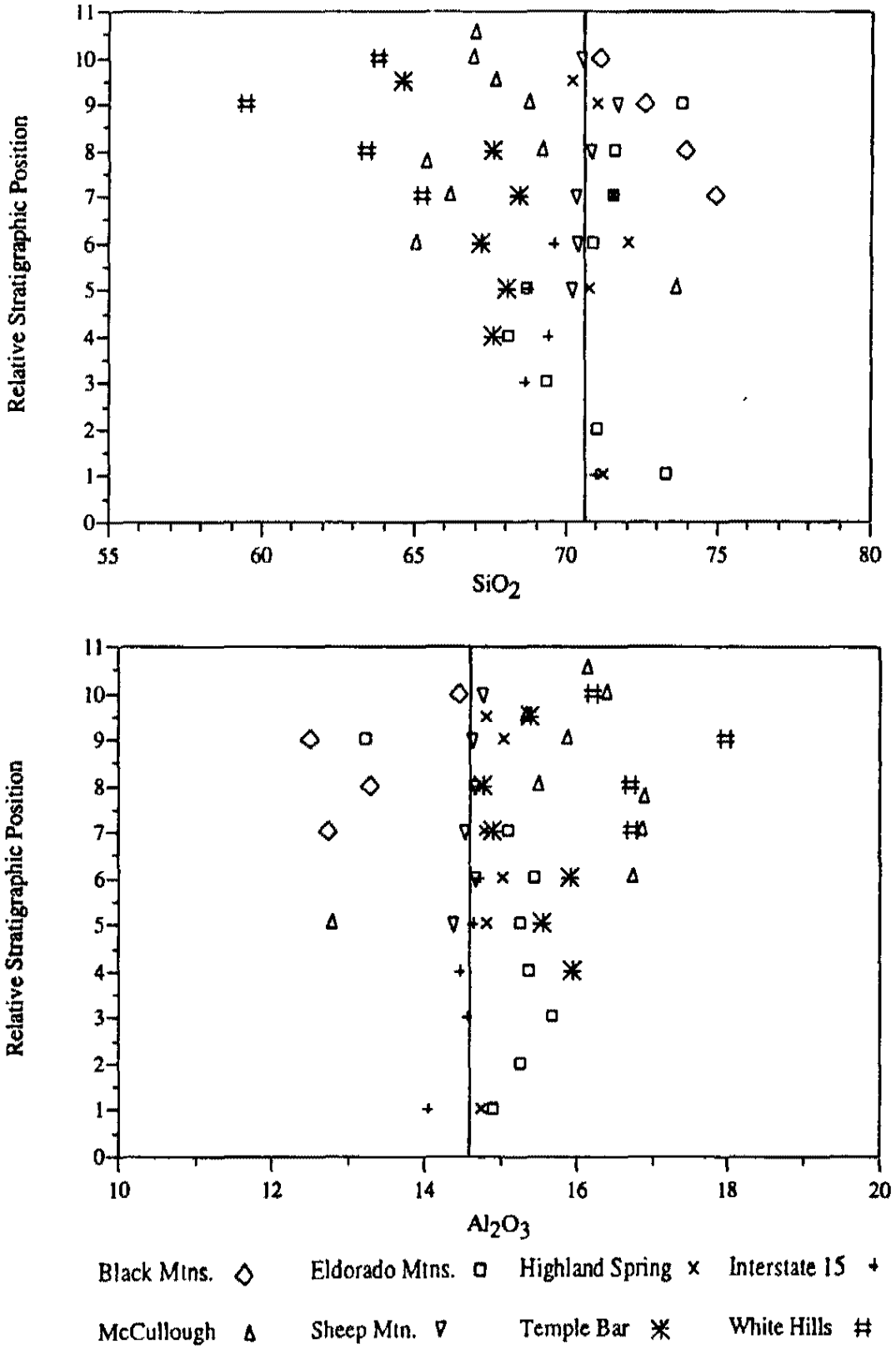

Figure 9. Plots of relative stratigraphic position vs. element concentration of Tuff of Bridge Spring sections. Average concentration value for each element indicated by vertical line.

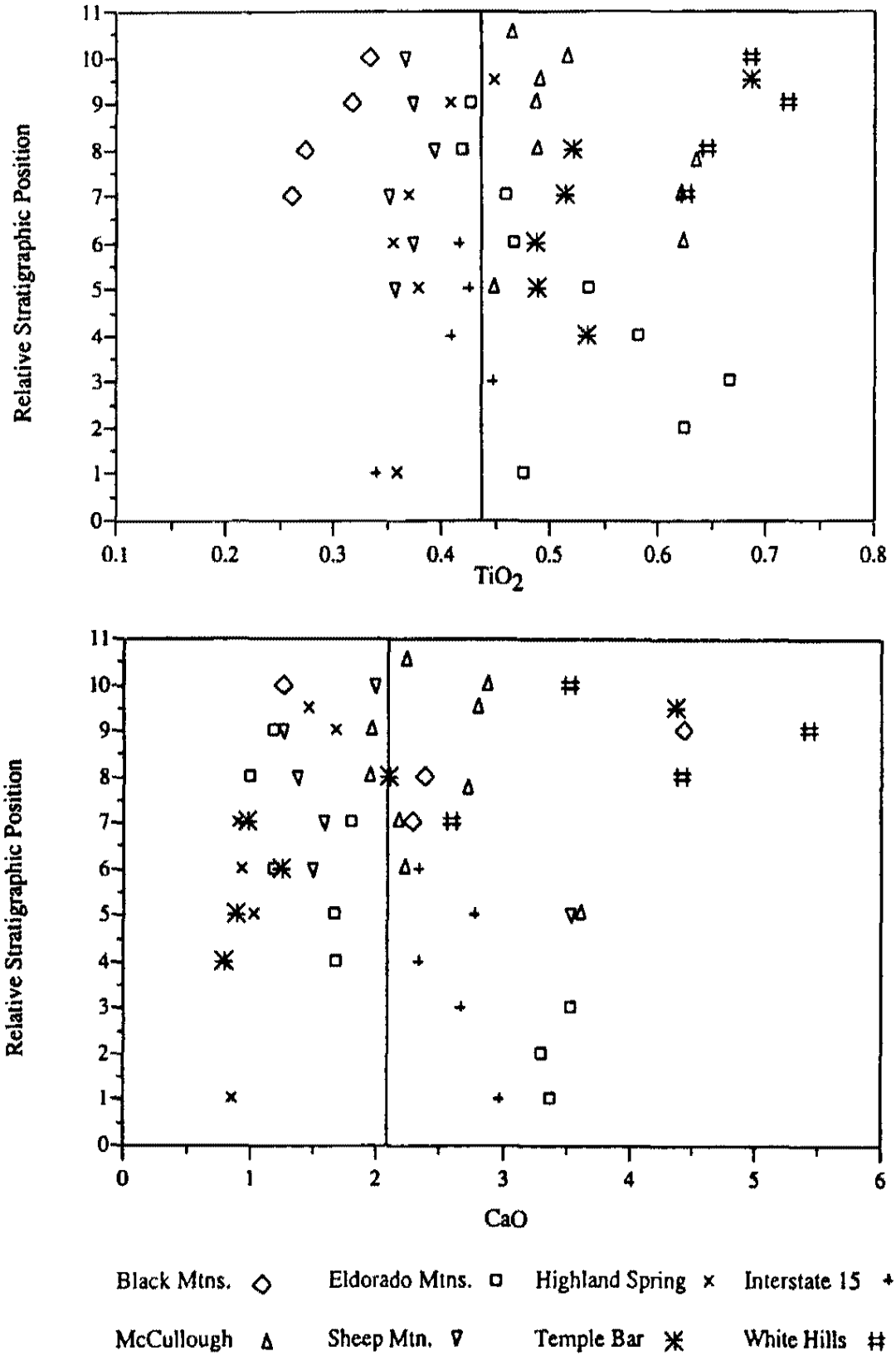

Figure 9, continued.

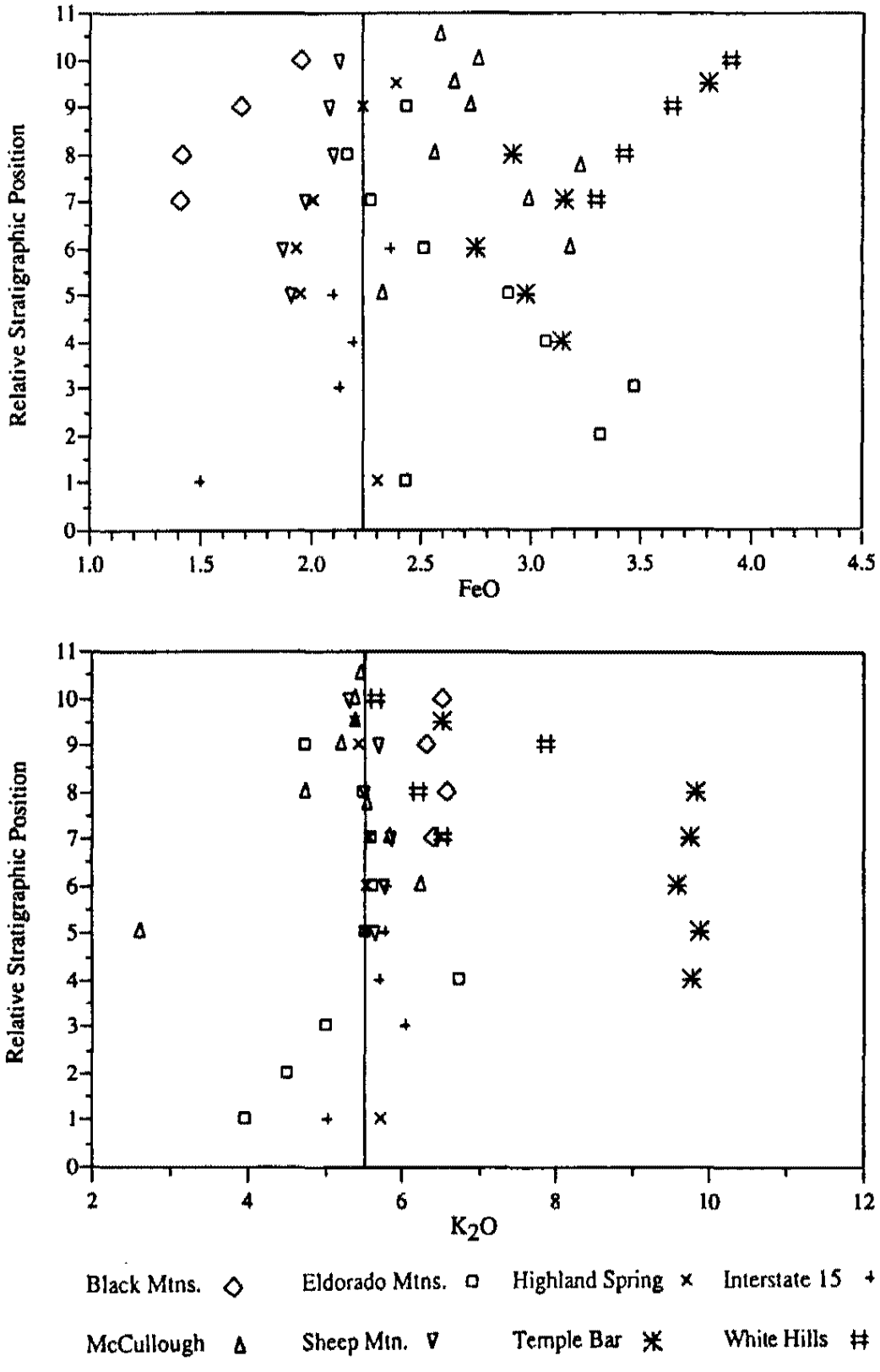

Figure 9, continued.

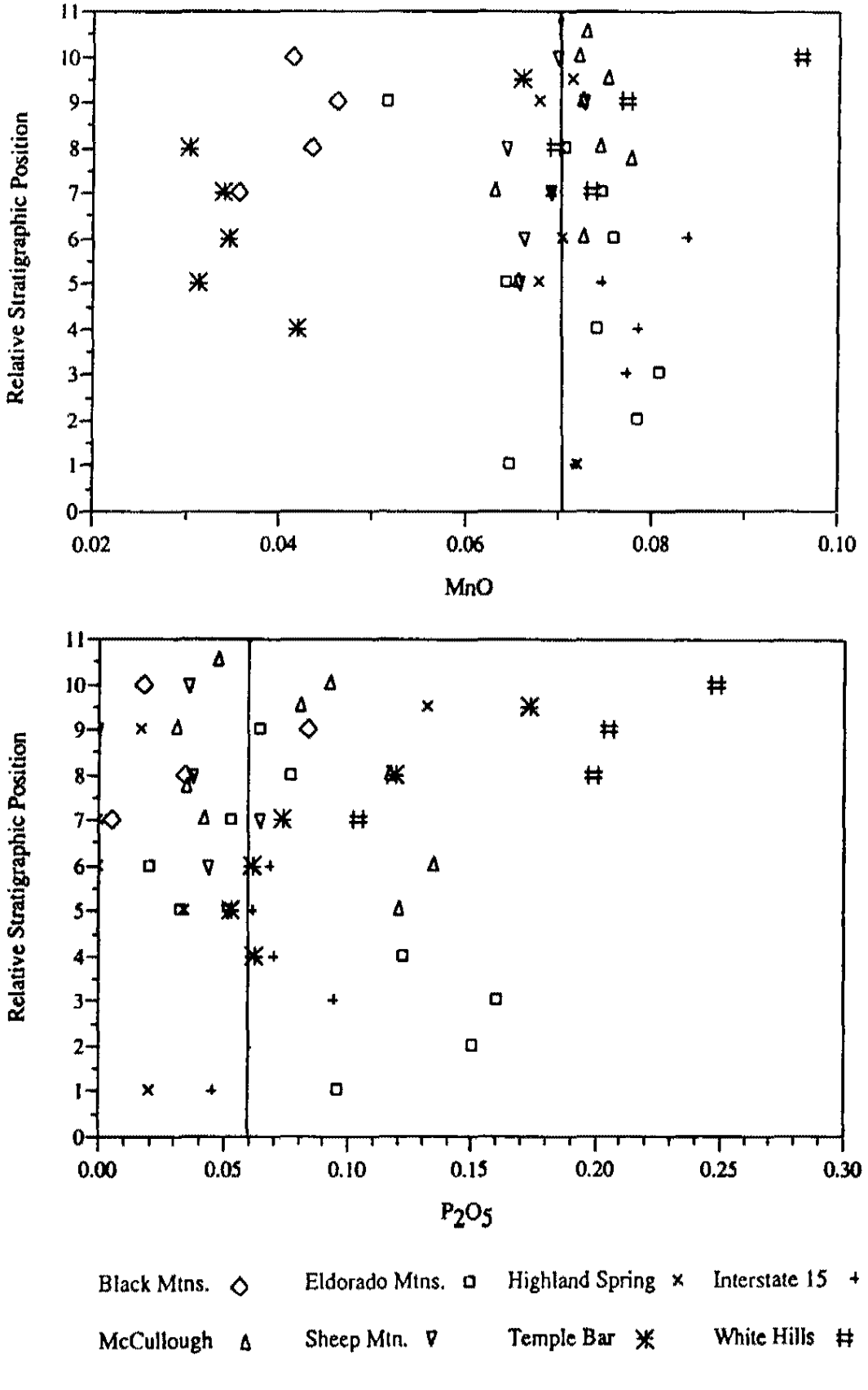

Figure 9, continued.

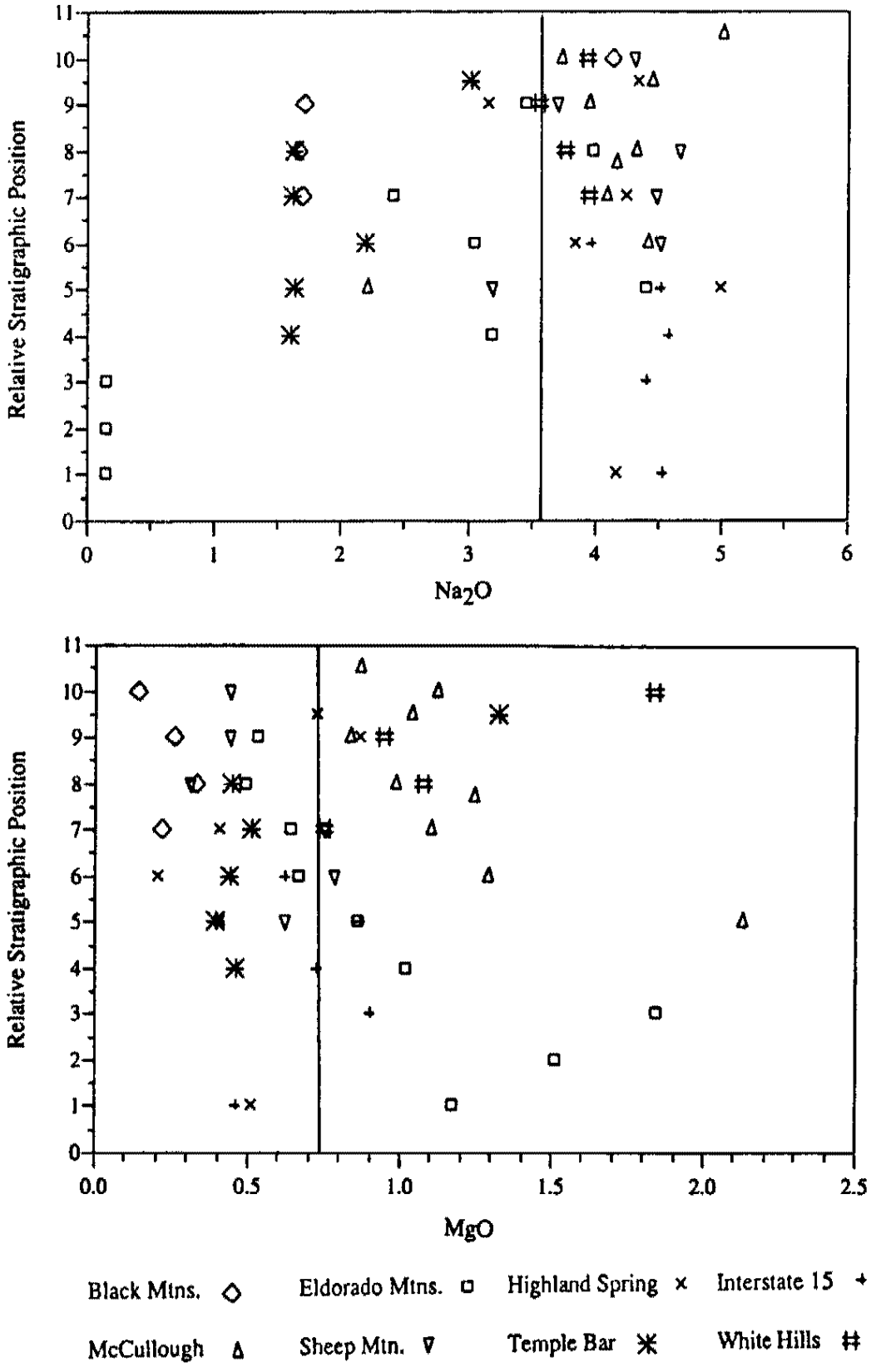

Figure 9, continued.

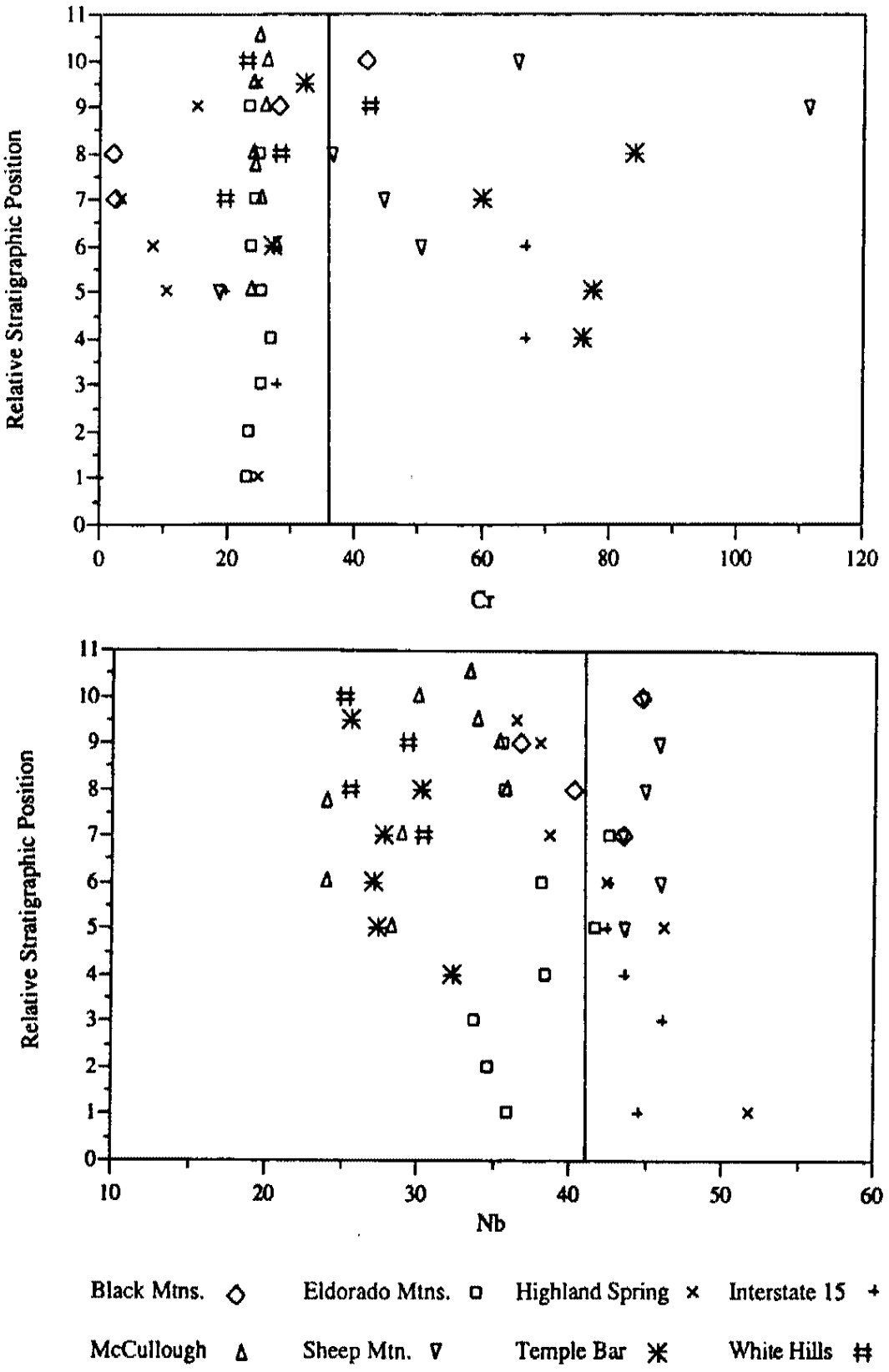

Figure 9, continued.

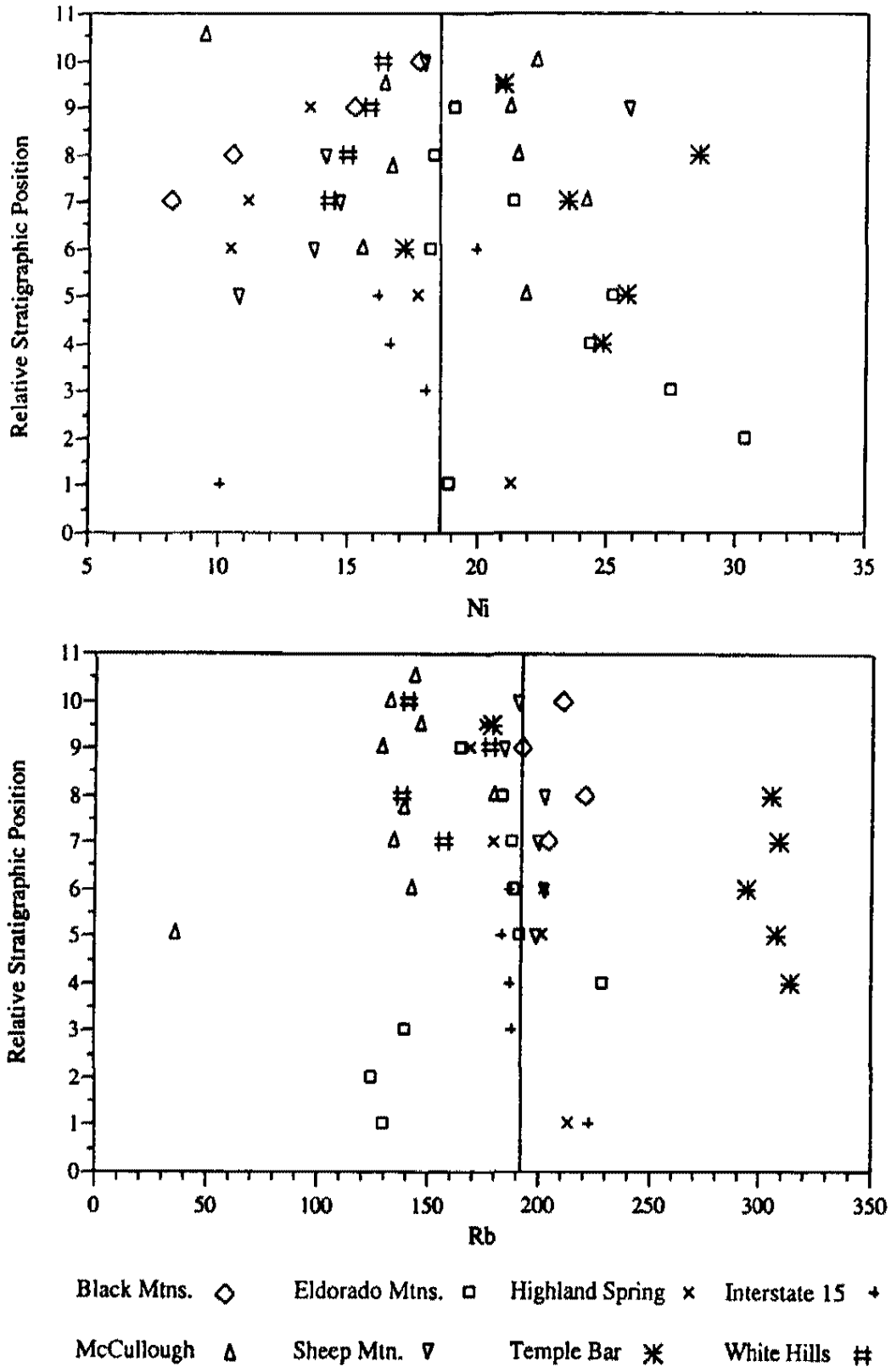

Figure 9, continued.

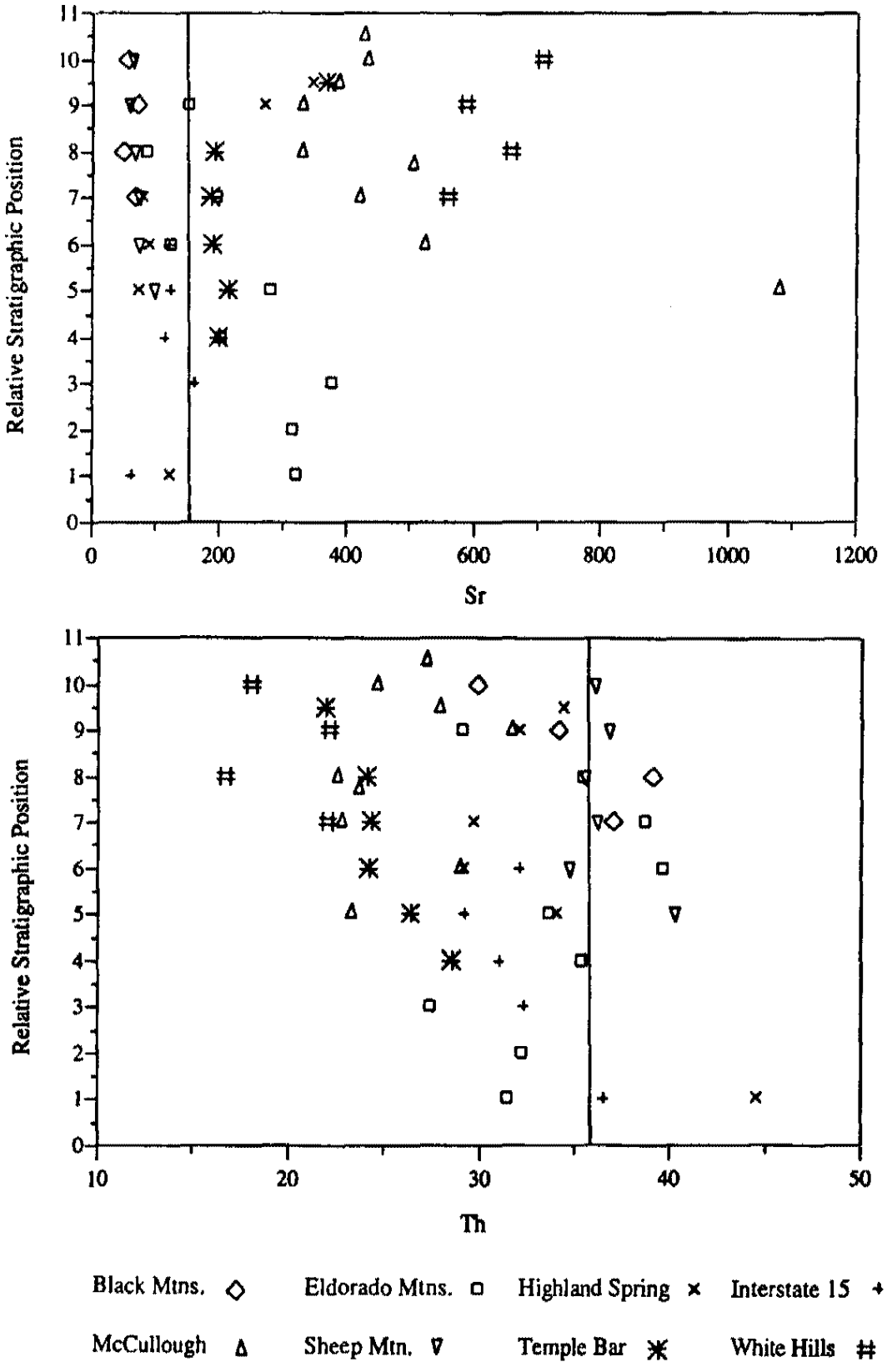

Figure 9, continued.

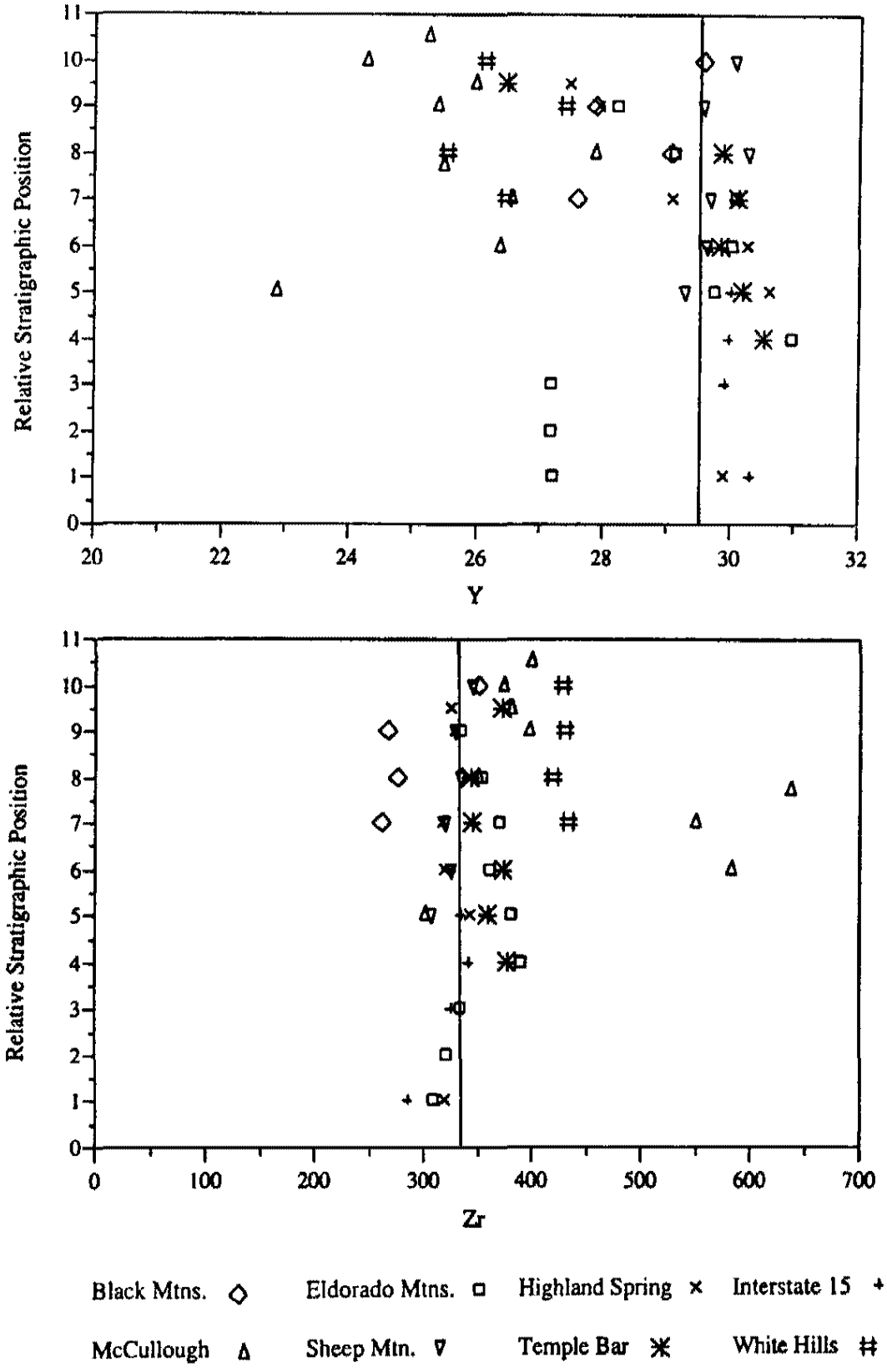

Figure 9, continued.

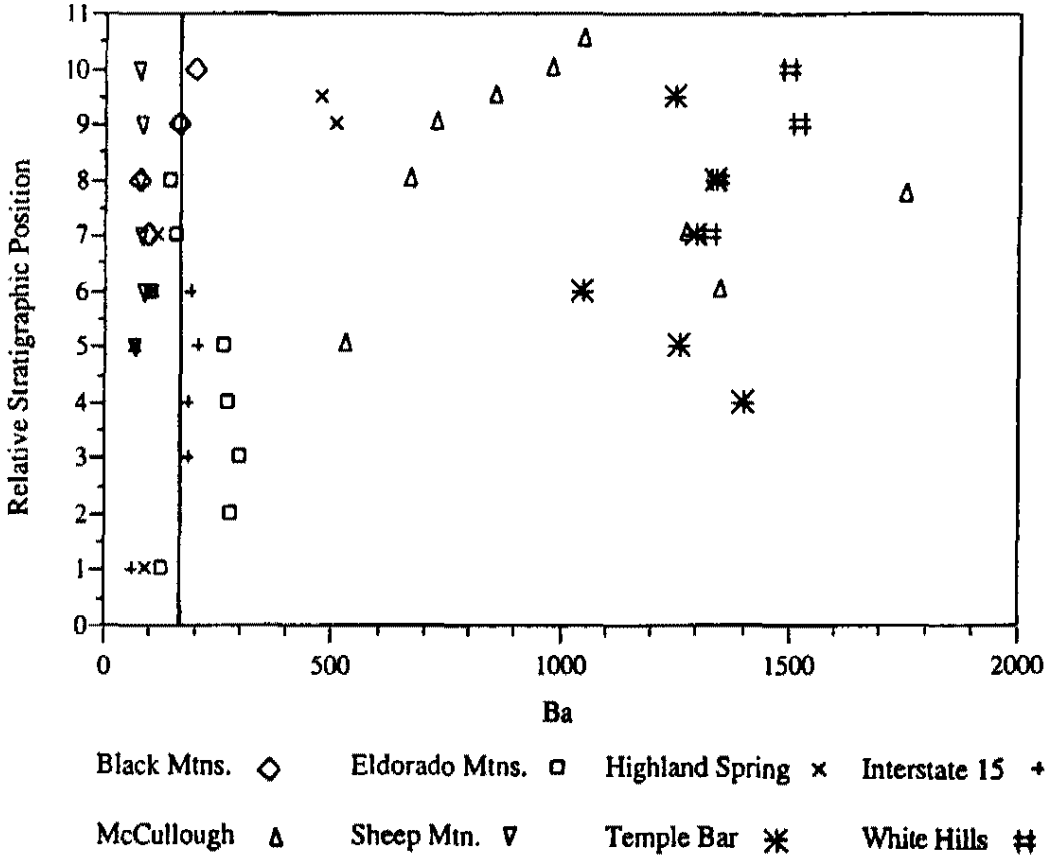

Figure 9, continued.

Table 5: Major and Trace Element Variation. Deviation is based on comparison of averaged section value to the base composition of each element. Base compositions are calculated by averaging analyses from Highland Spring, Eldorado Mtns., Sheep Mtn., and Interstate 15 sections. Major element oxides in wt.% and trace elements in ppm.

Section	Black Mountains					Dolan Springs				
	Minimum	Maximum	Range	Average	Deviation	Minimum	Maximum	Range	Average	Deviation
SiO2	71.08	74.91	3.83	72.995	2.28	73.69	75.59	1.90	74.64	3.92
Al2O3	14.00	12.76	1.24	13.38	-1.21	12.60	13.06	0.46	12.83	-1.76
TiO2	0.26	0.34	0.08	0.3	-0.13	0.28	0.24	0.04	0.26	-0.17
FeO	1.95	1.41	0.54	1.68	-0.55	1.22	1.66	0.44	1.44	-0.79
CaO	1.26	4.45	3.19	2.855	0.71	2.57	1.08	1.49	1.825	-0.32
K2O	6.34	6.60	0.26	6.47	0.95	4.65	5.43	0.78	5.04	-0.48
MnO	0.04	0.05	0.01	0.045	-0.02	0.04	0.06	0.02	0.05	-0.02
P2O5	0.00	0.08	0.08	0.04	-0.02	0.07	0.12	0.05	0.095	0.03
Na2O	1.66	4.15	2.49	2.905	-0.74	2.89	3.26	0.37	3.075	-0.57
MgO	0.14	0.33	0.19	0.235	-0.50	0.48	0.77	0.29	0.625	-0.11
Cr	2.2	41.9	39.7	22.05	-14.81	25.8	47.3	21.5	36.55	-0.31
Nb	36.7	44.6	7.9	40.65	-2.20	17.1	18.7	1.6	17.9	-24.95
Ni	8.2	17.7	9.5	12.95	-25.93	10.4	16.7	6.3	13.55	-25.33
Rb	193	221	28	207	15.75	108	143	35	125.5	-65.75
Sr	49	71	22	60	-98.88	125	196	71	160.5	1.63
Th	29.6	39.2	9.6	34.4	-0.82	13.2	15.9	2.7	14.55	-20.67
Y	27.6	29.6	2.0	28.6	-0.89	20.6	22.1	1.5	21.35	-8.14
Zr	261	350	89	305.5	-24.63	101	121	20	111	-219.13
Ba	75	205	130	140	-36.75	240	356	116	298	121.25

Table 5, continued.

Section	Eldorado Mountains					Highland Spring				
	Minimum	Maximum	Range	Average	Deviation	Minimum	Maximum	Range	Average	Deviation
SiO2	68.10	73.82	5.72	70.96	0.24	70.19	72.07	1.88	71.13	0.41
Al2O3	13.26	15.69	2.43	14.475	-0.11	14.74	15.06	0.32	14.9	0.31
TiO2	0.42	0.67	0.25	0.545	0.12	0.36	0.45	0.09	0.405	-0.03
FeO	2.16	3.47	1.31	2.815	0.59	1.93	2.39	0.46	2.16	-0.07
CaO	1.00	3.54	2.54	2.27	0.12	0.86	1.68	0.82	1.27	-0.88
K2O	3.98	6.76	2.78	5.37	-0.15	5.40	5.74	0.34	5.57	0.05
MnO	0.05	0.08	0.03	0.065	-0.00	0.07	0.07	0.00	0.07	0.00
P2O5	0.02	0.16	0.14	0.09	0.03	0.00	0.13	0.13	0.065	0.00
Na2O	0.16	4.41	4.25	2.285	-1.36	3.16	5.00	1.84	4.08	0.44
MgO	0.50	1.84	1.34	1.17	0.44	0.21	0.87	0.66	0.54	-0.19
										0.00
Cr	23.1	26.8	3.7	24.95	-11.91	3.3	25.0	21.7	14.15	-22.71
Nb	33.8	42.6	8.8	38.2	-4.65	36.5	51.9	15.4	44.2	1.35
Ni	18.2	30.4	12.2	24.3	5.90	10.5	21.4	10.9	15.95	-2.45
Rb	124	230	106	177	-14.25	169	213	44	191	-0.25
Sr	87	379	292	233	74.13	74	345	271	209.5	50.63
Th	27.4	39.7	12.3	33.55	-1.67	29.2	44.6	15.4	36.9	1.68
Y	27.2	31.0	3.8	29.1	-0.39	27.5	30.6	3.1	29.05	-0.44
Zr	309	390	81	349.5	19.38	319	344	25	331.5	1.38
Ba	106	300	194	203	26.25	69	511	442	290	113.25

Table 5, continued.

Section	Interstate-15					Lucy Gray Range				
	Minimum	Maximum	Range	Average	Deviation	Minimum	Maximum	Range	Average	Deviation
SiO2	68.66	71.00	2.34	69.83	-0.89	72.88	72.42	0.46	72.65	1.93
Al2O3	14.05	14.72	0.67	14.385	-0.20	14.21	14.31	0.10	14.26	-0.33
TiO2	0.34	0.45	0.11	0.395	-0.04	0.28	0.30	0.02	0.29	-0.14
FeO	1.50	2.37	0.87	1.935	-0.29	1.75	1.79	0.04	1.77	-0.46
CaO	2.33	2.97	0.64	2.65	0.50	0.71	0.87	0.16	0.79	-1.36
K2O	5.03	6.04	1.01	5.535	0.01	5.30	5.90	0.60	5.6	0.08
MnO	0.07	0.08	0.01	0.075	0.01	0.06	0.06	0.00	0.06	-0.01
P2O5	0.04	0.09	0.05	0.065	0.00	0.05	0.05	0.00	0.05	-0.01
Na2O	3.97	4.58	0.61	4.275	0.63	4.11	4.38	0.27	4.245	0.60
MgO	0.46	0.90	0.44	0.68	-0.05	0.21	0.34	0.13	0.275	-0.46
Cr	19.5	66.9	47.4	43.2	6.34	23.9	24.2	0.3	24.05	-12.81
Nb	42.5	46.1	3.6	44.3	1.45	30.6	32.1	1.5	31.35	-11.50
Ni	10.1	19.9	9.8	15	-23.88	19.1	19.8	0.7	19.45	-19.43
Rb	184	223	39	203.5	12.25	190	214	24	202	10.75
Sr	62	163	101	112.5	-46.38	35	43	8	39	-119.88
Th	29.2	36.6	7.4	32.9	-2.32	24.6	25.0	0.4	24.8	-10.42
Y	29.7	30.3	0.6	30	0.51	30.4	30.8	0.4	30.6	1.11
Zr	285	342	57	313.5	-16.63	258	261	3	259.5	-70.63
Ba	63	207	144	135	-41.75	28	102	74	65	-111.75

Table 5, continued.

Section	McCullough Range					Sheep Mountain				
	Minimum	Maximum	Range	Average	Deviation	Minimum	Maximum	Range	Average	Deviation
SiO2	65.05	73.65	8.60	69.35	-1.37	70.20	71.69	1.49	70.945	0.23
Al2O3	12.80	16.92	4.12	14.86	0.27	14.40	14.78	0.38	14.59	0.00
TiO2	0.45	0.64	0.19	0.545	0.12	0.35	0.40	0.05	0.375	-0.06
FeO	2.32	3.22	0.90	2.77	0.54	1.87	2.13	0.26	2	-0.23
CaO	1.95	3.62	1.67	2.785	0.64	1.26	3.54	2.28	2.4	0.25
K2O	2.62	6.26	3.64	4.44	-1.08	5.33	5.88	0.55	5.605	0.08
MnO	0.06	0.08	0.02	0.0715	0.00	0.06	0.07	0.01	0.065	-0.00
P2O5	0.03	0.14	0.11	0.0855	0.02	0.00	0.06	0.06	0.03	-0.03
Na2O	2.22	5.02	2.80	3.62	-0.02	3.19	4.68	1.49	3.935	0.29
MgO	0.84	2.13	1.29	1.485	0.75	0.31	0.78	0.47	0.545	-0.19
Cr	23.7	27.8	4.1	25.75	-11.11	18.7	111.6	92.9	65.15	28.29
Nb	24.0	35.8	11.8	29.9	-12.95	43.4	46.0	2.6	44.7	1.85
Ni	9.4	24.3	14.9	16.85	-22.03	10.8	25.9	15.1	18.35	-20.53
Rb	36	180	144	108	-83.25	184	203	19	193.5	2.25
Sr	330	1083	753	706.5	547.63	61	100	39	80.5	-78.38
Th	22.5	31.7	9.2	27.1	-8.12	34.8	40.3	5.5	37.55	2.33
Y	22.8	27.9	5.1	25.35	-4.14	29.3	30.3	1.0	29.8	0.31
Zr	301	638	337	469.5	139.38	306	346	40	326	-4.13
Ba	530	1753	1223	1141.5	964.75	69	89	20	79	-97.75

Table 5, continued.

Section	Salt Spring Wash					Temple Bar				
	Minimum	Maximum	Range	Average	Deviation	Minimum	Maximum	Range	Average	Deviation
SiO2	70.08	73.88	3.80	71.98	1.26	64.60	68.44	3.84	66.52	-4.20
Al2O3	11.58	15.15	3.57	13.365	-1.22	14.77	15.94	1.17	15.355	0.77
TiO2	0.37	0.50	0.13	0.435	0.00	0.49	0.69	0.20	0.59	0.16
FeO	2.12	2.66	0.54	2.39	0.16	2.75	3.81	1.06	3.28	1.05
CaO	0.50	2.99	2.49	1.745	-0.40	0.80	4.38	3.58	2.59	0.44
K2O	6.51	9.01	2.50	7.76	2.24	6.54	9.88	3.34	8.21	2.69
MnO	0.03	0.04	0.01	0.035	-0.03	0.03	0.07	0.04	0.05	-0.02
P2O5	0.02	0.11	0.09	0.065	0.00	0.05	0.17	0.12	0.11	0.05
Na2O	1.63	1.65	0.02	1.64	-2.00	1.61	3.02	1.41	2.315	-1.33
MgO	0.40	0.76	0.36	0.58	-0.15	0.40	1.33	0.93	0.865	0.13
Cr	13.5	23.0	9.5	18.25	-18.61	27.1	84.0	56.9	55.55	18.69
Nb	23.5	32.2	8.7	27.85	-15.00	25.6	32.3	6.7	28.95	-13.90
Ni	12.9	14.2	1.3	13.55	-25.33	17.2	28.6	11.4	22.9	-15.98
Rb	130	196	66	163	-28.25	179	314	135	246.5	55.25
Sr	56	112	56	84	-74.88	186	368	182	277	118.13
Th	18.1	23.8	5.7	20.95	-14.27	21.9	28.6	6.7	25.25	-9.97
Y	23.2	27.6	4.4	25.4	-4.09	26.5	30.5	4.0	28.5	-0.99
Zr	226	340	114	283	-47.13	344	378	34	361	30.88
Ba	388	392	4	390	213.25	1048	1400	352	1224	1047.25

Table 5, continued.

Section	White Hills					
	Minimum	Maximum	Range	Average	Deviation	Base Composition
SiO2	59.50	65.26	5.76	62.38	-8.34	70.72
Al2O3	16.22	18.00	1.78	17.11	2.52	14.59
TiO2	0.63	0.72	0.09	0.675	0.25	0.43
FeO	3.30	3.91	0.61	3.605	1.38	2.23
CaO	2.61	5.44	2.83	4.025	1.88	2.15
K2O	5.70	7.90	2.20	6.8	1.28	5.52
MnO	0.07	0.10	0.03	0.085	0.02	0.07
P2O5	0.10	0.25	0.15	0.177	0.11	0.06
Na2O	3.56	3.96	0.40	3.76	0.12	3.64
MgO	0.76	1.84	1.08	1.3	0.57	0.73
Cr	19.5	42.5	23.0	31	-5.86	36.86
Nb	25.2	30.4	5.2	27.8	-15.05	42.85
Ni	14.2	16.3	2.1	15.25	-3.15	18.40
Rb	138	178	40	158	-33.25	191.25
Sr	560	712	152	636	477.13	158.88
Th	16.7	22.2	5.5	19.45	-15.77	35.23
Y	25.5	27.4	1.9	26.45	-3.04	29.49
Zr	419	434	15	426.5	96.38	330.13
Ba	1330	1524	194	1427	1250.25	176.75

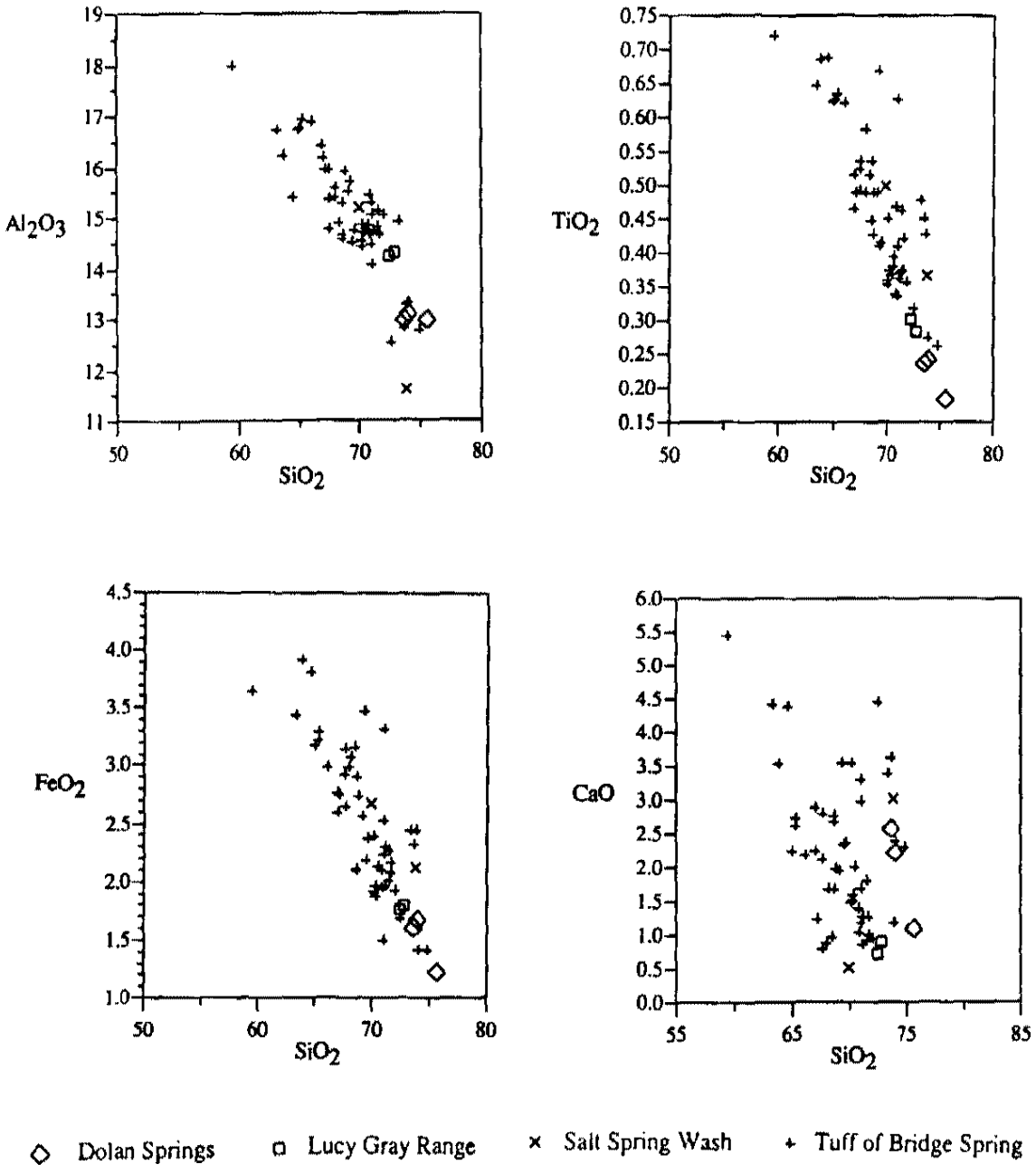

Figure 10. Harker variation plots of Tuff of Bridge Spring sections and three non-correlative tuffs: major element oxides and trace elements vs. SiO_2.

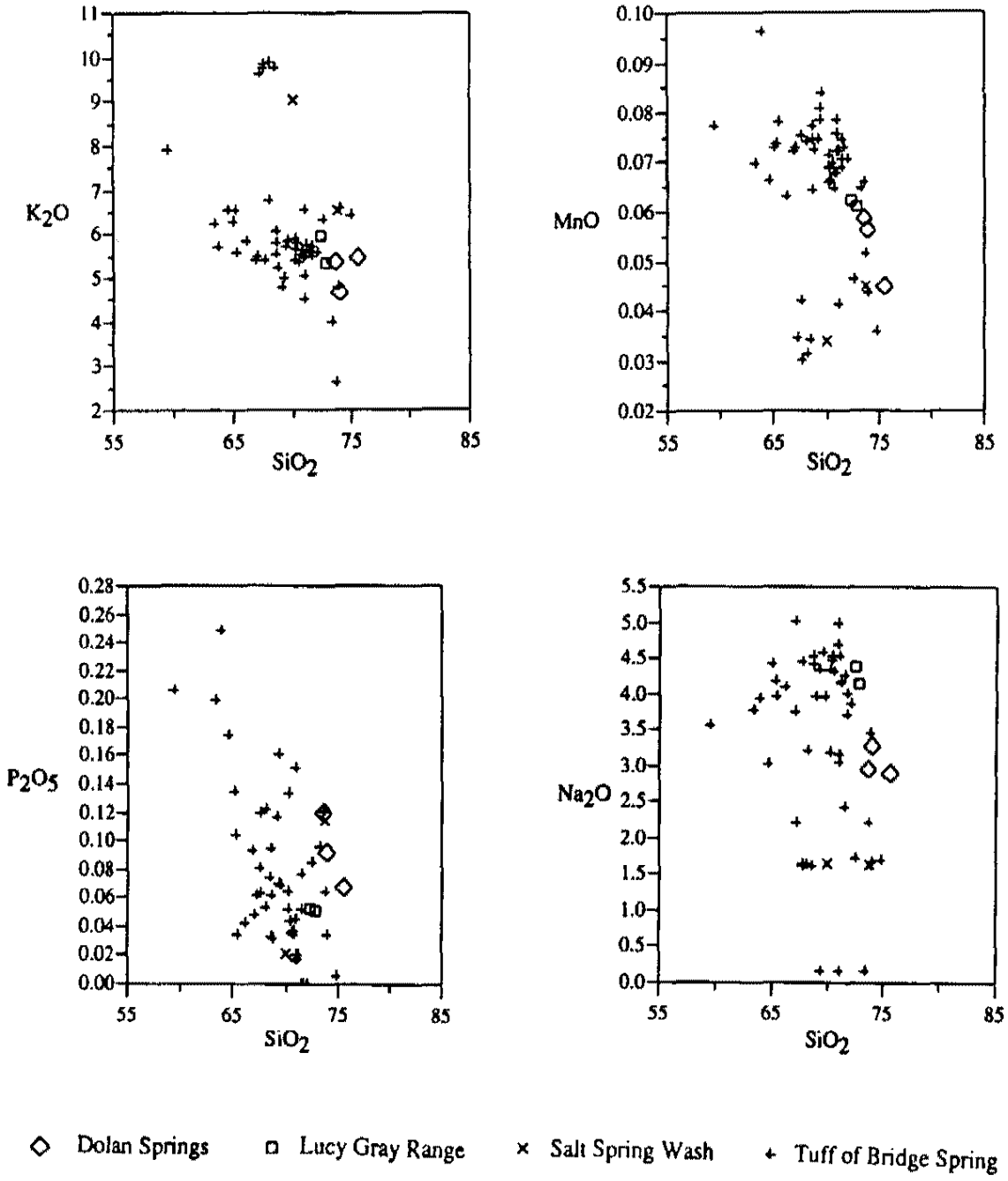

Figure 10, continued.

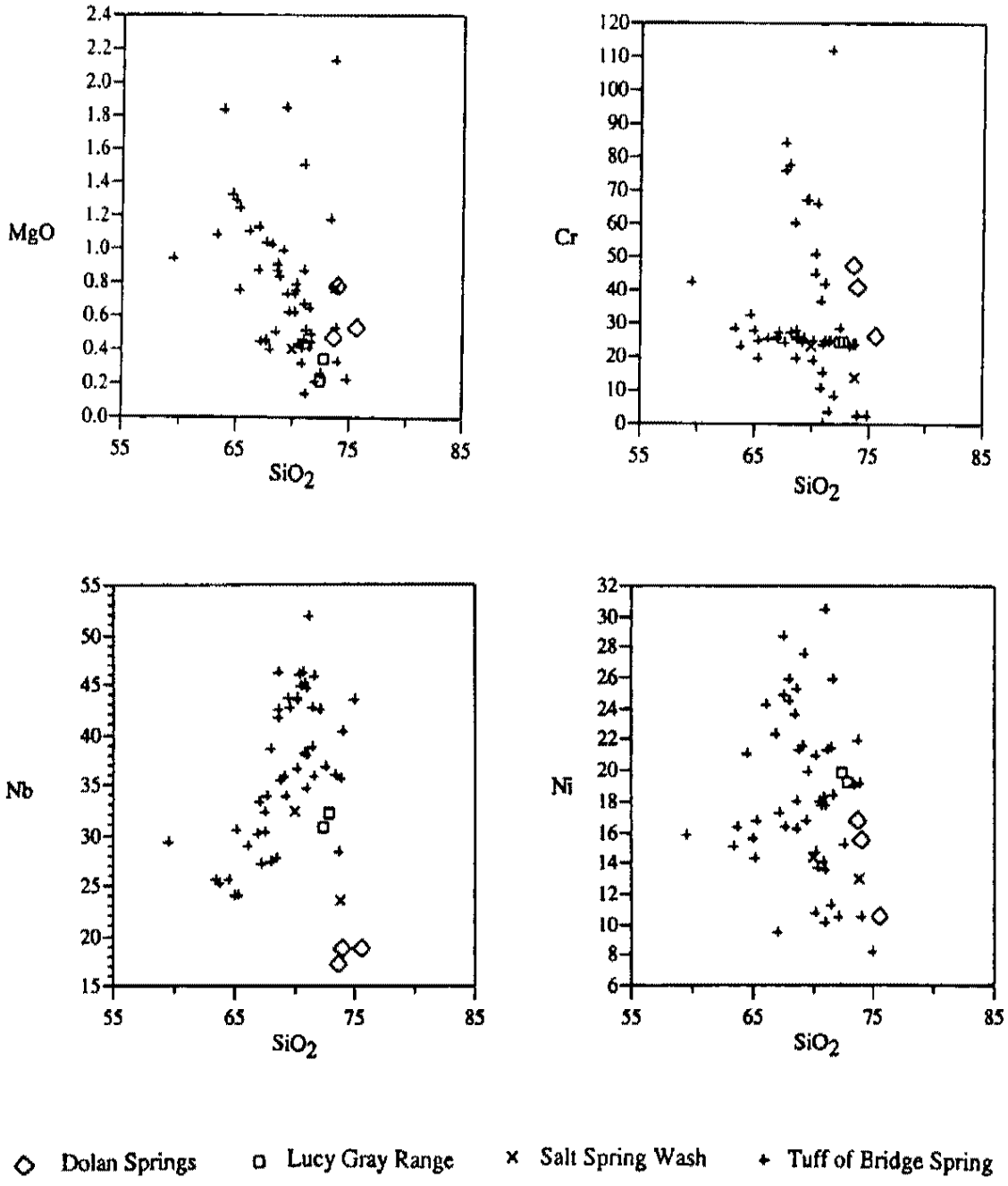

Figure 10, continued.

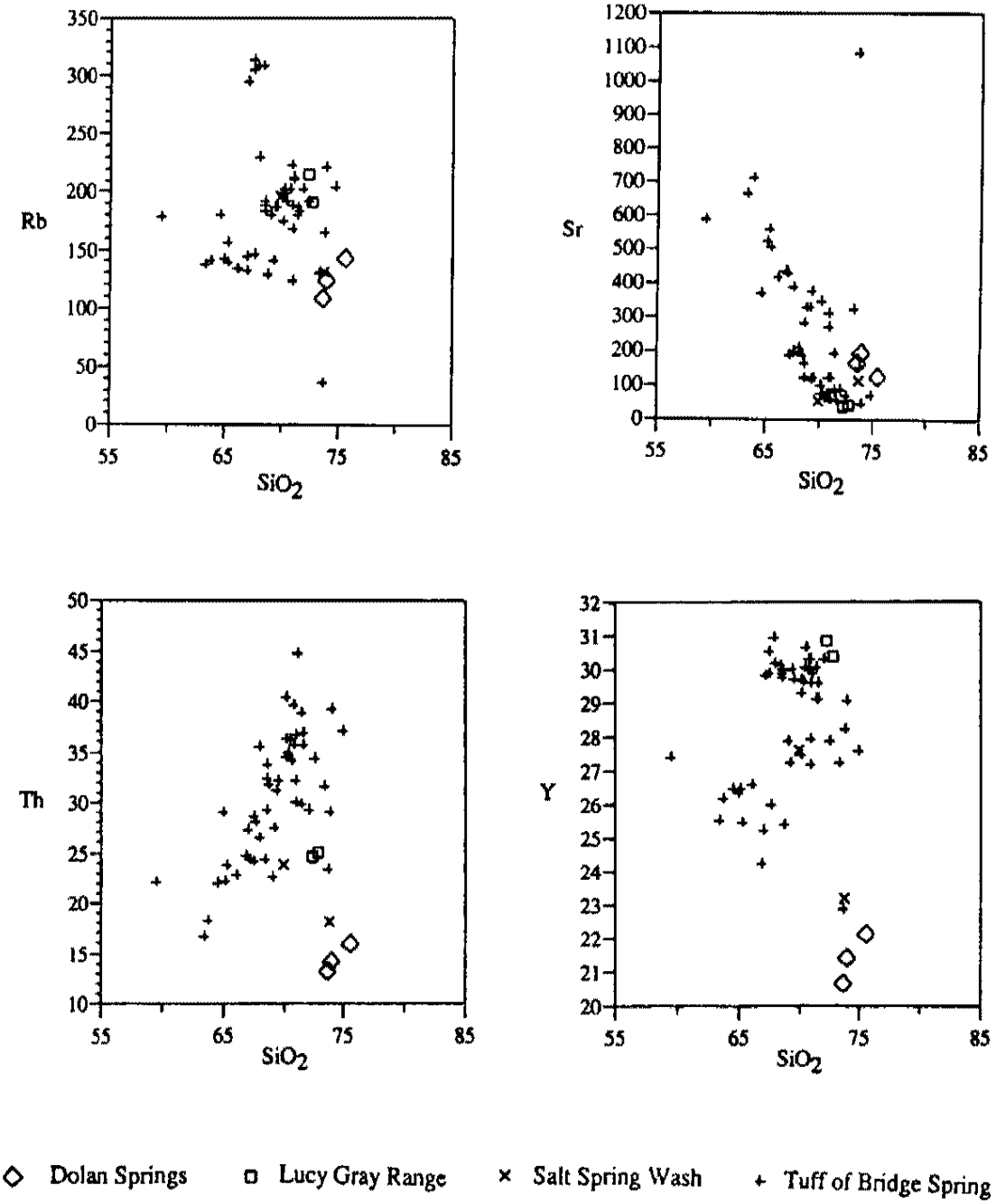

Figure 10, continued.

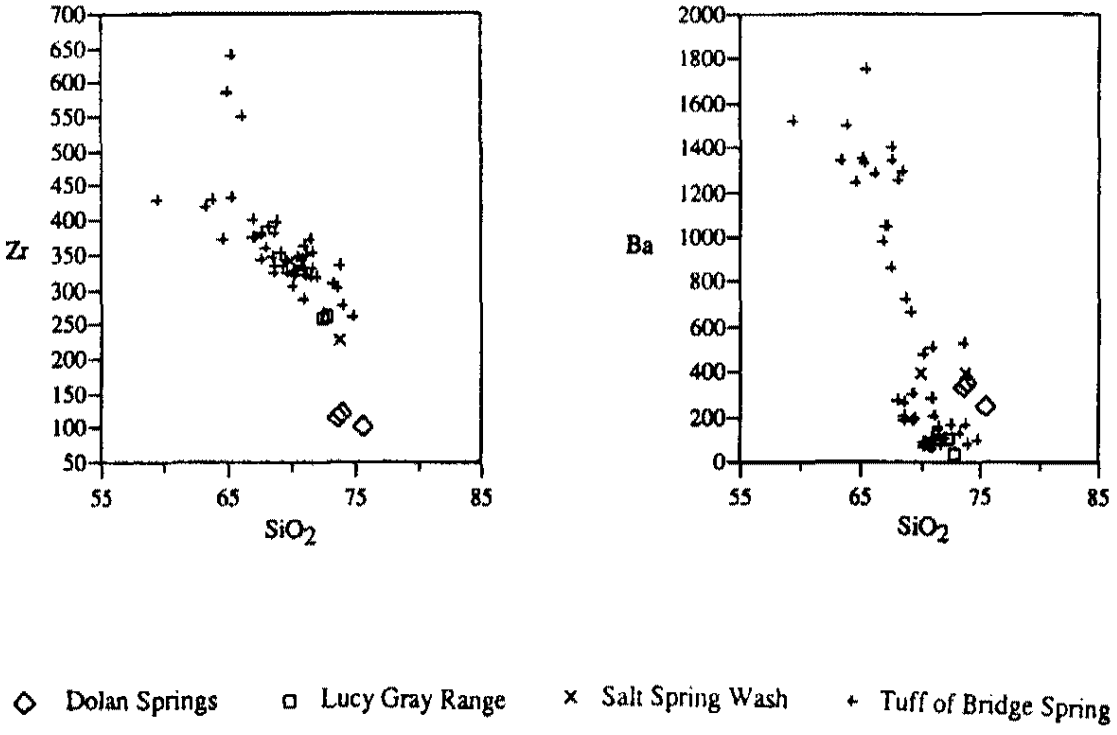

Figure 10, continued.

Regional Correlation

Isotopic Correlation of the Tuff of Bridge Spring

Previous regional correlations of the Tuff of Bridge Spring were based upon its modal mineralogy, distinctive lithology, and relative position in the Miocene volcanic section (Anderson, 1971; Anderson et al., 1972; Davis, 1985; Schmidt, 1987; Faulds, 1989; Bridwell, 1991; Cascadden, 1991). In this study, identification and correlation of the Tuff of Bridge Spring was established by determining its isotopic signature. Isotopic ratios are not altered by magmatic, eruptive, or weathering processes and consequently can be used as sensitive indicators to discriminate cogenetic magmatic suites. For this reason, isotopic ratios of H, O, Ar, Sr, Nd, and Pb are commonly used to correlate ash-flow tuffs (Hildreth and Mahood, 1985).

Eleven locations in the northern Colorado River extensional corridor in which the Tuff of Bridge Spring is either known or suspected to crop out were sampled and analyzed for Nd, Sr, and Pb isotopes (Fig. 6; Table 6). A plot of ε_{Nd} vs. $^{87}Sr/^{86}Sr$ for the Tuff of Bridge Spring (Fig. 11) shows that the majority of samples define a linear trend that varies from $^{87}Sr/^{86}Sr = 0.708653$ to 0.71036 and $\varepsilon_{Nd} = -8.070$ to -10.070.

Because cogenetic isotopic suites characteristically plot in tight clusters on ε_{Nd} vs. $^{87}Sr/^{86}Sr$ diagrams, the presence of a linear array suggests that the magmatic system evolved either as the result of open system magmatic processes, or developed under closed system conditions but was subsequently contaminated with isotopically-exotic xenoliths and/or xenocrysts. As will be discussed below, the linear isotopic array shown in Fig. 11 is interpreted to represent a cogenetic sequence that formed as the result of open system magmatic processes, and stratigraphic sections that preserve these isotopic values are interpreted to comprise the Tuff of Bridge Spring. These

sections include the McCullough Range, Eldorado Mountains, Highland Spring Range, and Sheep Mountain in Nevada, and the White Hills, Temple Bar, and Black Mountains in Arizona Also, for reasons discussed below, the Interstate 15, Nevada section will also be correlated with the Tuff of Bridge Spring.

It is important to note that correlation of sections to the Tuff of Bridge Spring cannot be established by isotopic signature alone, but must be confirmed by additional criteria such as geochemistry, mineralogy, lithology, and avaliable geochronology. Isotope-based correlations of the sections listed above to the Tuff of Bridge Spring are strongly supported by geochemical studies (see discussion of internal stratigraphy) which indicate the presence of distinct geochemical trends in the Tuff of Bridge Spring which can be correlated across its entire area of distribution.

There are, however, two examples of isotope-based correlations in which isotopic signatures are contradicted by other correlation criteria. In the first example, the isotope values of the Interstate 15 sample suggest it is not correlative to the Tuff of Bridge Spring, but the phenocryst mineralogy, lithology, and geochemistry of the section strongly suggest it is correlative to the Tuff of Bridge Spring (see discussion below). In the second example, the isotopic signature of the Dolan Springs section falls within the Tuff of Bridge Spring isotope array, but $^{40}Ar/^{39}Ar$ dating (see following discussion of other ash-flow tuffs) shows that the tuff is significantly older than the Tuff of Bridge Spring. In addition, it has a different phenocryst mineralogy.

In summary, based on evidence provided by non-isotopic correlation criteria, and contrary to isotopic evidence, the Interstate 15 section will be included in the Tuff of Bridge Spring. Using the same criteria, the tuff of Dolan Springs will be excluded from the Tuff of Bridge Spring.

Interstate 15

The Interstate 15 tuff plots outside of the Tuff of Bridge Spring isotopic array on ε_{Nd} vs. $^{87}Sr/^{86}Sr$ and $^{87}Sr/^{86}Sr$ vs. SiO_2 plots (Fig. 11 and Fig. 12, respectively) which indicates it is not cogenetic with the Tuff of Bridge Spring. However, the mineralogy, geochemistry and lithology of this section is similar to that of the Sheep Mountain section whose isotopic signature falls within the Tuff of Bridge Spring isotopic array (Fig. 11).

There are three possible explanations for the contradictions of the isotope and secondary correlation criteria data of the Interstate 15 section. First, the isotope analysis of the basal interval of Interstate 15 is spurious. Second, the basal interval of Interstate 15 is a locally-derived flow that is isotopically unrelated to the Tuff of Bridge Spring, but the unsampled interval of welded tuff overlying it is the Tuff of Bridge Spring. Third, the Interstate 15 section is entirely of local derivation (i.e., not correlative to the Tuff of Bridge Spring as indicated by the isotope analysis).

Re-analysis of the Interstate 15 basal pumiceous tuff and analysis of a densely-welded, uppermost interval from the Interstate 15 section will be conducted to determine the isotopic affinities of these units. Until these analyses are completed, the Interstate 15 section will be tentatively correlated with the Tuff of Bridge Spring.

Other Ash-flow Tuffs

Salt Spring Wash and Lucy Gray Range

The ε_{Nd} vs. $^{87}Sr/^{86}Sr$ plot (Fig. 11) of the Lucy Gray Range tuff implies it may be a felsic endmember to the Tuff of Bridge Spring mixing array, but this is contradicted by $^{87}Sr/^{86}Sr$ vs. SiO_2 plots (Fig. 12) which show that the Lucy Gray Range tuff plots away from the Tuff of Bridge Spring isotopic trend. The Salt Spring Wash isotope sample plots away from the Tuff of Bridge Spring array on both ε_{Nd} vs. $^{87}Sr/^{86}Sr$ and $^{87}Sr/^{86}Sr$ vs. SiO_2 diagrams (Figs. 11 and 12). Isotope plots indicate that both the Salt Spring Wash and Lucy Gray Range tuffs were derived from sources that are not cogenetic with the Tuff of Bridge Spring. This conclusion is supported by modeling of possible contaminants (see discussion of lithic contaminants below) which indicate these tuffs are not Tuff of Bridge Spring samples that have acquired hybridized isotopic signatures as the result of xenolith contamination.

Dolan Springs

Isotope-based correlation of the Dolan Springs volcanic complex to the Tuff of Bridge Spring is contradicted by an $^{40}Ar/^{39}Ar$ date of 16.09 ± 0.15 Ma (incremental release, biotite; this study) (Fig. 13). This date falls outside the uncertainty of the 15.23 ± 0.14 Ma date by Bridwell (1991) for the McCullough Range Tuff of Bridge Spring, and effectively eliminates the possibility that the Dolan Springs section is cogenetic with the Tuff of Bridge Spring. The exclusion of this section from the Tuff of Bridge Spring is also supported by significant differences of geochemistry and modal

mineralogy. The tuff of Dolan Springs, unlike the Tuff of Bridge Spring, contains abundant quartz phenocrysts.

Even though the tuff of Dolan Springs does not correlate with the Tuff of Bridge Spring, it is still of interest to this study. The similarity of isotopic compositions of the tuff of Dolan Springs and the Tuff of Bridge Springs suggests that the source of the tuff of Dolan Springs is isotopically similar to the Tuff of Bridge Spring. If the Tuff of Bridge Spring correlates with the Aztec Wash pluton in Nevada, this suggests that the source of the tuff of Dolan Springs and the Aztec Wash pluton were both derived from a regionally-extensive/isotopically similar crustal/mantle source. A date of 16.09 Ma for the Dolan Springs section also implies correlation with the 15.96 ± 0.04 Ma Mt. Perkins pluton (laser fusion $^{40}Ar/^{39}Ar$, sanidine) (Faulds, personal communication to E.I. Smith, 1993) (see later discussion of source).

Origin of the Tuff of Bridge Spring Data Array

Because rocks produced by closed system magma processes characteristically plot in tight clusters on ε_{Nd} vs. $^{87}Sr/^{86}Sr$ diagrams, the linearity of the Tuff of Bridge Spring data array indicates that the Tuff of Bridge Spring magma chamber evolved under open system conditions (see discussion of mixing trend below). Isotopic variablity in the Tuff of Bridge Spring occurs not only on the regional scale (i.e., between different sections widely separated across the distribution area of the tuff), but also within individual sections (e.g., Sheep Mountain and Eldorado Mountain sections) (Table 6).

Variablity of Nd/Sr, $^{87}Sr/^{86}Sr$, and SiO_2 values of the Tuff of Bridge Spring (Fig. 11 and Fig.12) may result from either the incomplete mixing of an isotopically-homogeneous, compositionally-zoned felsic magma body with a volumetrically smaller,

end member fraction of isotopically-dissimilar mafic magma, or the incorporation of xenoliths and/or xenocrysts during eruption and deposition of an isotopically homogeneous ash-flow tuff. The following discussion eliminates lithic contamination as a possible mechanism for variablity of isotopes in the Tuff of Bridge Spring, and suggests that the process of magma-mixing produced the linear Tuff of Bridge Spring isotopic array. The following discussion also demonstrates that the isotopic signatures of the Salt Spring Wash and Lucy Gray Range tuffs were not produced by contamination of Tuff of Bridge Spring with mafic and/or felsic lithic fragments.

Lithic Contamination

Possible sources of lithic contamination of the Tuff of Bridge Spring include Patsy Mine Volcanics, Precambrian crystalline basement, and alkali-olivine basalts that were derived from the melting of asthenospheric mantle.

Patsy Mine Volcanics

Xenoliths in the Tuff of Bridge Spring are predominantly mafic in composition (basaltic to basaltic andesite) and contain plagioclase, clinopyroxene, and Fe-oxide phenocrysts. A possible source of these xenoliths is the upper member of the Patsy Mine Volcanics. In the Eldorado Mountains, the Patsy Mine Volcanics consists of thick flows (457 ± 91 m) of plagioclase-, pyroxene-, olivine-, and magnetite-bearing basaltic andesite (Anderson, 1971). Coeval and lithologically equivalent units crop out in the McCullough Range (Schmidt, 1987), Highland Spring Range (Davis, 1985), Black Mountains (Faulds, 1989) and in the White Hills (Cascadden, 1991). Recent $^{40}Ar/^{39}Ar$ geochronology of lavas and tuffs in the northern Eldorado Mountains by

Faulds (personal communication to Smith, 1993) show that basaltic andesite flows located in the middle of the Upper Patsy Mine Member are 15.18 ± 0.07 m.y. old (laser fusion $^{40}Ar/^{39}Ar$ on plagioclase) which closely brackets the eruption of the Tuff of Bridge Spring at 15.12 ± 0.03 Ma (laser fusion $^{40}Ar/^{39}Ar$, sanidine).

Generation of the Tuff of Bridge Spring data array by lithic contamination requires that the contaminant have an isotopic composition that is sufficiently removed from the Tuff of Bridge Spring trend such that reasonably small amounts of contaminant can be assimilated to produce the trend. An example of this is shown in Fig. 14, which shows a hypothetical data array with two different contaminants. Generation of the data array by incorporation of a contaminant is calculated by adding successive amounts of pure contaminant to pure end member host rock. In these models, the composition of the contaminant represents 100 % assimilation and the composition of the uncontaminated tuff represents 0 % assimilation. When modeling the incorporation of a contaminant into a host rock to produce a succession of intermediate isotopic values, it is important to note that in order to produce the data trend, large amounts of contaminant must be assimilated when the composition of the contaminant is similar to that of the host rock. In Fig. 14, the isotope composition of Contaminant A requires that, in order to produce the data array, 100 % contaminant must be added to the pure end member host rock. Assimilation of Contaminant B, however, requires only 10 % contamination to produce the data array.

ε_{Nd} vs. $^{87}Sr/^{86}Sr$ values of clinopyroxene separated from two samples of Patsy Mine Volcanics (Upper and Lower Members) by Daley (1992) indicate that the isotope values of the Patsy Mine Volcanics are coincident with the lower portion of the Tuff of Bridge Spring field (Fig. 15). This similarity suggests that generation of the Tuff of Bridge Spring array by the incorporation of Patsy Mine Volcanics would require assimilation of very large quantities of Patsy Mine Volcanics (nearly 100 modal

percent). Incorporation of this much material is both unrealistic and not supported by modal analyses of the Tuff of Bridge Spring. The Tuff of Bridge Spring contains an average of 5.7 % lithic fragments (standard deviation = 6.6 %). Using this modal value, it is theoretically possible to generate the Tuff of Bridge Spring data array by incorporating a hypothetical mafic contaminant of lithospheric mantle derivation that has a calculated value of ε_{Nd} = -55.070 and $^{87}Sr/^{86}Sr$ = 0.7419. Rocks with this isotopic value are not known in the northern Colorado River extensional corridor, which effectively precludes the incorporation of Patsy-Mine type xenoliths as a possible mechanism for producing the Tuff of Bridge Spring data array.

Alkali Olivine Basalts

A second possible source of lithic contamination is asthenosphere-derived basalts. An example of a typical alkali olivine basalt in the northern Colorado River extensional corridor is the nepheline-normative Petroglyph Wash Basalt of the Fortification Hill volcanic field in Arizona (Feuerbach et al., in press). This rock, which has the values ε_{Nd} = 3.63, and $^{87}Sr/^{86}Sr$ = 0.0.70347 (Fig. 15), has isotopic affinities to contemporary oceanic island basalts (OIB). The ε_{Nd} and $^{87}Sr/^{86}Sr$ values of the Petroglyph Wash sample are significantly removed from the general trend of the Tuff of Bridge Spring array. This suggests the possibility that the array was generated as the result of contamination by xenoliths having OIB-type isotopic signatures. However, xenoliths of olivine-bearing alkali basalt are not present in the Tuff of Bridge Spring. This eliminates the incorporation of alkali basalt xenoliths as a controlling factor in producing the Tuff of Bridge Spring isotope array.

Precambrian Basement

Typical Early Proterozoic crystalline basement in the northern Colorado River extensional corridor consists of 1.7 Ga granitic and garnet-bearing gneisses, schists, and granite pegmatites (Anderson, 1971). These rocks belong to the Mojave crustal province (Wooden and Miller,1990; Bennett and DePaolo, 1987), which is defined in terms of regional Pb and Nd isotopic signatures (Fig. 16). Wooden and Miller (1990) estimate average initial Pb values of the Mojave crustal province as $^{206}Pb/^{204}Pb$= 16.1, $^{207}Pb/^{204}Pb$ = 15.38, and $^{208}Pb/^{204}Pb$= 35.65.

Pb isotope ratios of the Tuff of Bridge Spring range in value from $^{206}Pb/^{204}Pb$ = 18.030 to 18.240, $^{207}Pb/^{204}Pb$ = 15.557 to 15.586, and $^{208}Pb/^{204}Pb$ = 38.890 to 39.025 (Table 6). Superimposing plots of Tuff of Bridge Spring Pb values on $^{207}Pb/^{204}Pb$ vs. $^{206}Pb/^{204}Pb$ and $^{208}Pb/^{204}Pb$ vs. $^{206}Pb/^{204}Pb$ plots of early Proterozoic rocks of the Mojave and Arizona crustal provinces (Wooden and Miller, 1990) shows that the Tuff of Bridge Spring array is coincident with the Mojave province trend (Fig. 17). This similarity indicates that production of the Tuff of Bridge Spring by assimilation with Mojave Province-type crust is unlikely because a considerable amount of Mojave-type crust (nearly 100 %) would have to be added to the Tuff of Bridge Spring in order to produce the required changes in isotope values. This conclusion is supported by thin section and field studies which indicate that crystalline lithic fragments are not present in the Tuff of Bridge Spring.

Assimilation of Mojave-type crust is also contradicted by Rb and Sm geochemistry. Generation of the Tuff of Bridge Spring by assimilation of 10 % lithic fragments of Mojave-type crust would require a xenolith having a composition of ε_{Nd} = -30 and $^{87}Sr/^{86}Sr$ = 0.7294. Smaller amounts of contamination would force ε_{Nd}

values lower and $^{87}Sr/^{86}Sr$ values higher. Again, such isotopic values are not found in Mojave Province rocks.

Mixing Trend

Because the evidence presented above eliminates lithic contamination as a plausible mechanism for the origin of the Tuff of Bridge Spring isotope array, isotopic variation is interpreted to result from open system conditions in the Tuff of Bridge Spring magma chamber.

Open system magmatic processes include country rock assimilation and/or magma mixing. There is abundant evidence of magma mixing and assimilation in plutonic rocks of the northern Colorado River extensional corridor (e.g., Wilson Ridge, Mt. Perkins pluton, and the Aztec Wash pluton) (Larsen, 1990: Metcalf et al., 1992; Falkner et al., 1993). These features support the assumption that open system conditions were common in plutons that developed in this region during the Miocene, and implies similar mechanisms of origin for volcanic rocks of the region.

The Role of Contaminants in the Genesis of the Salt Spring Wash and Lucy Gray Range Tuffs

Contaminant modeling of both the tuff of the Lucy Gray Range tuff and the tuff of Salt Spring Wash indicate they were not generated as the result of contamination of the Tuff of Bridge Spring with xenoliths that have isotopic signatures typical of Patsy Mine Volcanics mafic rocks, OIB basalts, or Mojave-province Precambrian crystalline basement. Fig. 15 shows the plot of ε_{Nd} vs. $^{87}Sr/^{86}Sr$ of the Lucy Gray and Salt Springs Wash tuffs and the Tuff of Bridge Spring array. Assimilation of reasonable

volumes of xenoliths by the Tuff of Bridge Spring to produce the tuff of Salt Spring Wash requires contamination by a source that has values of $^{87}Sr/^{86}Sr$ that are not found in the extensional corridor. Likewise, generation of the tuff of the Lucy Gray Range by xenolith contamination requires assimilation of a source that has values of ε_{Nd} that are unrealistic for rocks of this area. These observations suggest that the isotopic signatures of these tuffs reflect derivation from different magmatic sources. Therefore, the Salt Spring Wash and Lucy Gray Range tuffs are not cogenetic with the Tuff of Bridge Spring.

Table 6: Isotope Analyses. (* = analysis pending.)

Section	Sample Number	87Sr/86Sr	Epsilon Nd	206Pb/204Pb	207Pb/204Pb	208Pb/204Pb
McCullough Range	91-M1-1	0.709534	-9.16	18.04	15.557	38.906
	91-M1-4	0.70901	-8.07	18.177	15.58	38.89
Eldorado Mountains	92-E3-5	0.708653	-8.61	*	*	*
	Duplicate	0.709112	*	*	*	*
Highland Spring Range	92-HS1-1	0.70964	-8.34	18.176	15.571	38.958
Sheep Mountain	91-SM1-1	0.70983	-9.28	18.052	15.563	39.025
	92-SM2-3	0.70958	-10.07	14.596	15.204	38.001
Temple Bar	92-TB3-4	0.70984	-8.83	18.24	15.586	38.988
White Hills	92-WH2-3	0.70902	-8.45	18.232	15.567	38.941
Black Mountains	92-BM1-3	0.71036	-9.43	18.038	15.562	39.016
Interstate 15	93-I151-1	0.714628	-10.11	18.038	*	*
Dolan Springs	92-DS1-1	0.71007	-9.56	*	*	*

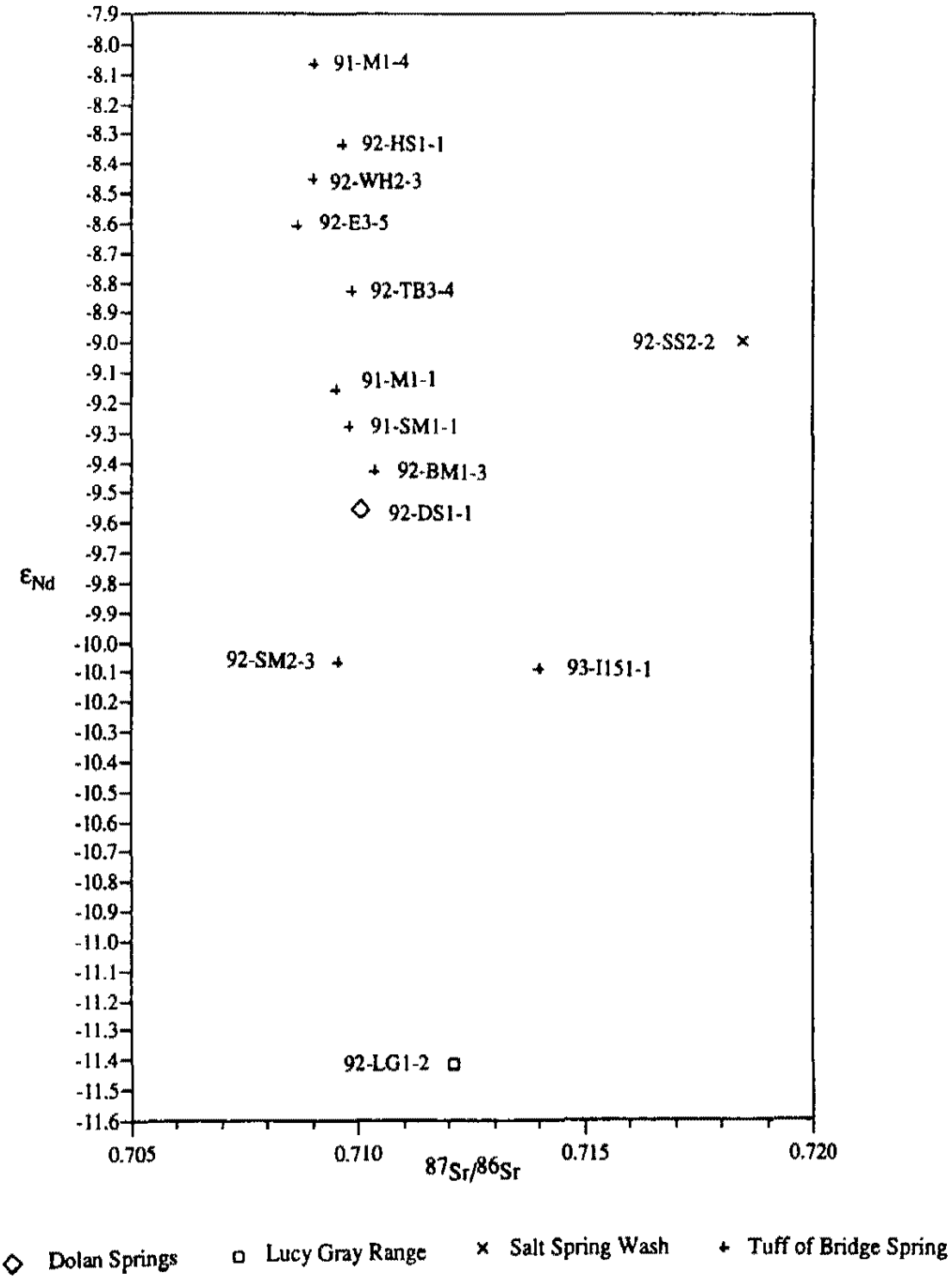

Figure 11: Plot of ε_{Nd} vs. $^{87}Sr/^{86}Sr$ of the Tuff of Bridge Spring and three non-correlative tuffs. Data points labeled with sample numbers.

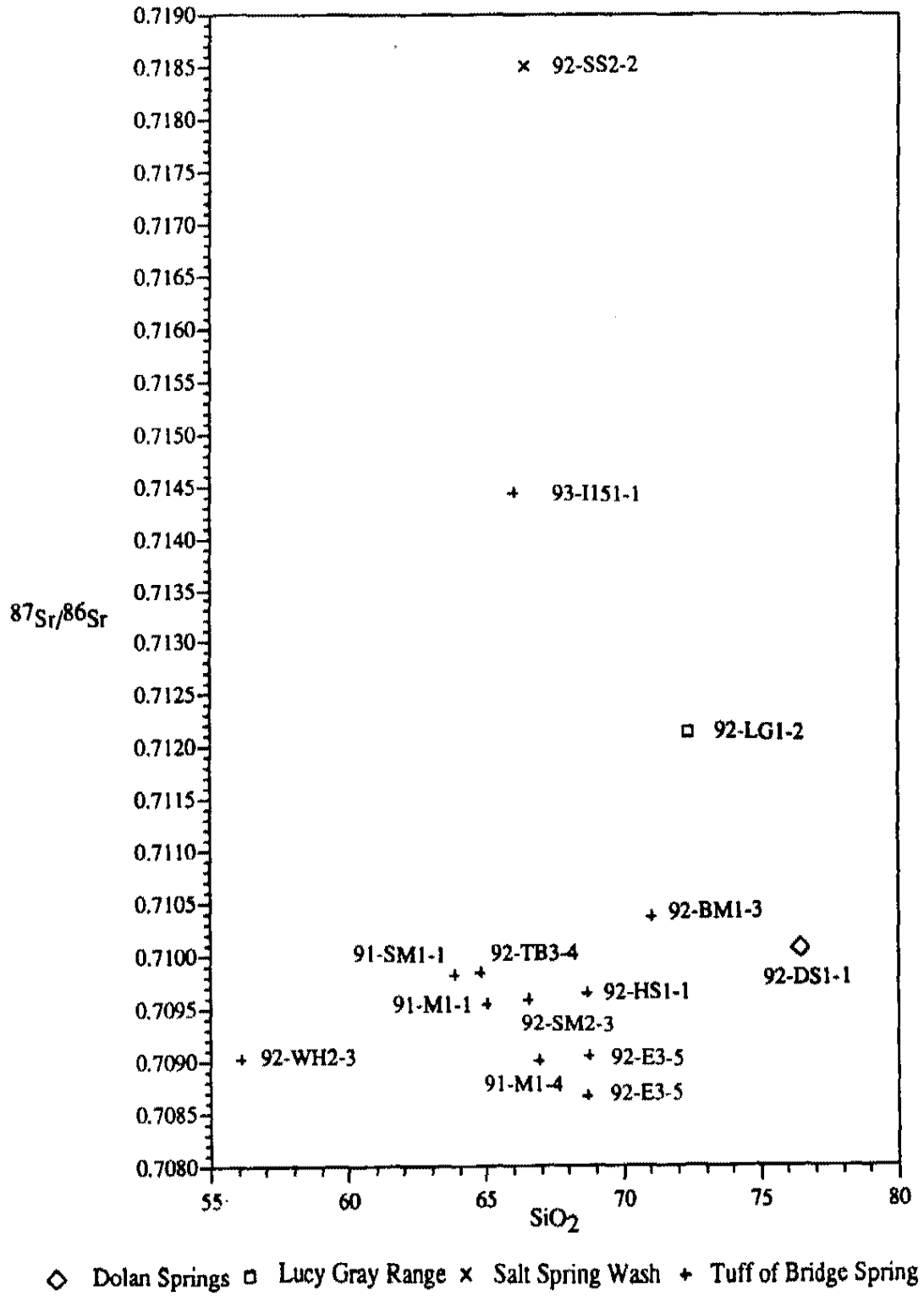

Figure 12. Plot of $^{87}Sr/^{86}Sr$ vs. SiO_2 of the Tuff of Bridge Spring and three non-correlative tuffs. Data points labeled with sample numbers.

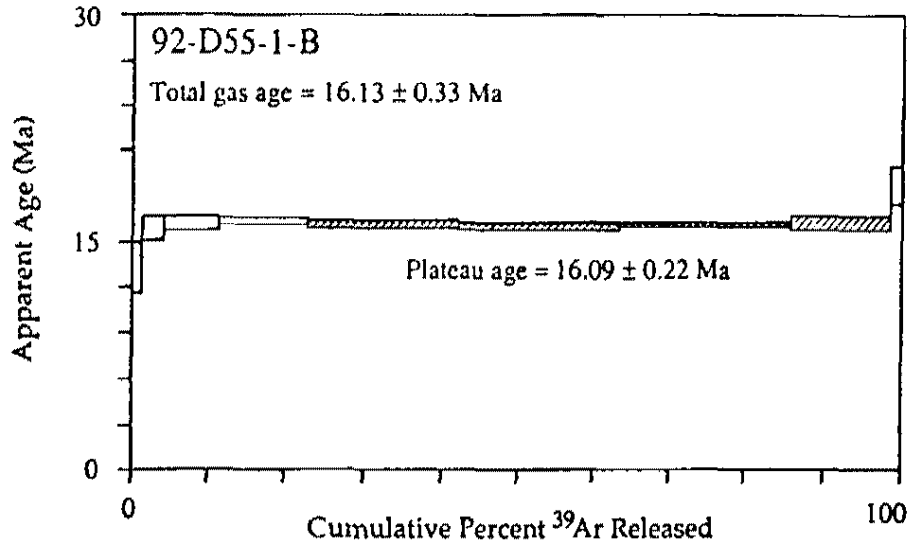

TEMP	40/39	37/39	36/39	MOLES 39	%TOTAL	% RAD	K/Ca	AGE (Ma)
		92-D55-1-B					J = .016479	
500	7.058	0.116	0.0223	125.0	1.2	6.3	4.22	13.25 ± 1.70
810	1.684	0.048	0.0038	298.6	2.8	31.9	10.30	15.89 ± 0.81
915	0.967	0.018	0.0014	764.8	7.3	56.7	27.26	16.22 ± 0.43
1815	0.779	0.011	0.0007	1207.0	11.5	71.0	45.07	16.37 ± 0.22
1080	0.762	0.013	0.0007	2034.2	19.3	71.3	37.81	16.08 ± 0.28
1180	0.783	0.023	0.0008	2225.8	21.1	69.0	20.98	16.00 ± 0.25
1245	0.798	0.034	0.0008	2375.4	22.6	68.3	14.37	16.12 ± 0.15
1310	0.790	0.051	0.0008	1327.3	12.6	69.1	9.61	16.17 ± 0.44
FUSE	1.031	0.124	0.0013	170.2	1.6	61.5	3.95	18.74 ± 1.24
TOTAL				10528.3	100.0			16.13 ± 0.31
PLATEAU AGE								16.09 ± 0.22

(Moles 39Ar X E-14)

Figure 13. ^{40}Ar/^{39}Ar incremental release age analysis (biotite) of the tuff of Dolan Springs.

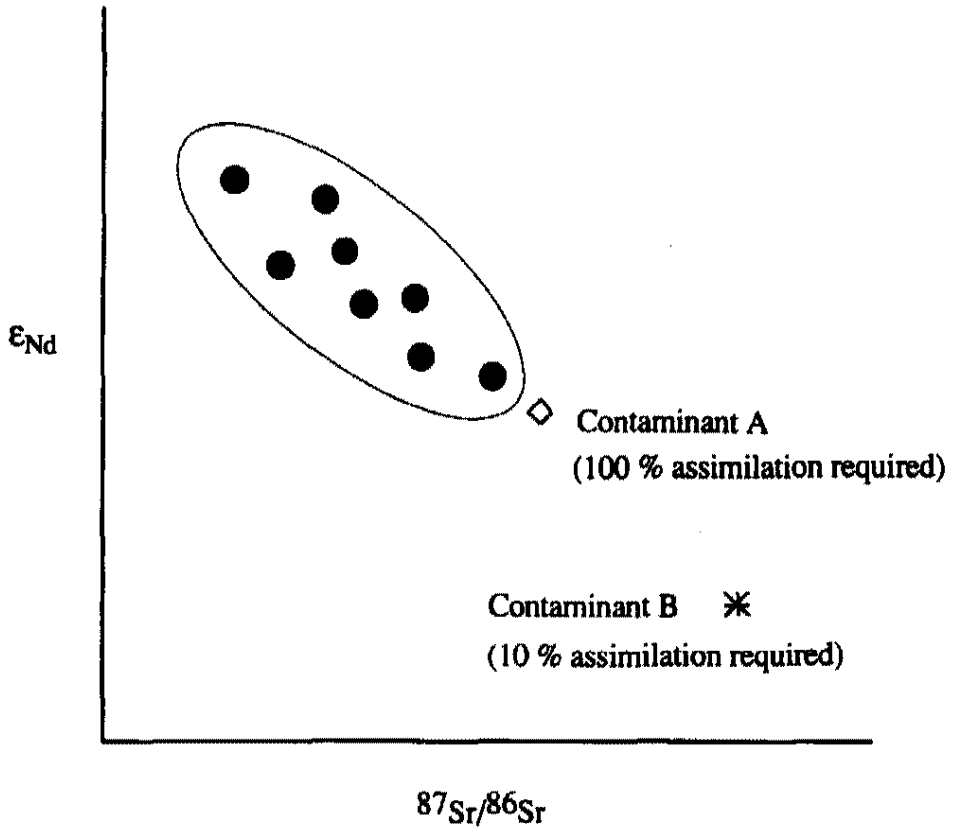

Figure 14. Generation of a hypothetical isotope array by xenolith contamination. See text for explanation.

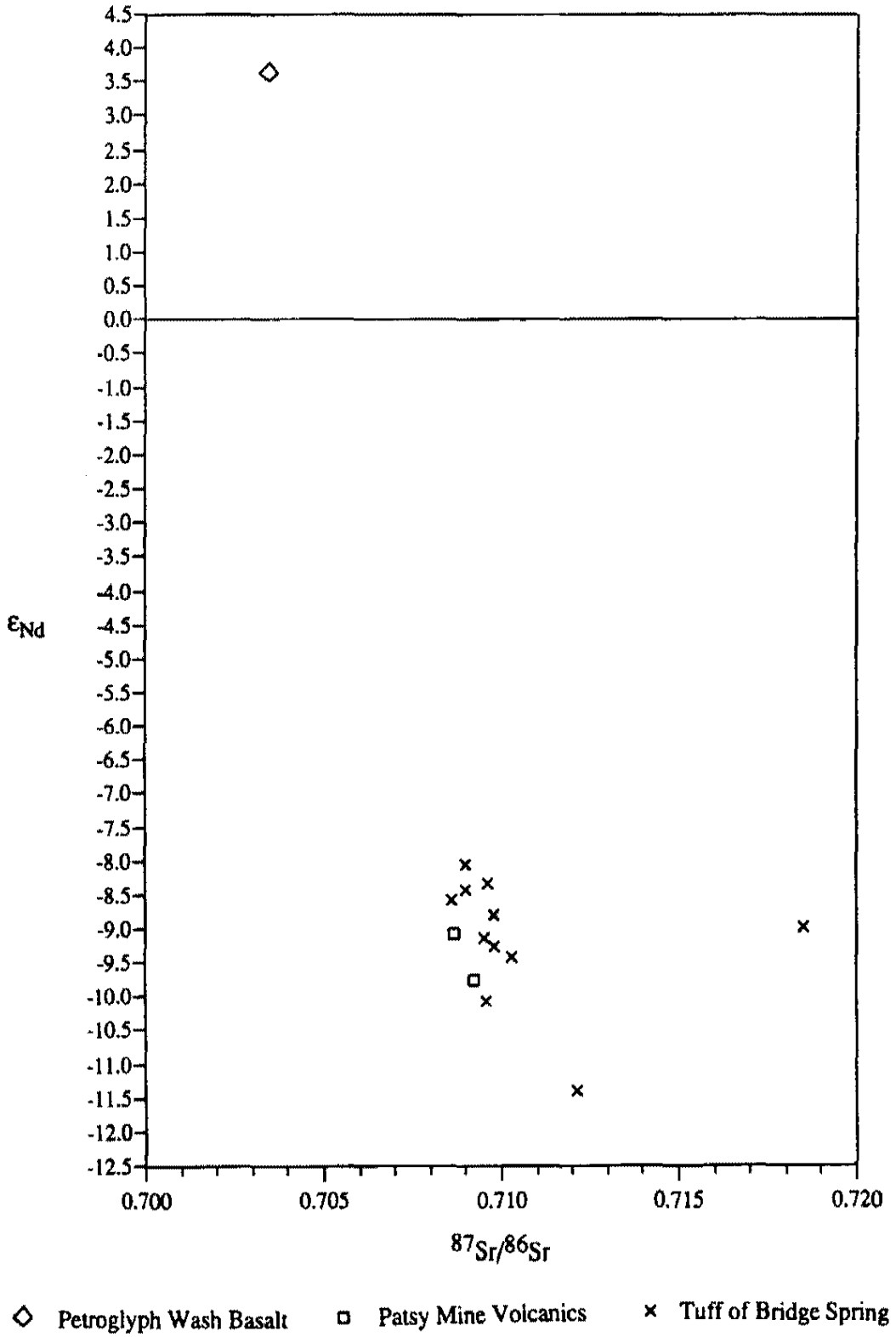

Figure 15. Plot of ε_{Nd} vs. $^{87}Sr/^{86}Sr$ for the Tuff of Bridge Spring, Patsy Mine Volcanics, and Petroglyph Wash Basalt.

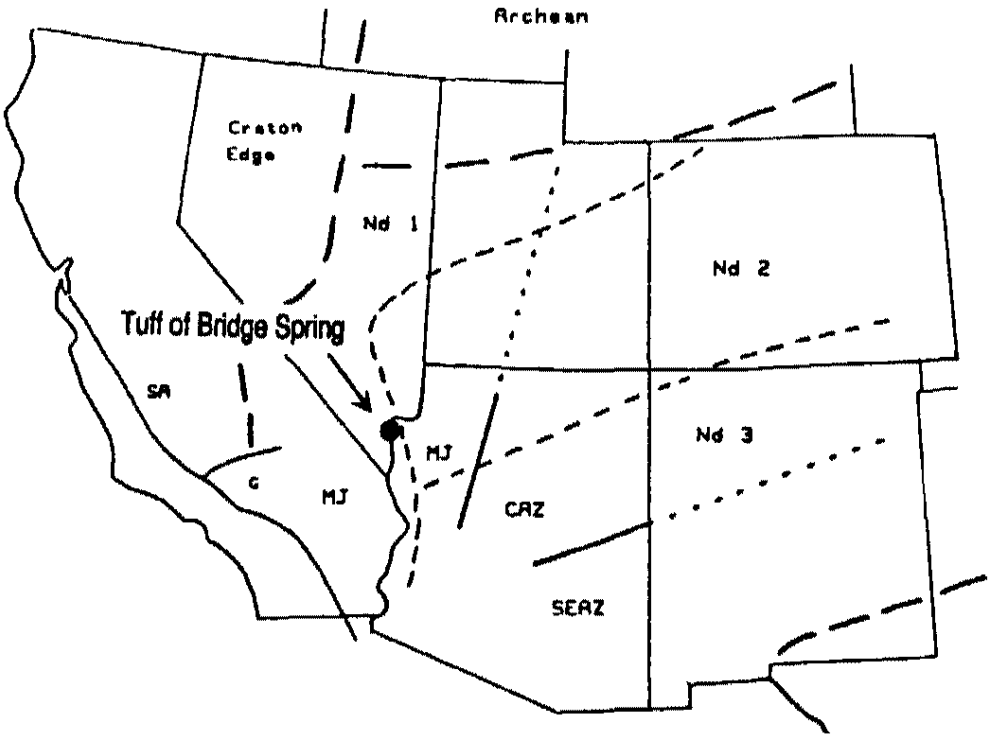

Figure 16. Appproximate geographic distribution of Early Proterozoic Nd and Pb provinces in the southwestern United States shown with the distribution area of the Tuff of Bridge Spring. Pb provinces: MJ = Mojave, CAZ = central Arizona, SEAZ = southeastern Arizona. Southwestern Arizona province boundaries are uncertain because of lack of data. From Wooden and Miller (1990).

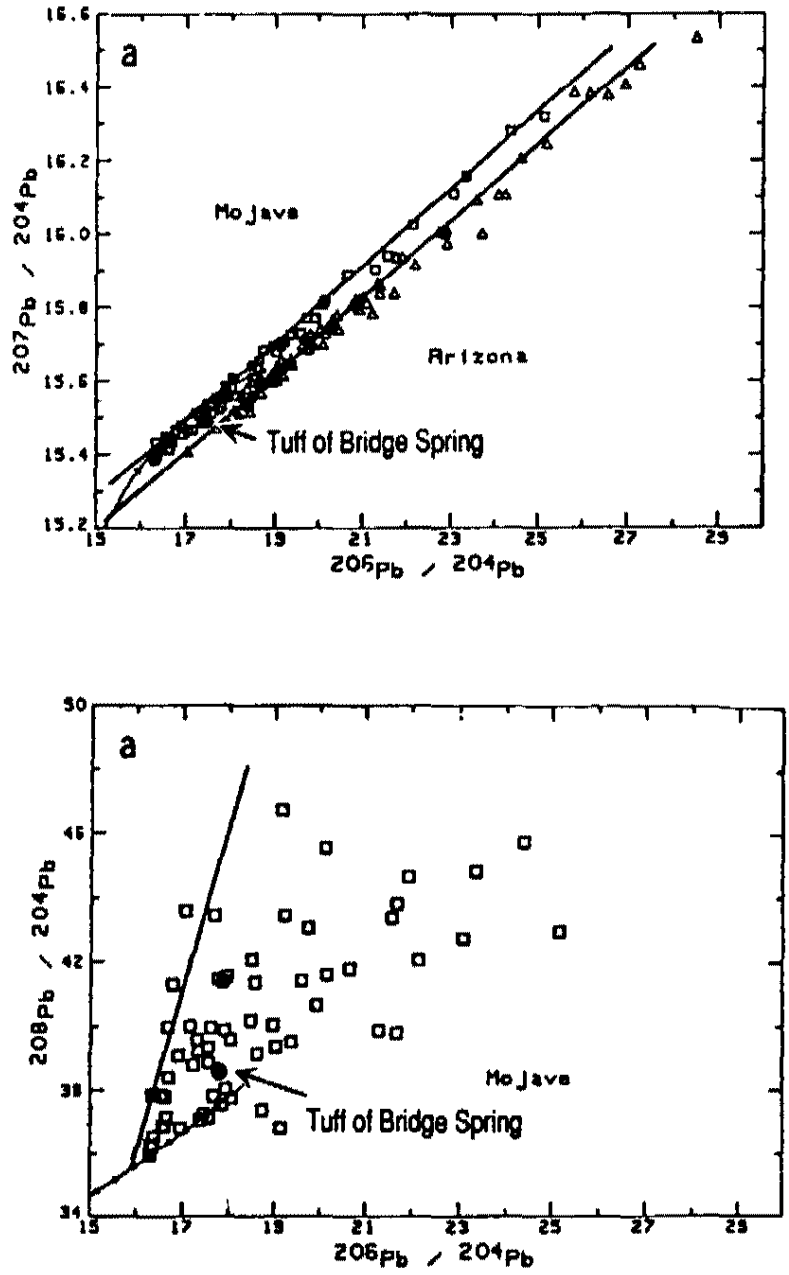

Figure 17. Pb isotope plots of a representative Tuff of Bridge Spring sample and samples of Mojave and Arizona Early Proterozoic crustal provinces rocks. Pb isotope analyses of crustal rocks from Wooden and Miller (1990).

processes may affect the degree of welding of ash-flow tuffs and the preservation of cooling breaks. Local zones of devitrification form in response to variations in the thickness of each ash flow which in turn are controlled by variations of pre-eruption topography. Because syn-and post-eruptive modification of ash-flow tuffs is common (Hildreth and Mahood, 1985), any division of ash-flow tuff internal stratigraphy that is based upon physical features of ash-flow tuffs (cooling breaks, phenocryst modes, degree of welding, color, etc.) that can be changed by secondary processes must be considered suspect.

In this study, the recognition of regionally-extensive chemical zonations in the Tuff of Bridge Spring (described below) indicates that secondary modification processes did not significantly alter the primary chemical signatures of the Tuff of Bridge Spring. This observation suggests that these signatures are magmatic in origin.

Determination of the internal stratigraphy of the Tuff of Bridge Spring is based upon the recognition of patterns of major/trace element enrichment and depletion of each section. In many cases, patterns can be linked to a specific outcrop features (e.g., cooling breaks) which correspond to distinct changes in the eruptive cycle. Recognition of the relationship between chemical patterns and outcrop features subsequently allows the division of each section into a series of eruptive units, which are the geochemically-defined equivalents of the conventional flow unit of Smith (1960). The presence of consistently reoccurring patterns of major and trace element variation across the distribution area of the Tuff of Bridge Spring allows division of the unit into two separate chemical members which formed in response to two different magmatic processes. Correlation of these chemical members across the distribution area of the Tuff of Bridge Spring leads to furthur division of the unit into three regional members. Persistence of regional chemical trends of the Tuff of Bridge Spring has important implications for understanding magma chamber processes.

Eruptive Units

Chemical Criteria

Plots of relative stratigraphic position vs. major element oxides and trace elements (Fig. 9) for the Tuff of Bridge Spring show trends of relative depletion and enrichment of each element. The pattern of these variations preserves a sequence of magmatic compositions that were present in the Tuff of Bridge Spring magma chamber immediately prior to eruption.

Plots of Tuff of Bridge Spring geochemistry on relative position vs. element concentration diagrams (Fig. 9) consists of alternating trends of elemental depletion or enrichment that are expressed as lines of changing slope. Two types of chemical breaks (interruptions) separate adjacent chemical trends on these plots (Fig. 18). The first type of chemical break is marked by a reversal in slope at an inflection point. The second, less frequently-occurring type of break is marked by the separation of two trends by a wide compositional gap between two trends of opposing slope, or between two trends with the same slope.

A certain amount of interpretation is required to locate chemical breaks in relative stratigraphic position vs. element concentration plots (see discussion below of Eldorado Mountains section). Such ambiguities can be resolved by using additional criteria for locating stratigraphic breaks in ash-flow tuffs such as cooling breaks, basal surge deposits, etc.

Although the pattern of elemental variation preserved in each section differs with each element, the relative stratigraphic position at which significant slope changes, inflection points, and/or compositional gaps occur is generally consistent in each section regardless of which element is being considered. These consistent patterns

define the chemical signatures of the Tuff of Bridge Spring and mark specific chemical horizons in the Tuff of Bridge Spring magma chamber. These signatures provide points of reference upon which division of the internal stratigraphy of the Tuff of Bridge Spring is based. Stratigraphic units defined on the basis of the chemical signature of the Tuff of Bridge Spring are referred to as "eruptive units" in this study.

An example of the division of a stratigraphic section into eruptive units is presented in Fig. 19, a compilation of relative stratigraphic position vs. normalized elemental oxide and trace element plots for the Eldorado Mountains stratigraphic section. These plots suggest that there are three major compositional trends in this section. These trends are formed by the grouping of intervals 1-3, 4-5, and 6-9. Corresponding chemical breaks occur above stratigraphic level 3, and 5. Fig. 20 summarizes the division of each Tuff of Bridge Spring stratigraphic section into successive eruptive units.

Field Evidence

The occurrence of cooling breaks are the main field evidence used to support geochemically-defined divisions of internal stratigraphy. In relatively short-lived magmatic systems, changes in magmatic chemistry do not necessarily occur isochronously with those types of chemical and physical changes in magmatic conditions that result in formation of cooling breaks.

Cooling breaks form during periods of eruptive quiescence. If the quiescent stage is of sufficient duration, the magma chamber may undergo complete re-equilibration, resulting in the formation of a normally-zoned magma chamber. In such cases, a period of quiescence is directly associated with the formation of cooling breaks, and because periods of eruptive quiescence are associated with major changes

of magma chamber chemistry, cooling breaks commonly coincide with the position of chemical breaks as well.

In some eruptive sequences, re-equilibration of a magma chamber may be interrupted by volatile saturation or by injection of mafic magma, two processes that may initiate eruption. If the re-equilibration process is interrupted by an ash-flow tuff eruption, the chemical signature of the resultant volcanic outflow will not differ significantly from older flows. In this case, formation of a chemical break that reflects an abrupt chemical gradient in the magma chamber will occur at a later time (i.e., above the most recent cooling break).

Field evidence supports the division of each Tuff of Bridge Spring stratigraphic section into a series of chemically distinctive eruptive units. Supporting field observations include (see Fig. 9 and 20, and Appendix C):

(1) Black Mountains: A poorly-exposed cooling break is present below stratigraphic interval 10, which correlates with chemical breaks shown by Th, Y, Ba, Cr, Rb, Sr, Mn, Mg, K, Fe, and Ti.

(2) Eldorado Mountains: Major chemical breaks occur below stratigraphic intervals 4 and 6, and a minor break occurs below interval 9. Placement of a chemical break below interval 4 is supported by the presence of gas-escape pipes, which are zones of concentrated lithic fragments that are typically preserved at the top of flow units (Fisher and Schmincke, 1985). A chemical break occurs between interval 5 and 6 (a massive vitrophyre and vapor phase zone, respectively), but cannot be associated with an obvious cooling break.

(3) Highland Spring: A sharp, laterally-continuous cooling break occurs between stratigraphic intervals 7 and 9. This cooling break correlates with a major geochemical break (Ti, Ca, K, Na, Mg, Mn, Zr, Sr, Rb, Ni, Nb, Cr, and Ba). A minor

chemical break occurring between the basal interval and interval 5 does not correlate to any specific outcrop feature.

(4) Interstate 15: Chemical breaks occur above the basal stratigraphic interval and between intervals 4 and 5. Isotope geochemistry (previously discussed) suggests that the basal interval is not cogenetic with the Tuff of Bridge Spring. The occurrence of a massive vitrophyre which may represent the base of a cooling unit at interval 6 weakly corresponds to the chemical break below interval 5.

(5) McCullough Range: A thin, pumice-rich interval of very poorly-welded crystal tuff occurs at stratigraphic interval 8, which correlates with a chemical break. Additional chemical breaks occur below the uppermost interval of the section (interval 10.5) and below the basal interval. A cooling break was not observed below the uppermost interval of the section. The basal interval of the McCullough Range section consists of a discontinuous, very-poorly welded lithic tuff which is possibly related to a pyroclastic surge deposit. This interval has a different chemical signature than the Tuff of Bridge Spring for most elements with the exception of P, Mn, Ni, Nb, and Th.

(6) Sheep Mountain: A possible cooling break occurs below a massive vitrophyre at interval 9. This cooling break correlates with a chemical break. Another chemical break separates the basal interval of the section from the units lying above it. This interval consists of a very poorly-welded, pumiceous vitrophyre that has a shard-rich matrix.

(7) Temple Bar: Chemical breaks occur between intervals 5 and 6, and 8 and 9.5, respectively. Obvious cooling breaks were not observed in the Temple Bar section.

(8) White Hills: A poorly exposed cooling break is present between stratigraphic intervals 8 and 9, which corresponds to a chemical break that is strongly established by variation of most trace elements.

Chemical Members of the Tuff of Bridge Spring

The dominant geochemical trend shown on Harker variation plots of the Tuff of Bridge Spring data involves Cr, an element which partitions into mafic mineral phases such as clinopyroxene (Fig. 21). The partitioning of Cr provides the basis of division of Tuff of Bridge Spring stratigraphic sections into two geochemically distinct members.

Assignment of sections to an appropriate geochemical member were made by examining numerous element/element and ratio/element plots. For reasons that will be discussed below, such assignments occasionally varied, depending upon the specific elements being considered in each plot. This requires that the final assignment of each stratigraphic section is based upon a consensus of many different plots that used many different combinations of elements and/or ratios. While the partitioning of Cr provides the best general criteria for division of the Tuff of Bridge Spring into two chemical members, the Eldorado Mountains section does not exhibit the same sensitivity to variation of Cr as the rest of the sections. Assignment of this section to an appropriate chemical member was based upon examination of element plots other than Cr vs. SiO_2.

The first chemical member of the Tuff of Bridge Spring generally exhibits a trend of relatively constant Cr and highly variable SiO_2, and includes the White Hills, McCullough Range, lower Eldorado Mountains (stratigraphic intervals 1-5), and upper Highland Spring Range (stratigraphic intervals 8-9), and upper Temple Bar (interval 9) stratigraphic sections. This chemical member will be refered to as the constant Cr member. The second Tuff of Bridge Spring chemical member generally exhibits a trend of highly variable Cr and moderately variable SiO_2, and includes the Black Mountain, Interstate 15, upper Eldorado Mountains (intervals 5-9), lower Highland Springs (intervals 1-7), lower Temple Bar (intervals 1-8), and Sheep Mountain sections. This group will be referred to as the variable Cr member.

As discussed above, division of the Tuff of Bridge Spring into chemical members is also shown in element /element plots (such as Cr vs. Sr and Y vs. Zr) (Fig. 22), and ratio/element plots (such as Ti/Sr vs. Fe and Zr/Ti vs. Ba) (Fig. 23 and 24, respectively). The interpretation of element/element and ratio/element diagrams relies both on the grouping of data within specific trends and the direction of the sequential path of changing chemistry within each stratigraphic section. For example, on the Zr/Ti vs. Ba diagram (Fig. 24), two groups are recognized on the basis of both trend and clustering of data. One group shows variable Zr/Ti and relatively constant Ba, and the second group shows variablity of both Zr/Ti and Ba.

Although the assignment of sections to different chemical groups may vary with the specific elements and elemental ratios being considered, the majority of plots support the chemical member designations described above. Deviations from these groupings for certain elements possibly reflect the use of whole-rock samples for geochemical analysis. The presence of xenoliths and phenocrysts in analyzed samples will cause compatible element concentrations to differ from magma (glass) concentrations. Since it is the contention of this study that the consistent separation of sections into two distinct chemical groups is the product of two distinct magmatic differentiation processes, only element and element ratios not appreciably affected by phenocrysts and /or xenoliths can be used to define chemical groups. The use of elements like Zr and Y, and to a lesser extent Cr may provide a means of bypassing the chemical "static" produced by phenocrysts and xenoliths to allow an undistorted view of the magmatic chemistry of the Tuff of Bridge Spring. A prime example of the role of chemical "static" in masking magmatic signatures involves the Eldorado Mountains section. Both the Harker variation plot of Cr and the Ti/Zr vs. Ba plot of this section indicate that entire section should be grouped in the variable Cr chemical member. Such an assignment, however, is strongly contradicted by the majority of Harker,

element/element, and ratio/element plots (e.g., Cr vs. Sr, Y vs. Zr, and Ti/Sr vs. Fe) (Fig. 22 and 23), which indicate that the section actually contains both chemical members.

Examination of the constant Cr chemical member indicates that two of the sections included in this group, (upper Highland Spring Range and upper Temple Bar sections), do show variance from both the constant Cr and variable Cr members for some elements, but for the most part exhibit the same geochemical signature as the rest of the constant Cr member sections in the majority of element/element and ratio/element plots. These differences suggest that the upper Highland Spring Range and upper Temple Bar sections were produced from a hybridized batch of magma in which the constant Cr signature is dominant, but which also preserves signatures that are intermediary between the signatures of both the constant Cr and variable Cr members.

Regional Members of the Tuff of Bridge Spring

Meaningful reconciliation of chemical member assignments with regional stratigraphic relationships of each Tuff of Bridge Spring section allows the division of the Tuff of Bridge Spring into three regionally-extensive ash-flow sheets, or regional members (Fig. 25). The stratigraphically lowest regional member of the Tuff of Bridge Spring (Member I) consists of the lower Eldorado Mountains, McCullough Range, and White Hills sections and is characterized by the constant Cr trend. The statigraphically intermediate regional member (Member II) exhibits the variable Cr trend and consists of the Interstate 15, Sheep Mountain, lower Highland Springs, upper Eldorado Mountains, Black Mountains, and lower Temple Bar sections. The stratigraphically uppermost member (Member III) has, for the most part (but with some differences),

the same chemical signature as the basal regional member (constant Cr trend) and includes the upper Highland Springs and the upper Temple Bar sections. Fig. 26 shows the areal distribution of the three regional members of the Tuff of Bridge Spring.

Fine Scale Chemical Variation

The plot of Zr/Ti vs. Ba (Fig. 26) provides a means of observing fine-scale chemical variations in the Tuff of Bridge Spring. Because these variations are preserved across the distribution area of the tuff, they probably reflect variations in the Tuff of Bridge Spring source magma chamber.

In the ratio Zr/Ti, Zr is an incompatible trace element that is partitioned only by the mineral zircon. Ti is slightly more compatible than Zr, and is partitioned into clinopyroxene and hornblende. Ba, the independent variable in this plot, is a compatible element which is fractionated by potassium feldspars and biotite. The relationship of Zr and Ti in the Tuff of Bridge Spring is unique for two reasons. First, changes in the Zr/Ti ratio seem to represent changes in magmatic compositions. Second, the direction of change of the ratio (relative increase or decrease) does not seem to be affected by the abundances of phenocrysts and/or lithic fragments in the samples.

The Zr/Ti vs. Ba plot (Fig. 24) separates the Tuff of Bridge Spring sections into two groups. The first group shows highly variable Zr/Ti in conjunction with relative invariablity of Ba. Stratigraphic sections with this geochemical signature include the Eldorado Mountains, Sheep Mountain, lower Highland Spring (stratigraphic intervals 1-7), Interstate-15, and Black Mountains sections. This group of sections corresponds closely to the sections that make up the constant Cr chemical member. The second group is characterized by variablity of both Zr/Ti and Ba. Sections with this signature

include the upper Highland Spring Range (intervals 8-9), McCullough Range, Temple Bar, and White Hills sections. This group of sections corresponds closely to the sections that make up the variable Cr chemical member.

Figure 27 is a compilation of the plots of each of the sections that have highly variable Zr/Ti, relatively invariable Ba plotted side by side (only the y-axis is functional in this plot; however, the magnitude of separation for Ba of the two parts of the Highland Spring section has been preserved). Numerals beside each data point denote its relative stratigraphic position in that particular section. If the pattern of enrichment and depletion of Zr/Ti within each stratigraphic section is followed from basal interval to stratigraphic top, a sequence or path of evolving chemistry can be traced. Each path consists of a series of vertical to slightly inclined segments that have alternating upward (increasing Zr/Ti) or downward (decreasing Zr/Ti) directed lines. The relative direction of each segment is controlled by the stratigraphic order of the analyzed samples. Data points in upward-directed segments have increasing Zr/Ti ratio values in the upsection direction. Data points in downward-directed segments have decreasing Zr/Ti ratio values in the upsection direction. The transition between adjacent segments is marked by inflection points where the Zr/Ti chemical path changes direction.

The sequence of increasing and decreasing Zr/Ti in the variable Zr/Ti, constant Ba trend forms similar patterns in each section. Each section may record only a part of the magmatic zoning that was present in the Tuff of Bridge Spring source chamber at the time of eruption. Complete reconstruction of the chemical profile of the chamber requires combining chemical path diagrams from different sections.

The stratigraphically uppermost inflection points of the variable Zr/Ti, constant Ba trend (i.e., interval 8 in the Eldorado Mountains, interval 7 in the Sheep Mountains, interval 8 in the Black Mountains, interval 6 in the Highland Spring Range, and interval 4 in the I-15 section) all occur at approximately the same Zr/Ti value (average = 538.2;

standard deviation = 41.4). Theoretically, this inflection point should occur at the same Zr/Ti value. Deviation from this value is expected to occur because the Zr/Ti ratio will change in response to changes in phenocryst and/or lithic fragment abundances, which will vary from section to section. This chemical inflection point is interpreted to represent a specific variable Zr/Ti, constant Ba magmatic horizon in the Tuff of Bridge Spring magma chamber that has been preserved in five sections spread over a distance of 90 km in the present day distribution area of the Tuff of Bridge Spring. This is perhaps the first report in the literature of such a widespread chemical marker horizon in ash-flow tuffs.

The variable Zr/Ti, constant Ba path of the upper interval of the Highland Spring section is separated from the lower part of the section by a significant change in Ba concentration (Fig. 24 and 27). This gap suggests that the rocks of the upper Highland Spring Range section were affected by magmatic processes that changed both Zr/Ti and Ba concentrations. Such a relationship is consistent with several other element vs. element and ratio vs. element plots of the Tuff of Bridge Spring in the Highland Spring Range (e.g., Cr vs. Sr) and indicates that this stratigraphic section preserves a major chemical transition that formed in the Tuff of Bridge Spring magma chamber.

The chemical path concept also has implications for location of the source of the Tuff of Bridge Spring (see source section).

Magma Chamber Processes

Differential retention of Cr in the two Tuff of Bridge Spring chemical members suggests that two different differentiation processes dominated the petrogenesis of the

Tuff of Bridge Spring at different points in its evolution. The trend of increasing SiO_2 and relatively constant Cr indicate that differentiation of the constant Cr chemical member occurred without the involvement of mafic minerals such as clinopyroxene. These conditions are suggestive of differentiation of the upper levels of a normally zoned felsic magma body. The trend of variable SiO_2 and Cr of the variable Cr member suggests magma differentiation by either subtraction or addition of clinopyroxene and perhaps olivine from a mafic magma. These conditions are more typical of the lower parts of a magma chamber. Coexistence of these two trends suggests that the Tuff of Bridge Spring originated from a magma chamber with a felsic top and a basal part that was injected with mafic magma which indicates that magma mixing may have been a dominant mechanism in the development of the chamber. This model is supported by both Harker variation plots and abundant lithologic evidence of magma mixing.

Harker variation plots of the Tuff of Bridge Spring show cyclical patterns of variation for several major and trace elements (Fig. 28), which suggests hybridization of a felsic-dominated magma chamber by an influx of mafic magma, and subsequent re-equilibration of the system to more felsic compositions.

Lithologic evidence that magma mixing occurred in the source chamber of the Tuff of Bridge Spring include the occurrence of (1) glomerocrysts, (2) mafic enclaves, and (3) disequilibrium textures in feldspars.

Glomerocrysts are ubiquitous in thin sections of the Tuff of Bridge Spring. The presence of crystal clusters is evidence of magma hybridization processes. These processes can include magma mixing (Davidson et al., 1990; Seaman and Ramsey, 1992).

The presence of disequilibrium textures in feldspars indicate re-equilibration in response to changes in magma composition. Such changes may be due to magma

mixing processes (Hyndman, 1985). Disequilibrium textures in Tuff of Bridge Spring feldspar phenocrysts include resorbed margins in sanidine phenocrysts, sieve textures in plagioclase and sanidine, and mantling of plagioclase phenocrysts by sanidine.

Macroscopic indicators of magma mixing in the Tuff of Bridge Spring include the occurrence of banded fiamme and mafic enclaves (see field description section). Mills (1991, 1993) interpreted the presence of banded, compositionally-mixed pumice in the Rainier Mesa and Ammonia Tanks Members of the Timber Mountain Tuff, Nevada, and mafic enclaves in the Tuff of Hoover Dam, Nevada/Arizona as the volcanic equivalent of the classic magma mixing textures described in northern Colorado River extensional corridor intrusive rocks (e.g., Naumann, 1987; Larsen, 1990; Larsen and Smith, 1990; Metcalf et al., 1992, 1993). The occurrence of banded fiamme at the Bridge Spring type locality (unpublished field observation, Smith, 1993), and several small, porphyritic mafic inclusions (< 3.0 cm wide) in the Eldorado Mountains and Temple Bar sections are interpreted here to be mafic enclaves. These inclusions have crenulate margins but lack the characteristic chilled, glassy margins and coarser-grained interiors of "typical" mafic enclaves (Koyaguchi, 1986).

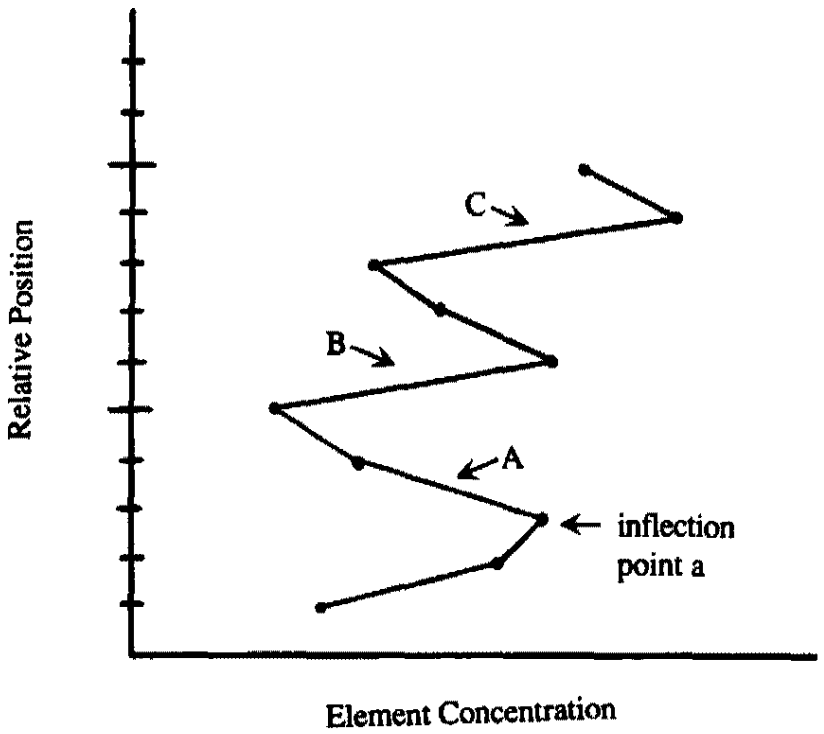

Figure 18. Diagram showing different types of chemical breaks. (A) Chemical break occurs between two trends that have opposite slopes. Reversal in slope occurs at inflection point a. (B) Chemical break occurs between two trends that have the same slope. Trends are separated by a wide chemical gap. (C) Chemical break occurs between two trends that have opposite slopes. Trends are separated by a wide chemical gap.

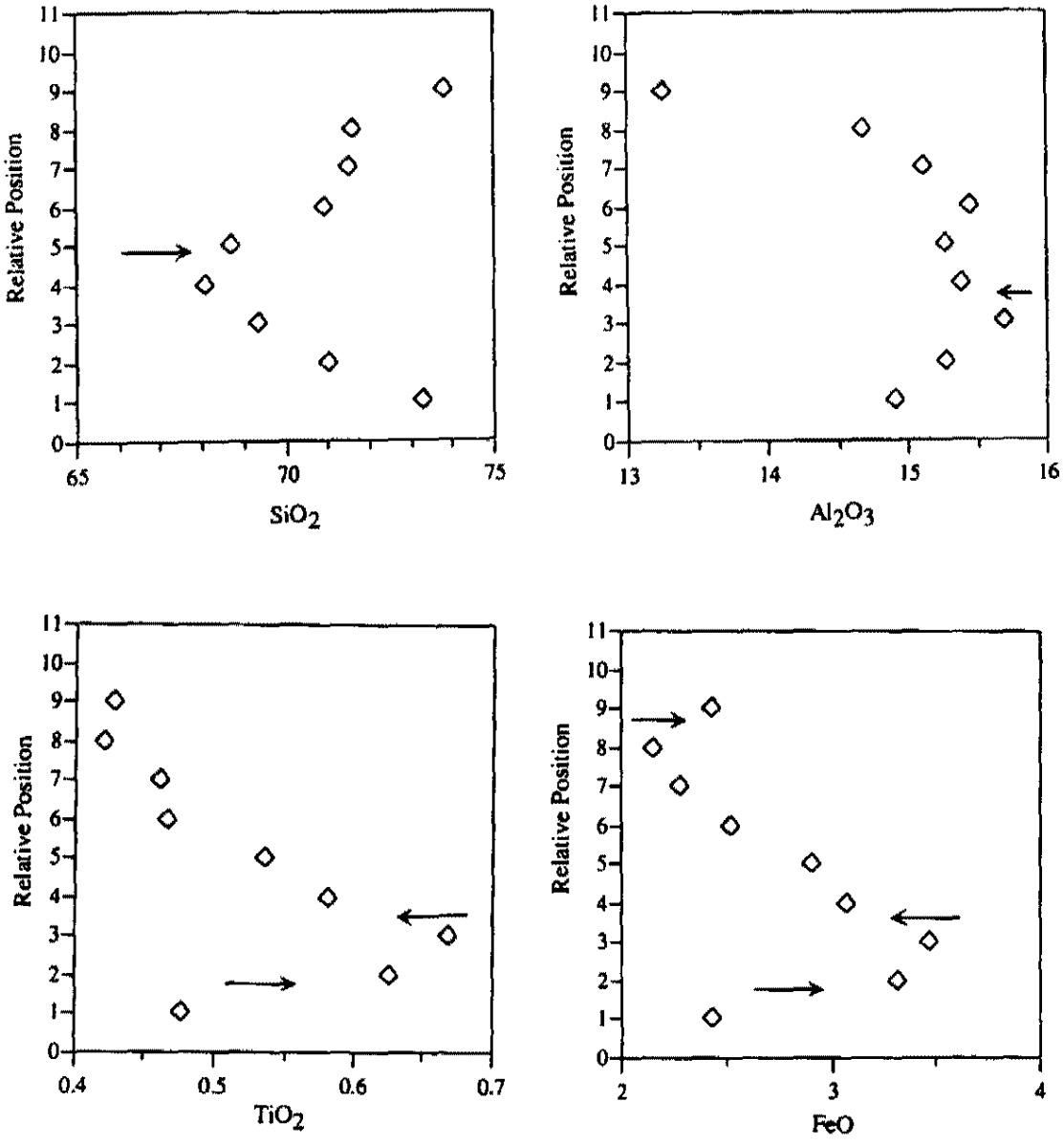

Figure 19. Plot of relative position vs. element concentration for the Eldorado Mountains section showing chemical breaks. Arrows indicate positions of chemical breaks.

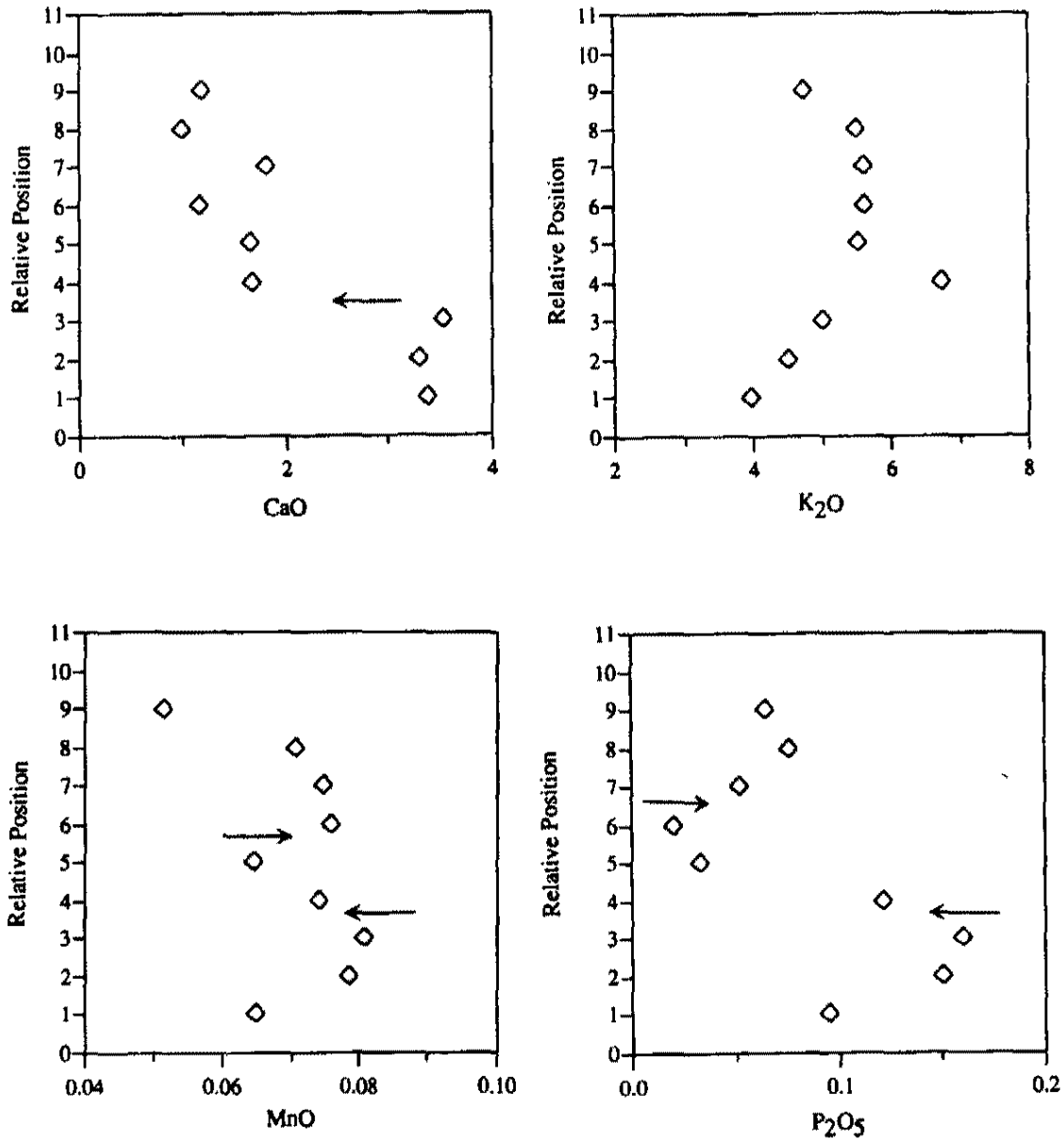

Figure 19, continued.

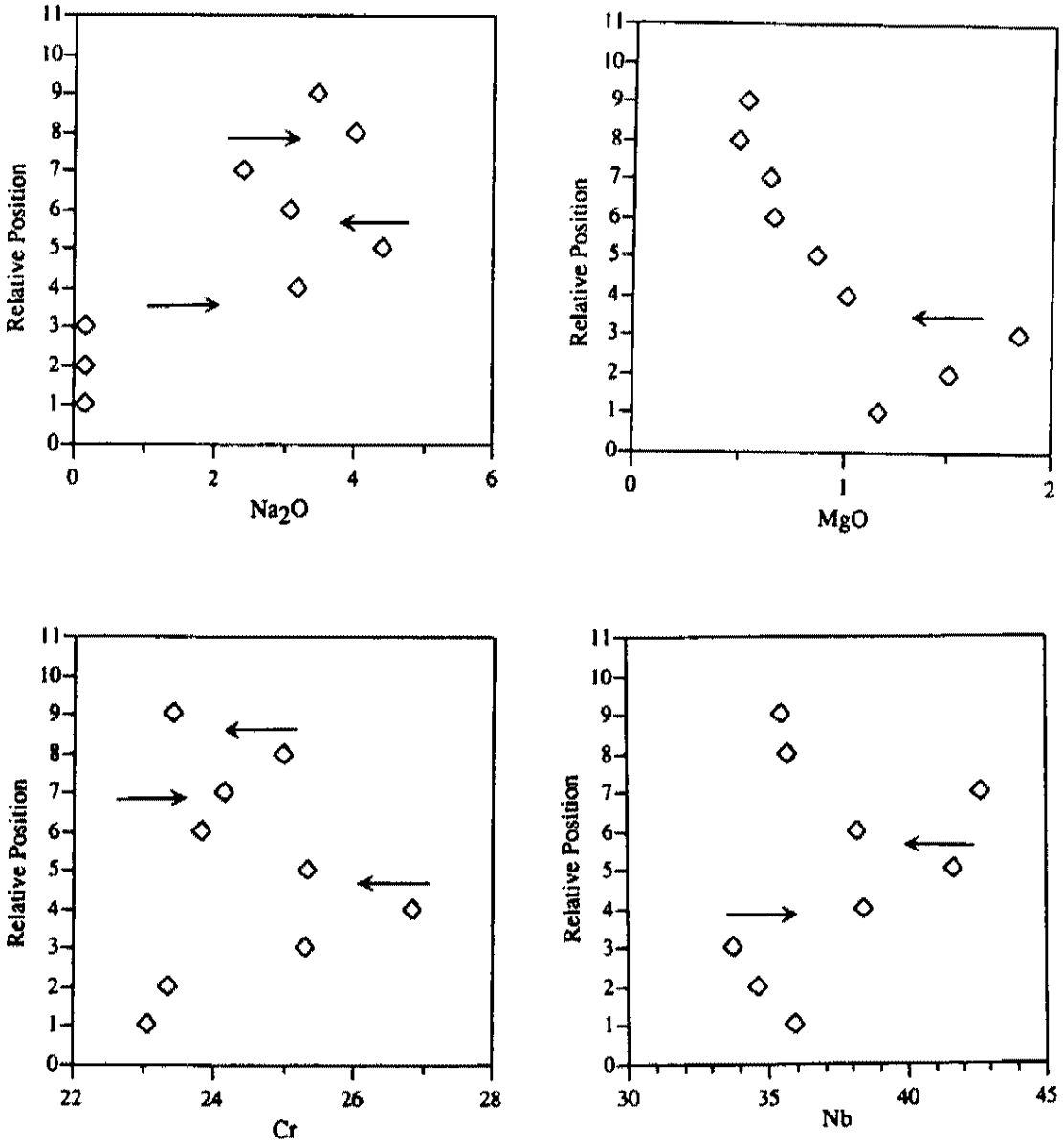

Figure 19, continued.

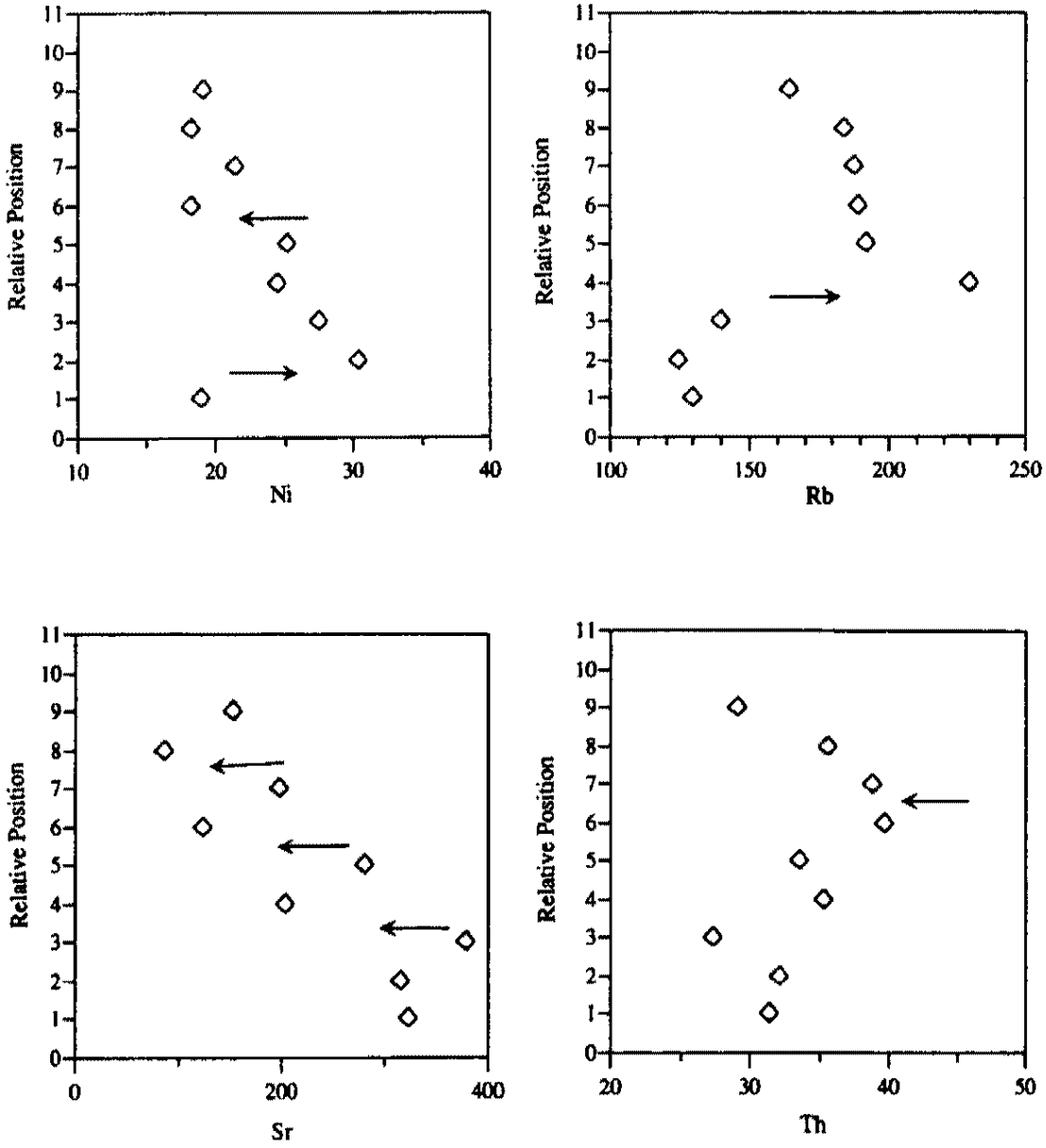

Figure 19, continued.

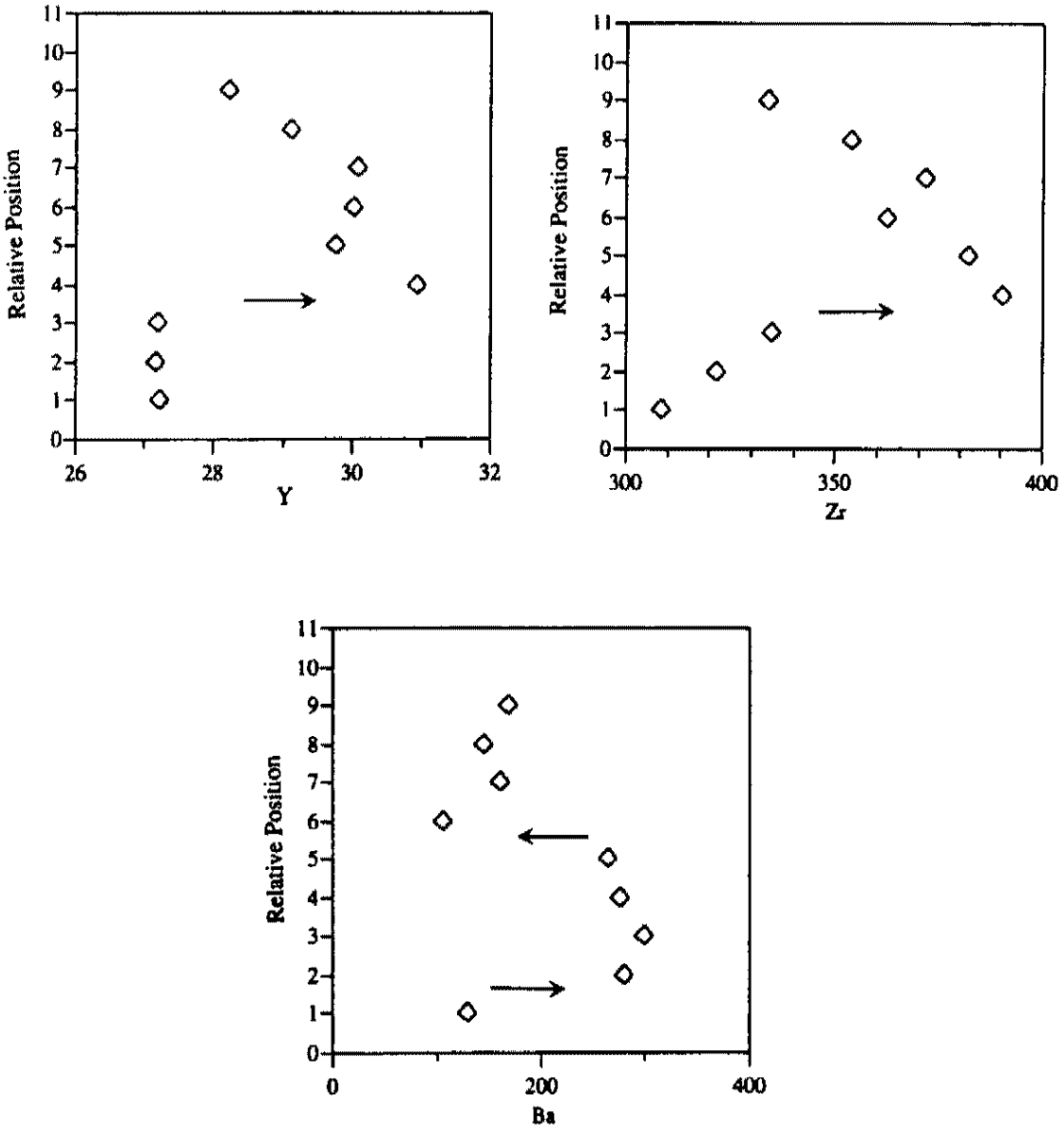

Figure 19, continued.

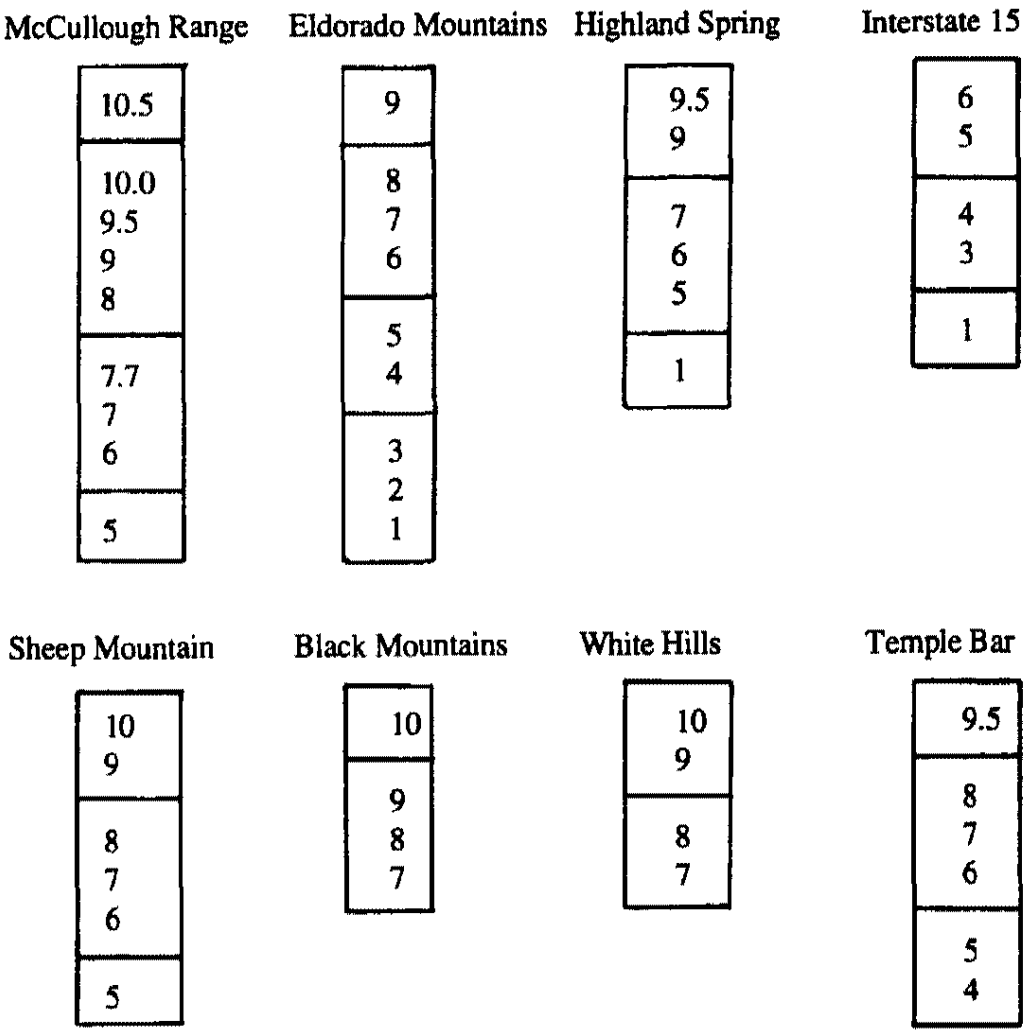

Figure 20. Division of Tuff of Bridge Spring stratigraphic sections into eruptive units. Numbers indicate relative stratigraphic position of each interval.

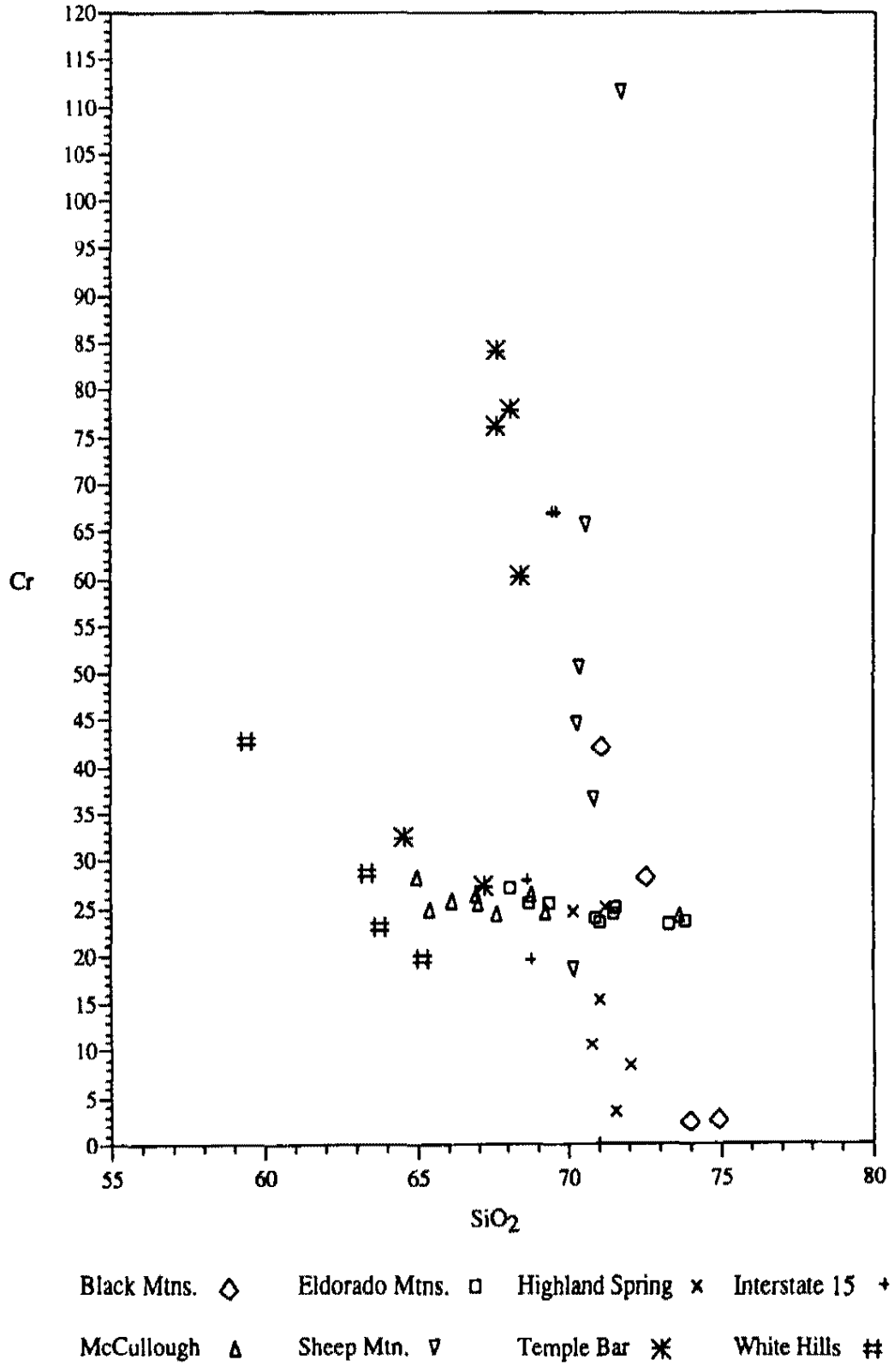

Figure 21. Plot of Cr vs. SiO_2 showing division of the Tuff of Bridge Spring into constant Cr and variable Cr members. See text for explanation.

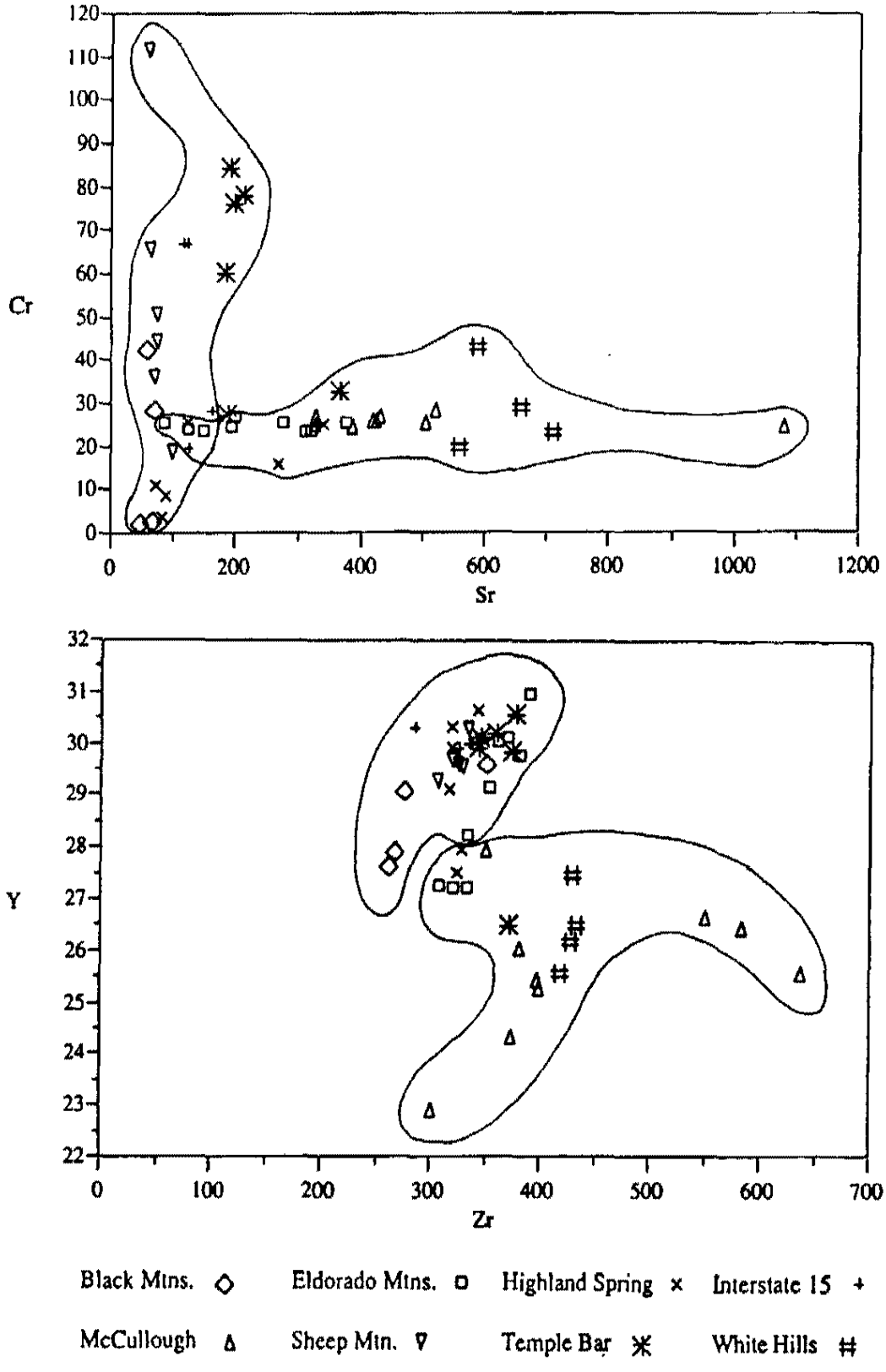

Figure 22. Plots of Cr vs. Sr and Y vs. Zr. See text for explanation.

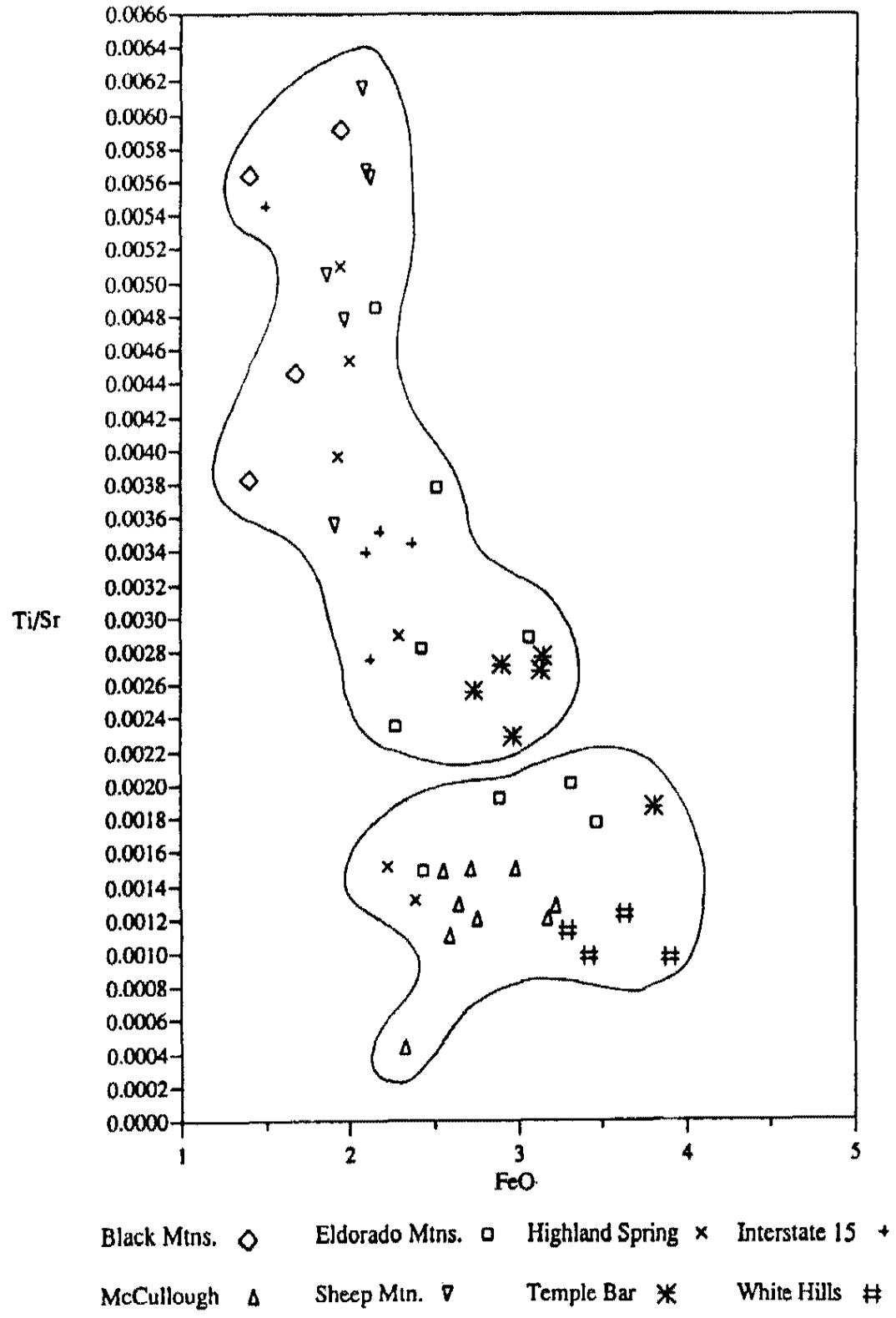

Figure 23. Plot of Ti/Sr vs FeO. See text for explanation.

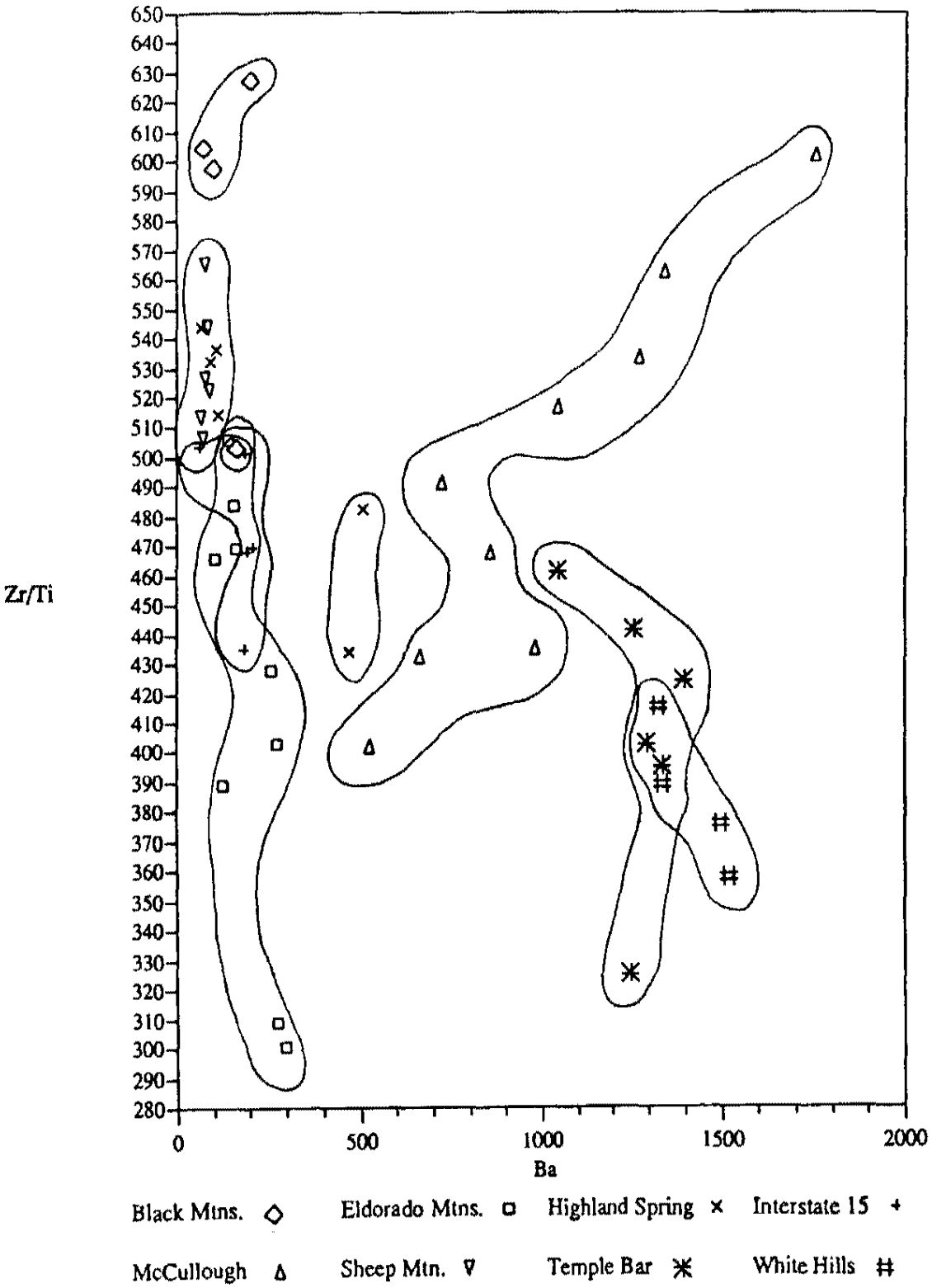

Figure 24. Plot of Zr/Ti vs. Ba showing division of the Tuff of Bridge Spring into variable Zr/Ti, constant Ba group (constant Cr member), and variable Zr/Ti, variable Ba group (variable Cr member).

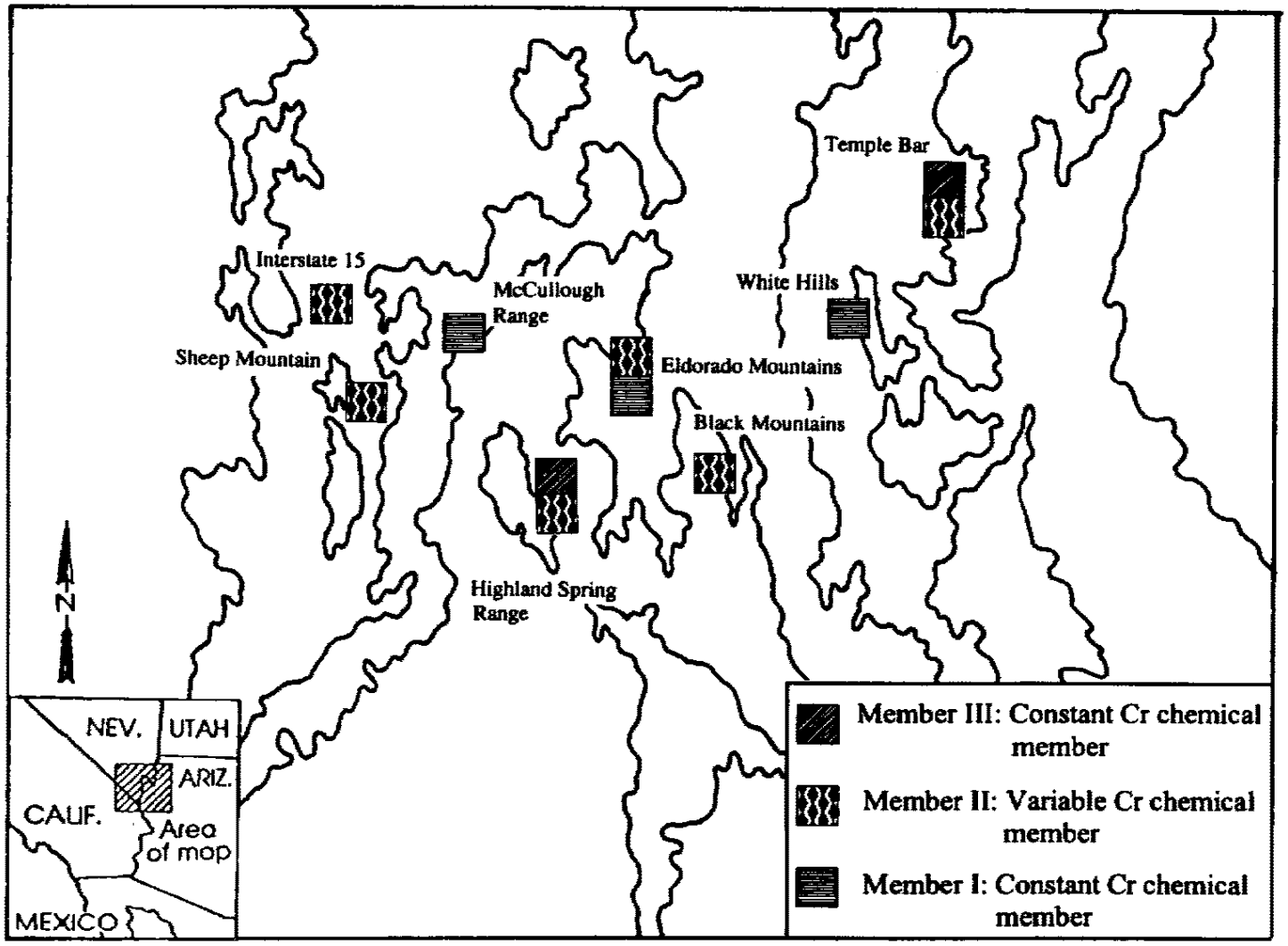

Figure 25. Regional members of the Tuff of Bridge Spring. See text for explanation.

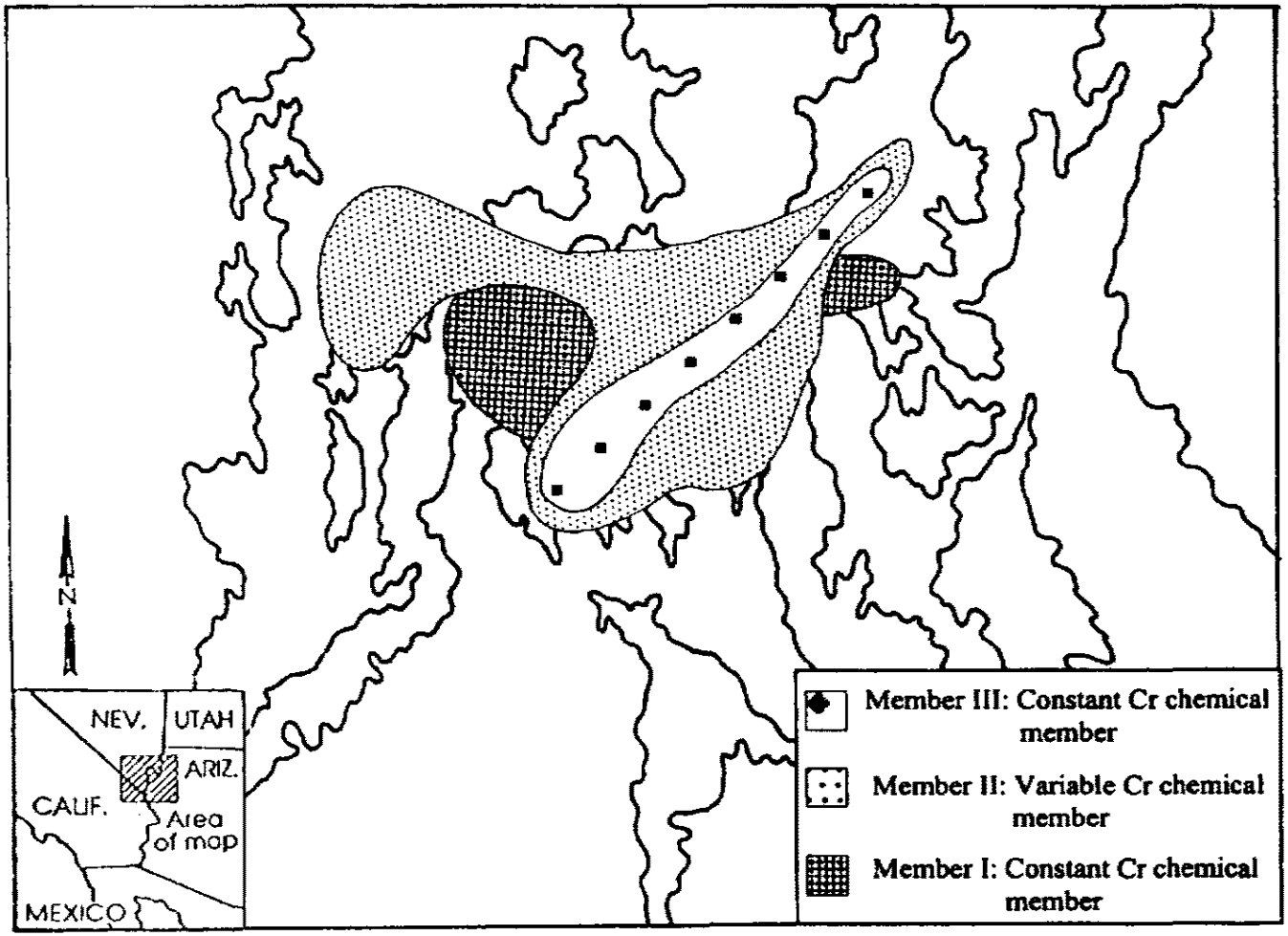

Figure 26. Distribution of the regional members of the Tuff of Bridge Spring.

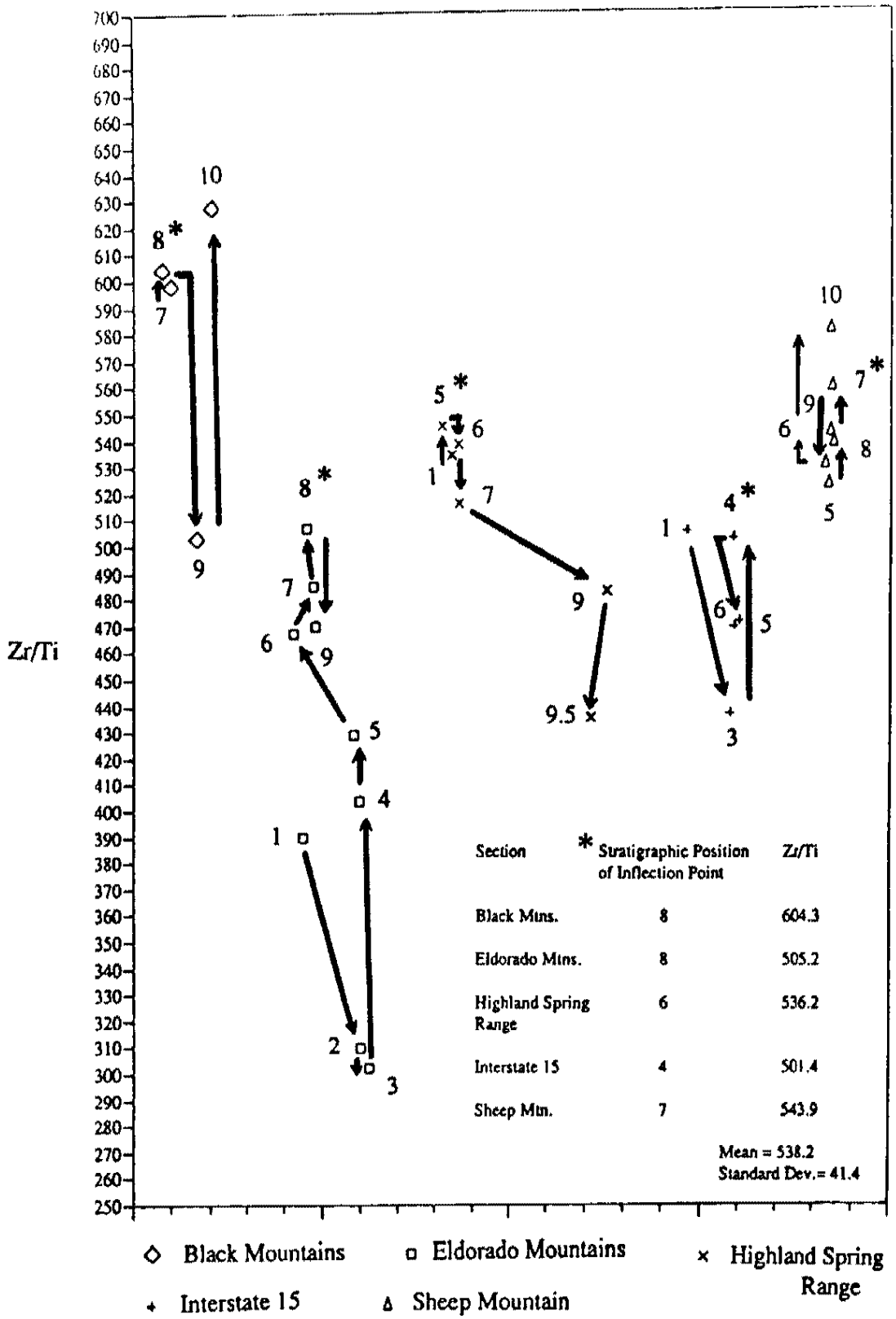

Figure 27. Compilation of plots of sections with variable Zr/Ti, constant Ba showing chemical paths and inflection points. See text for explanation.

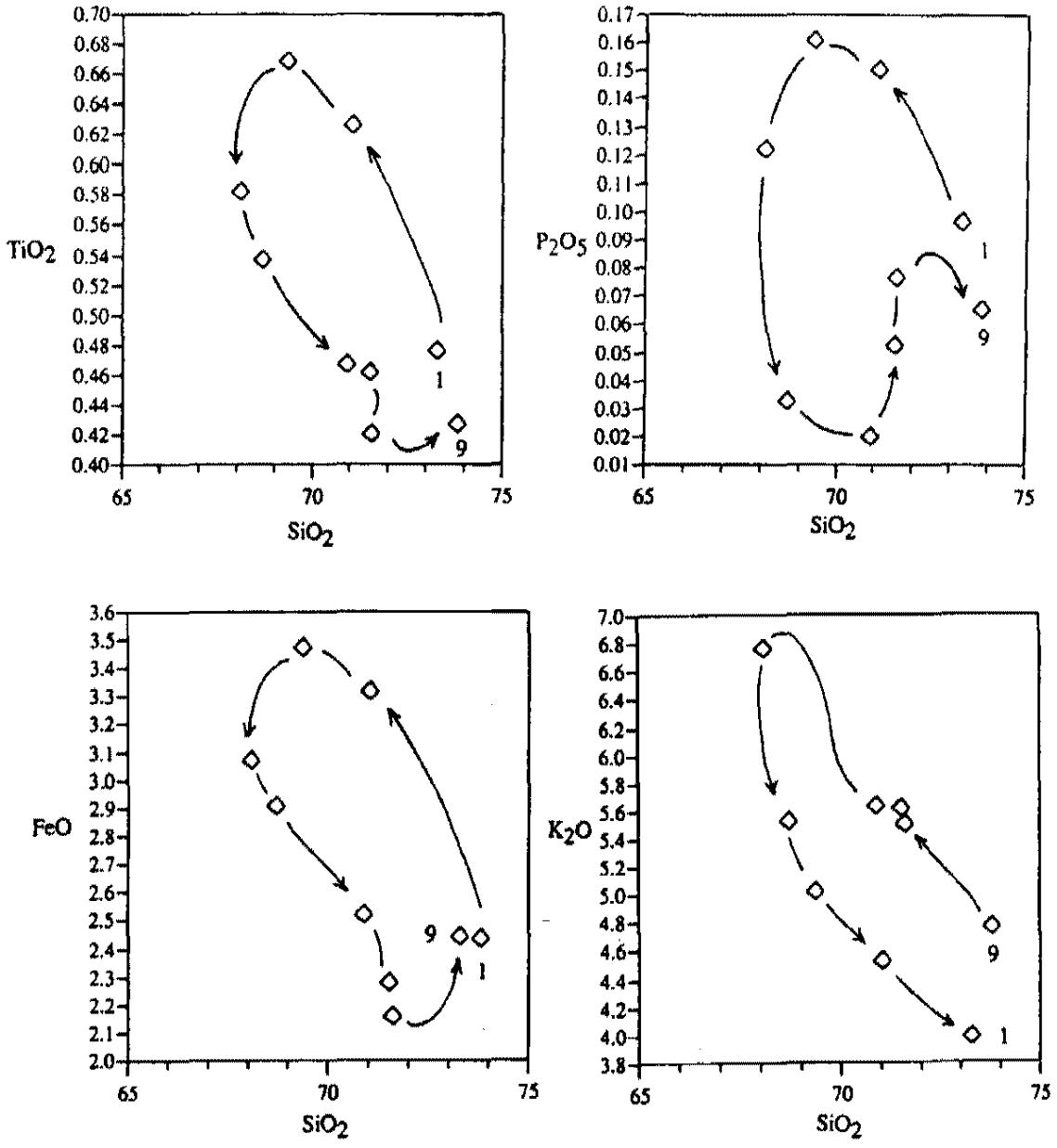

Figure 28. Harker variation plots of the Eldorado Mountains section showing cyclical variation. Numbers indicate relative stratigraphic position of each sample.

Location of Source

Introduction

Several investigators who have utilized the Tuff of Bridge Spring as a marker horizon have also inquired as to the location of its source. Anderson (1971) suggested that the source of the Tuff of Bridge Spring is located in the Chemehuevi Valley, California based on similarities of lithology and phenocryst mineralogy of these rocks to the Tuff of Bridge Spring in the Eldorado Mountains (Fig. 1). Analysis of flow direction indicators in the Tuff of Bridge Spring in the Eldorado Mountains by Brandon (1979) indicated a source to the southwest, perhaps in the Mojave Desert of California. Walker et al. (1981) speculated that the source of the Erie Tuff (the Interstate 15 member of the Tuff of Bridge Spring, this study) is the Devil Peak volcanic complex in the southern Spring Range of Nevada. Hewett (1956) suggested that the Erie Tuff erupted from a source in the western McCullough Range.

In general, correlation of ash-flow tuffs to specific source calderas is difficult in structurally-complex regions like the northern Colorado River extensional corridor. Because regions of intense structural disruption may also be subjected to high rates of erosion and sedimentation, it is probable that the characteristic topographic and lithologic features of calderas and associated intracaldera deposits (e.g., deeply-embayed topographic margins, megabreccia deposits, thick intracaldera fill deposits) may be obscured or obliterated in tectonically-active areas. In the Great Basin, over one hundred ash-flow tuffs of Oligocene to Miocene age are known compared to fewer than 70 caldera structures (Best et al., 1989). The deficit of known calderas compared to outflow sheets indicates that correlations based on "conventional" field studies in highly deformed regions are likely to be unsuccessful or inconclusive.

Because the characteristic features of calderas that crop out in structurally-disrupted regions may either be destroyed or so distorted that field-based identification of these structures is not possible, correlation of outflow sheets to their source (this may be a caldera or a pluton depending upon the degree of erosion) must be established by corroboration of several different criteria. These criteria can include: radiogenic and/or stable isotopes, geochronology, geochemistry, microscopic or macroscopic flow indicators, paleomagnetic signatures, and field relationships. The present study uses radiogenic isotopes as the primary criteria for correlation of the Tuff of Bridge Spring to possible plutonic sources of equivalent age in the extensional corridor. Geochronology (where available), major/trace element analysis, field relationships and associated petrologic studies are used to support isotope-based correlations.

Examination of the data generated during the course of this study indicates that the Aztec Wash pluton, Nevada, and the Mt. Perkins pluton, Arizona are both likely candidates for the intrusive source of the Tuff of Bridge Spring.

Although the Dolan Springs volcanic section does not correlate with the Tuff of Bridge Spring (see correlation section), it is still of considerable interest in this study because the association of the Dolan Springs ash-flow tuff with proximal-type pyroclastic deposits suggests that a caldera structure is located nearby. Also of interest is the close proximity of the Dolan Springs section to the 15.96 Ma Mt. Perkins pluton (Metcalf et al., 1992, 1993). The similarity of the isotopic signatures and ages of the Dolan Springs section and Mt. Perkins pluton and the presence of a major detachment structure (the Mockingbird Mine fault) between the two blocks has important implications for the correlation of the Mt. Perkins pluton to the Dolan Springs section (see discussion below).

Radiogenic Isotopes

Isotopic ratios are not altered by magma fractionation, eruptive, or weathering processes, which makes them excellent indicators of magmatic source (see internal stratigraphy discussion). Variation of isotopic ratios is controlled by conditions which are unique to each magma chamber. These conditions include: the isotopic signature of the contaminant, the amount of contaminant incorporated, and the isotopic signature of the host rock. Consequently, each cogenetic pluton/caldera/outflow suite should possess an unique isotopic signature which can be used as a correlation reference.

Fig. 29 shows the plot of the ε_{Nd} vs. $^{87}Sr/^{86}Sr$ values for the Tuff of Bridge Spring and several plutonic and volcanic suites in the northern Colorado River extensional corridor. This plot indicates that the array of the Tuff of Bridge Spring is distinct from both the River Mountains and the White Hills fields, but is coincident with the Nelson/Aztec Wash pluton and the Mt. Perkins pluton data sets. These comparisons suggest that the Tuff of Bridge Spring is cogenetic with both the Aztec Wash and Mt. Perkins plutons.

In general, Pb isotopes are more sensitive indicators of isotopic change (particularly crustal contamination) in evolving magmatic systems than are values of ε_{Nd} and $^{87}Sr/^{86}Sr$ (Wilson, 1989). Given this sensitivity, correlation of outflow sheets to possible plutonic equivalents using Pb is generally not attempted. However, several interesting relationships are present in the Tuff of Bridge Spring Pb system that warrant a brief description here.

The plot of $^{87}Sr/^{86}Sr$ vs. $^{206}Pb/^{204}Pb$ (Fig. 30) for the Tuff of Bridge Spring and selected northern Colorado River extensional corridor plutons/volcanic sequences shows that the Tuff of Bridge Spring is isotopically distinct from the Boulder City and Wilson Ridge plutons as well as from the general trend of rocks of the White Hills and

River Mountains. The plot also shows that the trend of the Tuff of Bridge Spring is generally parallel to, but not coincident with, the trend of the Nelson/Aztec Wash plutons. $^{87}Sr/^{86}Sr$ vs. $^{206}Pb/^{204}Pb$ values of Mt. Perkins quartz diorite and diorite fall significantly off the Tuff of Bridge Spring trend. The isotopic values of the Mt. Perkins pluton granodiorite and gabbro, however, lie at either end of the Tuff of Bridge Spring data array. This relationship suggests that magmatic compositions similar to granodiorite and gabbro of the Mt. Perkins pluton are end members of the Tuff of Bridge Spring mixing array.

Geochronology

An important criterion for correlation of outflow sheets to cogenetic intrusive rocks is radiometric dating (Hildreth and Mahood, 1985; Best et al., 1989). Due to the utility of the Tuff of Bridge Spring as a stratigraphic marker horizon, a considerable number of radiometric age analyses of the Tuff of Bridge Spring are available for comparison to ages of selected plutons. Presently, geochronology of the Tuff of Bridge Spring consists of three $^{40}Ar/^{39}Ar$ analyses (two incremental release and two laser fusion analyses) and six K/Ar analyses (Table 7). The presence of substantial discrepancies between $^{40}Ar/^{39}Ar$ and K/Ar analyses of the Tuff of Bridge Spring (discussed below) indicates that any final determination of the age of the Tuff of Bridge Spring cannot be made without obtaining additional incremental release $^{40}Ar/^{39}Ar$ data on the Tuff of Bridge Spring. In lieu of this work, however, an age of 15.23 ± 0.14 Ma (incremental release Ar/Ar, sanidine, Bridwell, 1991) will be tentatively accepted in this study as being representive of the true age of the Tuff of Bridge Spring. Comparison of this date to radiometric age analyses of the Aztec Wash and Mt. Perkins plutons will also be presented below.

Discrepancies in Tuff of Bridge Spring Geochronology

$^{40}Ar/^{39}Ar$ dates of the Tuff of Bridge Spring range from 15.12 ± 0.03 Ma to 15.24 ± 0.01 Ma, and K/Ar analyses range from 14.4 ± 0.5 to 16.6 ± 0.5 Ma (Table 7). In general, inconsistencies in dates generated by the two analytical methods are significant and can be summarized as follows: (1) K/Ar dates are generally 0.80 to 1.37 Ma older than $^{40}Ar/^{39}Ar$ values; (2) Tuff of Bridge Spring samples collected from different areas and analyzed using the same method have different dates; and (3) samples collected at different stratigraphic postions from the same section and analyzed by the same method have different dates.

Differences in radiometric dates of the Tuff of Bridge Spring may have resulted from one or more of the following factors: (1) differences in retention of Ar and K in sanidine and biotite; (2) differences due to geographic origin of the sample being analyzed; (3) differences associated with stratigraphic position of the sample; (4) differences generated by the method of analysis chosen; and (5) non-agreement of cross laboratory data (unpublished study, Morikawa, 1993). Although it is generally conceded that the small sample size requirements and high precision of the laser fusion $^{40}Ar/^{39}Ar$ method makes it the technique of choice in correlations of ash-flow tuffs (Hildreth and Mahood, 1985), the presence of substantial inconsistencies between $^{40}Ar/^{39}Ar$ and K/Ar analyses of the Tuff of Bridge Spring indicate that more information is required to evaluate the effects of these factors on the calculated age of the Tuff of Bridge Spring. Until the reason for these inconsistencies are understood, all dates of the Tuff of Bridge Spring should be regarded with suspicion.

Comparative Geochronology

A recently completed U/Pb analysis by Calvin Miller (personal communication to E.I. Smith, 1993) indicates that the Aztec Wash pluton is 15.12 ± 0.6 Ma old. Laser fusion $^{40}Ar/^{39}Ar$ analysis (sanidine) of the Mt. Perkins pluton by Faulds (personal communication to E.I. Smith, 1993) indicates a date of 15.96 ± 0.04 Ma. While the older date of the Mt. Perkins pluton appears to preclude it from consideration as the source of the Tuff of Bridge Spring, it is the contention of this study that any correlation of the Tuff of Bridge Spring to a specific pluton/caldera that is based on either K/Ar or $^{40}Ar/^{39}Ar$ geochronology should be considered inconclusive based on the arguments presented above. The U/Pb age of the Aztec Wash pluton, on the other hand, is analytically consistent within uncertainty to the 15.23 ± 0.14 Ma age of the Bridwell (1991) analysis of the Tuff of Bridge Spring. The large uncertainty of the Aztec Wash pluton analysis, however, severely limits its usefulness for correlation purposes.

In summary, correlation of the Tuff of Bridge Spring with the Mt. Perkins and Aztec Wash plutons cannot, at this time, be made on the basis of comparative geochronology due to inconsistencies between K/Ar and $^{40}Ar/^{39}Ar$ analyses of the Tuff of Bridge Spring and the large uncertainty of the Aztec Wash pluton analysis.

Geochemistry

Conventional geochemistry-based correlations of volcanic outflow to cogenetic intrusive rocks (e.g., Weber and Smith, 1987) cannot be applied in this study due to lack of available geochemistry of either the Mt. Perkins or the Aztec Wash plutons. Geochemistry-based correlation of both the Aztec Wash and Mt. Perkins plutons to the

Tuff of Bridge Spring is limited, at this time, to two empirical observations. First, the three magmatic systems are highly variable in composition. The Aztec Wash pluton ranges in composition from an olivine gabbro to an aplite (SiO_2 = ca. 50 to 76 wt. %) (Falkner et al., 1993). The Mt. Perkins pluton ranges in SiO_2 composition from 43 to 73 wt. % (Metcalf et al., 1993). The Tuff of Bridge Spring varies from andesite to rhyolite in composition (SiO_2 = 57.467 to 74.912 wt. %). The second observation is that the three magmatic systems generally exhibit geochemical signatures that suggest that magma mixing was important in their petrogenesis (Falkner et al., 1993; Metcalf et al., 1993).

Presented below is a more unconventional technique of geochemistry-based correlation developed for this study that uses Zr/Ti vs. Ba chemical paths (previously introduced in the internal stratigraphy section) as points of reference to determine the completeness with which a particular stratigraphic section preserves the chemical evolution of the Tuff of Bridge Spring. This information can then be used to distinguish proximal sections from distal sections, and, by inference, which sections are located closest to the Tuff of Bridge Spring caldera.

Chemical path correlation

Chemical paths, as described previously in the internal stratigraphy section, preserve a sequential chemical record of the magmatic evolution of the Tuff of Bridge Spring. In addition to their utility in regional correlation of Tuff of Bridge Spring flow units, chemical paths can also be used to roughly quantify how completely the chemical record is preserved in a given stratigraphic section. Since proximal pyroclastic deposits contain more complete accumulations of pyroclastic material than more distally located deposits, those sections which are characterized by chemical paths which preserve the

most complete magmatic histories of the Tuff of Bridge Spring, by inference, were deposited in relatively more proximal positions. Determination of the relative proximity of selected sections can then be used much in the same manner as conventional stratigraphic fence diagrams to pinpoint the location of the Tuff of Bridge Spring source.

Fig. 31 shows a plot of an idealized Zr/Ti versus Ba chemical path that preserves the entire magmatic history of a hypothetical, complete stratigraphic section. Also shown is a diagramatic representation of an idealized, incompletely mixed magma chamber with several Zr/Ti chemical paths. Assuming that the chemical paths preserve a sequential chemical record of the magmatic evolution of the Tuff of Bridge Spring, any point on the chemical path represents a specific magmatic composition that was present in a zoned magma chamber prior to eruption of the Tuff of Bridge Spring. More distally located sections will preserve only fragments of the complete chemical path and more proximal sections will contain more complete records of the path.

The Zr/Ti versus Ba plot of the Tuff of Bridge Spring (Fig. 24) shows that of the five stratigraphic sections that comprise the constant Cr chemical member, the chemical path of the Eldorado Mountains Tuff of Bridge Spring section preserves the most complete record of magmatic evolution of the upper and intermediate levels of the Tuff of Bridge Spring source magma chamber. This implies that the Eldorado Mountains section is the most proximally located of these sections. Similarly, the chemical path of the Highland Spring section, which is the most incomplete of the constant Cr chemical member, implies that early and late occurring flows of the Tuff of Bridge Spring never reached the Highland Spring Range, which was located at the edge of the Tuff of Bridge Spring distribution area. Similarly, chemical path records of both the Sheep Mountain, Interstate 15, and Black Mountains sections preserve magmatic

variations that were present during the middle and late stages of the Tuff of Bridge Spring eruptive sequence.

A proximal deposit should preserve a complete chemical record of a magmatic sequence erupted from a zoned parent chamber. Hypothetically, the chemistry of the most proximally located section of the Tuff of Bridge Spring should have the most complete chemical path on a Zr/Ti vs. Ba plot (i.e., a plot of such a section should preserve both the variable Zr/Ti, constant Ba trend as well as the variable Zr/Ti, variable Ba trend) (Fig. 24). Paradoxically, the Eldorado Mountains section does not preserve such a chemical record. Magmatic variations that characterize the lower levels of the evacuated Tuff of Bridge Spring magma chamber are missing from the chemical path record of this section. This discrepancy may be an artifact of either incomplete sampling or incomplete preservation. The presence of large-scale flow lobes in the Tuff of Bridge Spring in the Eldorado Mountains suggest that ash-flow tuff deposition was laterally discontinuous in the Eldorado Mountains (see field criteria section). This observation suggests that the stratigraphic section chosen for geochemical sampling in the Eldorado Mountains is incomplete. Sampling of a series of sections in the Eldorado Mountains would be required to overcome the effects of laterally-discontinuous exposures.

Field and Petrologic Studies

Conventional field-based correlations of ash-flow tuffs to cogenetic intrusive rocks in tectonically-disrupted regions such as the western United States may be inconclusive or unsuccessful due to problems of preservation, exposure, and/or extreme distortion of contact relationships. However, field studies and related petrographic studies are useful adjuncts to the other correlation criteria employed in this study.

There are many distinctive field indicators that can be used to aid correlation of ash-flow tuffs to cogenetic intrusive rocks. These feature include: (1) outcrop-scale field indicators of distal/proximal deposition (these include cooling breaks, coignimbrite lag breccias, differences in modal phenocryst populations, gas segregation features, stratigraphic thicknesses, lobate outcrop habit, surge/airfall deposits, and pumice-rich deposits) (Fisher and Schmincke, 1984); (2) geographical location and spatial relationships of pluton to outflow; and (3) the presence of features commonly associated with calderas including megabreccia deposits, topographic caldera rim, thick intracaldera accumulations, etc.; and (4) the occurrence of magmatic mixing textures in both intrusive and extrusive members of the same cogenetic suite.

Several lines of field evidence support the isotope-based correlation of the Tuff of Bridge Spring to the Aztec Wash pluton (Fig. 4). These include: (1) field indicators of proximal deposition; (2) geographical location of the Aztec Wash pluton with respect to the Tuff of Bridge Spring distribution area; and (3) presence of mixing textures in both the Tuff of Bridge Spring and the Aztec Wash pluton.

Field Indicators

Field indicators of proximal deposition that are present in the Tuff of Bridge Spring in the Eldorado Mountains include lobate bedforms and coignimbrite lag deposits. The presence of complex, large-scale lobate (pinch-and-swell) bedforms exposed in outcrop is one of the most striking outcrop features of the Tuff of Bridge Spring in the Eldorado Mountains. The presence of lobate bedforms indicate ash-flow tuff deposition in either very rough, incised terrain, or in near-vent depositional environments (Fisher and Schmincke, 1984).

Coignimbrite lag deposits, another indicator of near-vent deposition (Fisher and Schminke, 1984), were observed in exposures of Tuff of Bridge Spring that crop out at the Bridge Spring type locality. Tuff of Bridge Spring coignimbrite lag deposits consists of an approximately 1 m thick, laterally-discontinuous interval of lithic tuff that is composed of approximately 39 volume percent of angular to subrounded clasts (< 2 cm) of andesite and basaltic andesite in a glomerocrystic, devitrified matrix that contains phenocrysts of sanidine, plagioclase, biotite, and clinopyroxene.

Location of Pluton

The location of the Aztec Wash pluton in the center of the distribution area of the Tuff of Bridge Spring suggests it is the source of the Tuff of Bridge Spring (Fig. 2). Calderas commonly occur in the centers of radially-distributed outflow sheets in other areas of the Basin and Range (Best et al., 1989). The elongated shape of the present outcrop distribution of the Tuff of Bridge Spring probably resulted from extensional deformation of an ash flow sheet which originally had a circular distribution pattern (c.f., Best et al., 1989).

Magmatic Mixing Textures

The occurrence of magmatic mixing textures in the Tuff of Bridge Spring and in both the Aztec Wash and Mt. Perkins plutons lends support to the hypothesis that the Tuff of Bridge Spring may be related to either one of these intrusive bodies. Falkner et al. (1993) documented impressive magmatic mixing textures in the Aztec Wash pluton including mafic enclaves and the late stage occurrence of mafic and felsic dikes.

Metcalf et al. (1993) reported similar magmatic mixing textures in the Mt. Perkins pluton.

Evidence of magma mixing in the Tuff of Bridge Spring includes the occurrence of banded fiamme in outcrop near the formation's type section, and the possible occurrence of mafic enclaves in outcrop (see lithology section). Microscopic-scale indicators of magma mixing processes present in the tuff include: (1) glomerocrysts, (2) altered mafic enclaves, and (3) disequilibrium textures in plagioclase and potassium feldspar phenocrysts (see lithology section). These characteristics are interpreted here as comprising additional evidence of the occurrence of magma mixing processes in the Tuff of Bridge Spring.

The Dolan Springs Volcanic Section

Similarity of the Nd and Rb isotopic signature of the proximal volcanic deposits of the Dolan Springs section with the Mt. Perkins pluton, their similar ages, and the close proximity of the two magmatic systems (approximately 15 km) suggests they are cogenetic (see regional correlation section). An eastward dipping, low-angle detachment fault, the Mockingbird Mine fault, crops out between the Dolan Springs section and the Mt. Perkins pluton (Faulds, 1989). At the present time, the kinematics of this structure is unknown (Faulds, personal communication to Smith, 1993). Definitive correlation of the Dolan Springs section to the Mt. Perkins pluton must be deferred until the geochemistry and isotope chemistry of the Mt. Perkins pluton is determined, and the kinematics of the Mockingbird Mine fault are understood.

Summary and Conclusion

Correlation of the Tuff of Bridge Spring to the Aztec Wash pluton, Nevada is supported by similarities of isotopic signature, highly variable geochemistry, chemical signatures that are suggestive of magma mixing processes, the presence of magma mixing textures in outcrop, and the occurrence of lobate flow features, coignimbrite lag deposits, and several other field indicators of proximal deposition that are present in the Tuff of Bridge Spring of the Eldorado Mountains. Correlation is also supported by the location of the Aztec Wash pluton near the center of the distribution area of the Tuff of Bridge Spring.

Radiogenic dates of the Tuff of Bridge Spring and the Aztec Wash pluton overlap within uncertainty, but the large error of the Pb date analysis of the Aztec Wash pluton makes any correlation that is based upon radiometric age analyses questionable.

Correlation of the Tuff of Bridge Spring to the Mt. Perkins pluton, Arizona is supported by similarities of isotopic signature, highly variable geochemistry, chemical signatures that are suggestive of magma mixing processes, and the presence of magma mixing textures in outcrops. However, these similarities may indicate that the two entities are not cogenetic, but were derived from similar isotopic reservoirs, and formed by magmatic processes that were operating on a regionally-extensive scale in this area during the middle Miocene. Similarities between the Tuff of Bridge Spring and the Mt. Perkins pluton are also contradicted by the significant differences in age analyses of the two entities. However, correlation of the Mt. Perkins pluton to the Tuff of Bridge Spring cannot be ruled out solely on the basis of radiometric age analyses because the $^{40}Ar/^{39}Ar$ and K/Ar geochronology of the Tuff of Bridge Spring has not been satisfactorily resolved.

Final correlation of either pluton to the Tuff of Bridge Spring is dependent upon the identification of intracaldera features in the Eldorado Mountains Tuff of Bridge Spring or in the volcanic cover of the Mt. Perkins pluton.

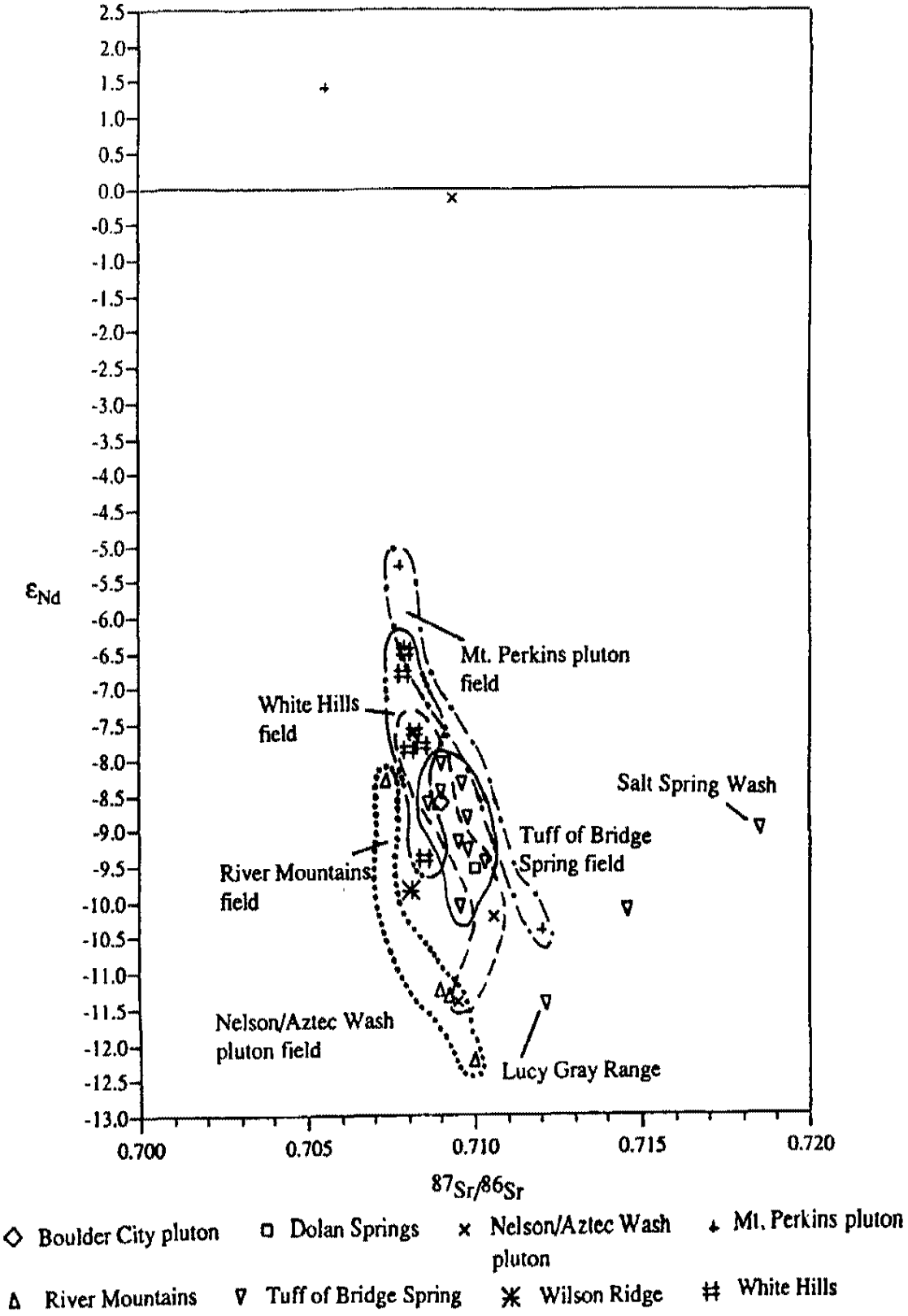

Figure 29. Plot of ε_{Nd} vs. $^{87}Sr/^{86}Sr$ for the Tuff of Bridge Spring and selected plutons and volcanic suites of the northern Colorado River extensional corridor.

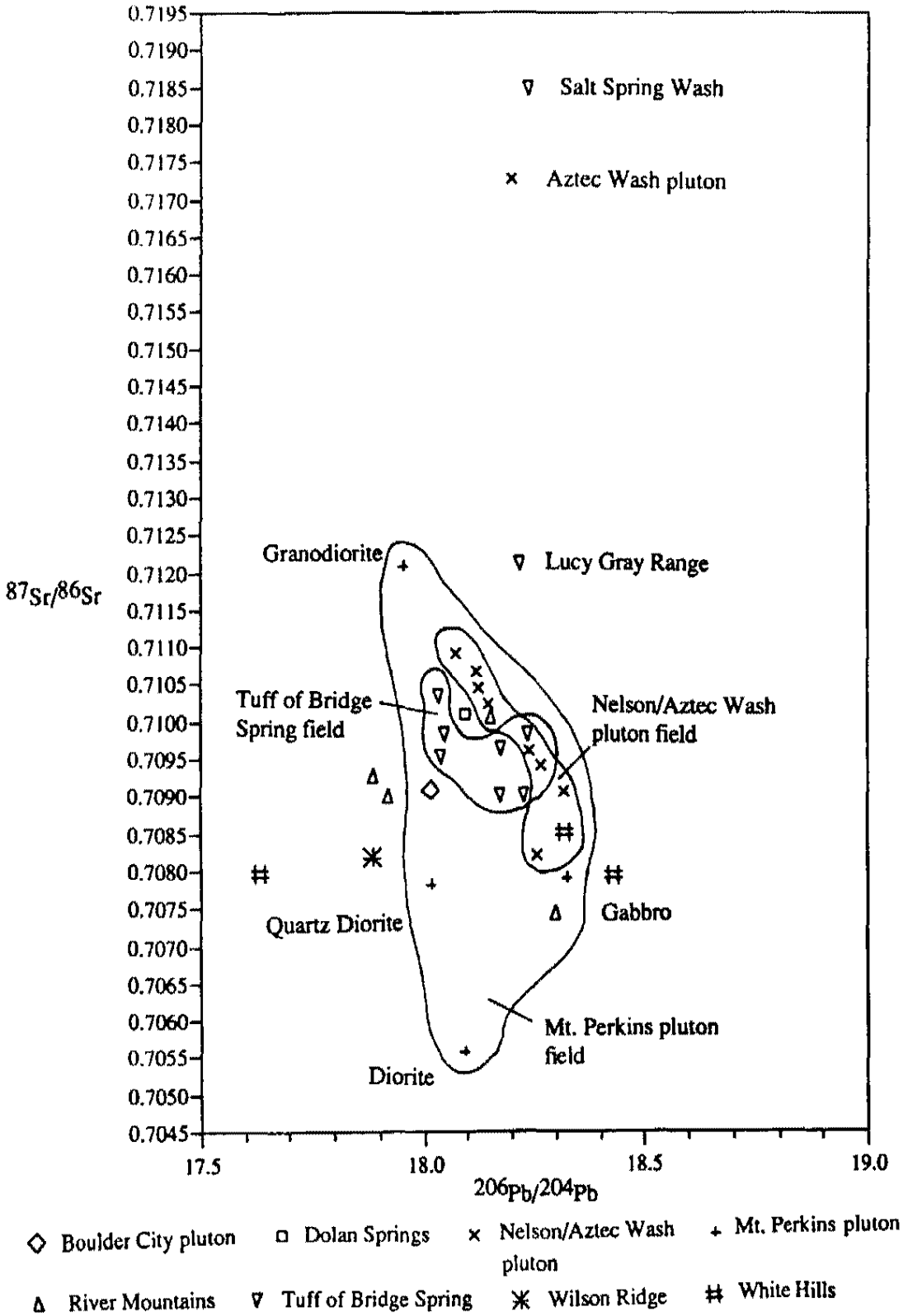

Figure 30. Plot of $^{87}Sr/^{86}Sr$ vs. $^{206}Pb/^{204}Pb$ for the Tuff of Bridge Spring and selected volcanic complexes and plutons of the northern Colorado River extensional corridor.

Table 7: $^{40}Ar/^{39}Ar$ Geochronology of the Tuff of Bridge Spring

Method: $^{40}Ar/^{39}Ar$	
Northern Eldorado Mountains, NV	**15.12 ± 0.03** Ma (personal commun., (basal cooling unit) Faulds, 1993) (laser fusion-sanidine)
Black Mountains, AZ	**15.24 ± 0.01** Ma (personal commun., Faulds, 1993) (laser fusion- sanidine)
McCullough Range, NV	**15.23 ± 0.14** Ma (Bridwell, 1991) (incremental release-sanidine)
Method: K/Ar	
Eldorado Mountains, NV	**15.92 ± 0.36** Ma (Faulds et al., 1992) (biotite)
Eldorado Mountains, NV	**14.5 ± 0.6** Ma (Anderson et al., 1972) (sanidine)
	14.4 ± 0.5 Ma (Anderson et al., 1972) (biotite)
Black Mountains, AZ	**16.43 ± 0.36** Ma (Faulds et al., 1992) (biotite)
McCullough Range, NV	**16.6 ± 0.4** Ma (Bridwell, 1991) (biotite)
White Hills, AZ	**16.4 ± 0.5** Ma (Cascadden, 1991) (biotite)

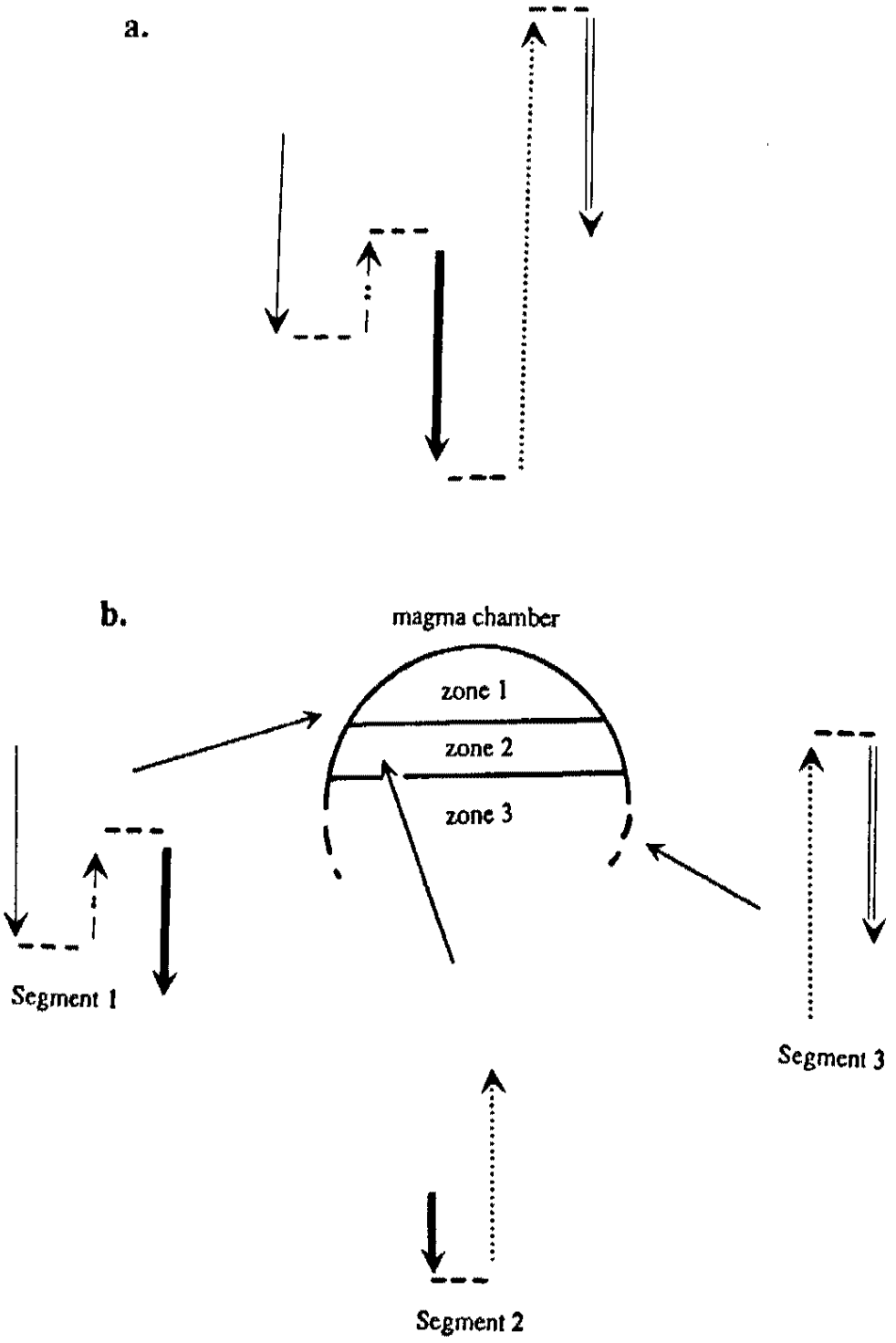

Figure 31. Hypothetical Zr/Ti vs. Ba chemical path diagram. (a) Complete Zr/Ti chemical path. (b) Three incomplete Zr/Ti path segments derived from three different chemical zones in a magma chamber.

Summary and Conclusion

The Tuff of Bridge Spring (15.23 ± 0.14 Ma) (Bridwell, 1991), a regionally-extensive ash-flow tuff, ranges in composition from andesite to rhyolite (59.50 to 74.91 wt. % SiO_2). The average composition of the Tuff of Bridge Spring is dacite (67 wt. % SiO_2). Phenocrysts include sanidine, plagioclase feldspar, biotite, clinopyroxene, sphene, opaque iron oxide, ± zircon, and ± apatite. Hornblende is rare and possibly xenocrystic. Quartz is a not primary phase in the Tuff of Bridge Spring.

Samples of the Tuff of Bridge Spring form linear data arrays on Sm, Rb, and Pb isotope diagrams. The linearity of these data arrays suggest that the Tuff of Bridge Spring is a cogenetic suite that formed as the result of magma mixing. Modelling using crustal and mantle derived contaminants that were present in this region during the Mid-Miocene (i.e., Patsy Mine Volcanics, Precambrian crystalline basement, and alkali olivine basalts) eliminates the possibility that the linear isotope arrays were produced by contamination. Based on these interpretations, and supported by geochemistry, petrology, and geochronology, the following stratigraphic sections are included within the Tuff of Bridge Spring; in Nevada, the Eldorado Mountains, Highland Spring Range, Interstate 15 (near Sloan), Sheep Mountain, and the McCullough Range, and in Arizona, the Black Mountains, Temple Bar, and White Hills. Isotope analyses of the Lucy Gray Range and Salt Spring Wash sections suggest that they are not cogenetic with the Tuff of Bridge Spring. The isotope signature of the Dolan Springs volcanic section falls within the Tuff of Bridge Spring data array, but an incremental release $^{40}Ar/^{39}Ar$ date of 16.01 ± 0.15 Ma (biotite; this study, 1993) shows that the section is significantly older that the Tuff of Bridge Spring. These relationships suggests that, although the Dolan Springs section does not correlate with the Tuff of Bridge Spring, the two rock types were derived from a common, regionally-extensive crustal/mantle

source that was present in the extensional corridor during the mid-Miocene. The overlap of ages of the Dolan Springs section with the Mt. Perkins pluton, and the presence of a low-angle detachment structure, the Mockingbird Mine Fault (Faulds, 1981) between the two bodies suggests that the Dolan Springs section may be the volcanic cover of the Mt. Perkins pluton.

The chemical variation in the Tuff of Bridge Spring is remarkably large and exists not only on the regional scale but on the scale of the stratigraphic section. Radical changes in chemical variation within each section form chemical boundaries which can be used to divide each section into a series of eruptive units which are the chemical equivalents of pyroclastic flow units (Smith, 1960). Because the formation of chemical boundaries is controlled by chemical re-equilibration of the magma chamber during periods of quiescence, chemical boundaries do not always coincide with cooling breaks. However, cooling breaks are not always preserved due to devitrification and/or vapor phase crystallization of ash-flow tuffs, which makes the use of chemical breaks and the eruptive unit concept extremely useful for determination of the internal stratigraphy in ash-flow tuffs.

The differential partitioning of elements such as Zr, Y, Cr, Sr, and Ba in the Tuff of Bridge Spring provide a means of dividing the formation into two chemically-distinct members. The constant Cr chemical member, which includes the McCullough Range, lower Eldorado Mountains, White Hills, upper Highland Spring Range, and upper Temple Bar sections, exhibits geochemical trends in which concentrations of Cr generally remain constant with respect to SiO_2. The variable Cr chemical member exhibits trends in which both Cr and SiO_2 are variable. This chemical member includes the Black Mountain, Interstate 15, upper Eldorado Mountains, lower Highland Spring, lower Temple Bar, and Sheep Mountain sections.

The division of the Tuff of Bridge Spring into three regional-extensive stratigraphic members is based on chemical member assignments and regional stratigraphic relationships. The stratigraphically lower and upper regional members belong to the constant Cr trend and the stratigraphically-intermediate regional member is part of the variable Cr trend. The regional members of the Tuff of Bridge Spring consist of the following (listed in ascending stratigraphic order): (1) Regional Member I: lower Eldorado Mountains, McCullough Range, and White Hills sections; (2) Regional Member II: Interstate 15, Sheep Mountain, lower Highland Springs, upper Eldorado Mountains, and lower Temple Bar; (2) Regional Member III: upper Highland Springs and upper Temple Bar.

Fine-scale chemical variations in the Tuff of Bridge Spring can be used as a stratigraphic marker horizon horizon. A single Zr/Ti vs. Ba chemical marker horizon occurs across 90 km of the tuff's distribution area. The presence of this horizon and the consistent patterns of geochemical partitioning found in the Tuff of Bridge Spring suggests that these patterns reflect chemical boundaries that were present in the Tuff of Bridge Spring magma system at the time of eruption. The presence of the Zr/Ti vs. Ba horizon also implies that, for certain elements, the chemical signatures exhibited by the Tuff of Bridge Spring are magmatic signatures that are not affected by changes in abundances of phenocrysts and/or xenoliths in whole rock samples. For these elements, and especially for Zr, Ti, and Ba, the signature imparted by the tuff's matrix is strong enough to overprint the non-magmatic signature or chemical "static" imparted from phenocrysts and xenoliths incorporated in the tuff.

The different behavior of Cr, Sr, Ba, and other elements in the Tuff of Spring suggests that petrogenesis of the tuff was controlled by two contrasting magmatic processes. The first process involved normal differentiation of a felsic magma in the top of the magma chamber. The second process involved injection of a mafic magma

into the lower part of the chamber and subsequent incomplete mixing of the two. The occurrence of these two processes are reflected in the assignments of the three regional members of the Tuff of Bridge Spring. The chemical signature of Regional Member I (constant Cr, variable SiO_2) reflects derivation from the top of a normally-zoned, felsic magma chamber. The chemistry of Regional Member II reflects derivation from a magma batch whose variable Cr, variable SiO_2 signature indicates injection and incomplete incorporation of a mafic magma into a felsic magma. The chemical signature of Regional Member III (constant Cr. variable SiO_2) indicates the return of the magma chamber to more felsic conditions. This model is supported by petrologic evidence including disequilibrium textures in feldspars and the rare presence of mafic enclaves.

Correlation of the Tuff of Bridge Spring to various plutons in the northern Colorado River extensional corridor by means of isotopic analysis suggests that both the Aztec Wash pluton, Nevada and the Mt. Perkins pluton, Arizona are likely sources for the Tuff of Bridge Spring. Isotope-based correlation of the Aztec Wash pluton to the Tuff of Bridge Spring is supported by several field indicators of proximal deposition, the presence of magma mixing textures, location near the center of the tuff's distribution center, and similarities in geochronology. Although the isotope signature of the Mt. Perkins pluton falls within the Tuff of Bridge Spring array, correlation of the Tuff of Bridge Spring to the Mt. Perkins pluton is not as well supported as the correlation with the Aztec Wash pluton. Also, dates of the two rock types are significantly different. However, the presence of consistent discrepancies between $^{40}Ar/^{39}Ar$ and K/Ar dates for the Tuff of Bridge Spring indicates that the geochronology of the tuff has not been adequately constrained. Therefore, correlation of the Mt. Perkins to the Tuff of Bridge cannot be ruled out.

Future Work

The following studies are recommended for future research in order to resolve several unanswered questions concerning the Tuff of Bridge Spring.

(1) Confirmation and refinement of the chemical member concept requires that analysis of Tuff of Bridge Spring for rare-earth elements (REE) geochemistry be completed.

(2) Microprobe analysis of tuff matrix and phenocrysts/xenoliths in whole rock tuff samples could not only be used to confirm the role of matrix in controlling the isotopic signature of the Tuff of Bridge Spring, but theoretically also could be used to numerically model/quantify the effects of chemical interferences imparted by phenocrysts/xenoliths.

(3) Resolution of the problems concerning $^{40}Ar/^{39}Ar$ and K/Ar analyses of the Tuff of Bridge Spring would require extensive dating of several sections using both incremental release and laser fusion $^{40}Ar/^{39}Ar$ techniques on both sanidine and biotite.

(4) Correlation of the Tuff of Bridge Spring to either the Mt. Perkins pluton or the Aztec Wash pluton is dependent on locating a caldera in the vicinity of either of those plutons. However, locating such a structure may not be possible. Correlation of the Tuff of Bridge Spring specifically to the Aztec Wash pluton could be strengthened by geochemical comparison.

(5) Correlation of the Dolan Springs section to the Mt. Perkins pluton requires detailed mapping of both the Mockingbird Mine fault and the Dolan Springs volcanic section.

References Cited

Anderson, R.E., 1971, Thin skin distension in Tertiary rocks of southeastern Nevada: Geological Society of America Bulletin, v. 82, p. 43-58.

Anderson, R.E., 1973, Large-magnitude late Tertiary strike-slip faulting north of Lake Mead, Nevada: U.S. Geological Survey Professional Pater 794, 18 p.

Anderson, R.E., Longwell, Cr.R., Armstrong, R.L., and Marvin, R.F., 1972, Significance of K-Ar ages of Tertiary rocks from the Lake Mead region, Nevada-Arizona: Geological Society of America Bulletin, v. 83, no. 2, p. 273-288.

Bennett, V.C., and DePaolo, D.J., 1987, Proterozoic crustal history of the western United States as determined by neodymium isotopic mapping; Geological Society of America Bulletin, v. 99, p. 674-685.

Best, M.G., Christiansen, E.H., Deino, A.L., Gromme, C.S., McKee, E.H., and Noble, D.C., 1989a, Eocene through Miocene volcanism in the Great Basin of the western United States: New Mexico Bureau of Mines and Mineral Resources Memoir 47, p. 91-133.

Brandon, C.F., 1979, Flow direction studies of the Tuff of Bridge Spring, Nevada: Senior Project, University of Wisconsin-Parkside (unpublished).

Bridwell, H.L., 1991, The Sloan Sag: a mid-Miocene volcanotectonic depression, north-central McCullough Mountains, southern Nevada [M.S. thesis]: Las Vegas, Nevada, University of Nevada, 147 p.

Carmichael, I.S.E., Turner, F.J., and Verhoogan, J., 1974, Igneous Petrology: New York, McGraw Hill Book company, 739 p.

Cas, R.A.F., and Wright, J.V., 1987, Volcanic successions: Ancient and modern: London, United Kingdom, Allen and Unwin, 528 p.

Cascadden, T.E., 1991, Style of volcanism and extensional tectonics in the eastern Basin and Range province: northern Mojave County, Arizona [M.S. thesis]: Las Vegas, Nevada, University of Nevada, 156 p.

Choukroune, P., and Smith, E.I., 1985, Detachment faulting and its relationship to older structural events on Saddle Island, River Mountains, Clark County, Nevada: Geology, v. 13, p. 421-424.

Cole, E.D., 1989, Petrogenesis of late Cenozoic alkalic basalt near the eastern boundary of the Basin-and-Range: Upper Grand Wash Trough, Arizona and Gold Butte, Nevada [M.S. thesis]: Las Vegas, Nevada, University of Nevada, 68 p.

Daley, E.E., 1992, Temporal and spatial variations in compositions of young mafic volcanic rocks of the southwestern Basin and Range: Isotopic constraints on the relationship between thinning in the lithosphere and extensional deformation in the upper crust [Phd. dissertation]: Berkeley, California, University of California, 205 p.

Darval, P., 1991, Normal faulting in the Eldorado Mountains, southeastern Nevada: Geological Society of America Abstracts with Programs, v. 23, no. 2, p. 17.

Davidson, J.P., De Silva, S.L., Holden, Peter, and Halliday, A.N., 1990, Small-scale disequilibrium in a magmatic inclusion and its more silicic host: Journal of Geophysical Research, v. 95, p. 17661-17675.

Davis, S.O., 1984, Structural geology of the central portion of the Highland Spring Range, Clark County, Nevada [M.S. thesis]: Los Angeles, California, University of California, 190 p.

Duebendorfer, E.M., and Smith, E.I., 1991, Tertiary structure, magmatism, and sedimentation in the Lake Mead region, southern Nevada, *in* Seedorf, E., Tertiary Geology and Volcanic-hosted Gold Deposits of the Southern Great Basin and Vicinity; Geological Society of Nevada, Special Publication no.13, p. 66-86.

Duebendorfer, E.M., and Wallin, E.T., 1991, Basin development and syntectonic sedimentation associated with kinematically-coupled strike-slip and detachment faulting, southern Nevada: Geology, v. 19, p. 87-90.

Duebendorfer, E.M., Sewell, A.J., and Smith, E.I., 1990, The Saddle Island detachment; An evolving shear zone in the Lake Mead area, Nevada: *in* Wernicke, B.P., ed., Basin and Range extensional tectonics near the latitude of Las Vegas, Nevada: Geological Society of America Memoir 176, p. 77-97.

Falkner, C.M., Miller, C.F., and Wooden, J.L., 1993, Petrology of the Aztec Wash pluton, Eldorado Mountains, southern Nevada: Geological Society of America Abstracts with Programs, v. 25, no. 5, p. 36.

Faulds, J.E., 1989, Structural development of a major extensional accommodation zone in the Basin and Range province, northwestern Arizona and southern Nevada: Implications for kinematic models of continental extension [Ph.D. dissertation]: Albuquerque, New Mexico, University of New Mexico, 263 pgs.

Faulds, J.E., Geissman, J.W., and Mawer, C.K, 1990, Structural development of a major extensional accommodation zone in the Basin and Range province, northwestern Arizona and southern Nevada; Implications for kinematic models of continental extension: *in* Wernicke, B.P., ed., Basin and Range extensional tectonics near the latitude of Las Vegas, Nevada: Geological Society of America Memoir 176, p. 37-76.

Faulds, J.E., Geissman, J.W., and Shafiqullah, Muhammad, 1992, Implications of paleomagnetic data on Miocene extension near a major accommodation zone in the Basin and Range province, northwestern Arizona and southern Nevada: Tectonics, v. 11, no. 2, p. 204-227.

Feuerbach, D.L., Smith, E.I., Walker, J.D., and Tangeman, J.A., 1993, The role of the mantle during crustal extension: Constraints from geochemistry of volcanic rocks in the Lake Mead area, Nevada and Arizona: Geological Society of America Bulletin (in press).

Fisher, R.V., and Schmincke, H.-U., 1984, Pyroclastic Rocks: Berlin, Germany, Springer-Verlag, 472 p.

Hewett, D.F., 1956, Geology and mineral resources of the Ivanpah Quadrangle, California and Nevada: U.S. Geological Survey Professional Paper 275, 172 p.

Hildreth, W., and Mahood, G.A., 1985, Correlation of ash-flow tuffs: Geological Society of America Bulletin, v. 96, p. 968-974.

Hutchison, C.S., 1974, Laboratory Handbook of Petrographic Techniques: New York, John Wiley and Sons, 527 p.

Koyaguchi, T., 1986, Textural and compositional evidence for magma mixing and its mechanism, Abu volcano group, southwestern Japan: Contributions in Mineralogy and Petrology, v. 93, p. 33-45.

Larsen, L.L., 1990, Significance of mafic enclaves in the Wilson Ridge pluton, Mojave County, Arizona [M.S. thesis]: Las Vegas, Nevada, University of Nevada, 81 p.

Larsen, L.L., and Smith, E.I., 1990, Mafic Enclaves in the Wilson Ridge pluton, northwestern Arizona: Implications for the generation of a calc-alkaline intermediate pluton in an extensional environment: Journal of Geophysical Research, v. 95, no. B11, p. 17693-17716.

Lipman, P.W., 1976, The roots of ash flow calderas in western North America: Windows into the tops of granitic batholiths: Journal of Geophysical Research, v. 89, p.8801-8841.

Longwell, C.R., 1963, Reconnaissance geology between Lake Mead and Davis Dam, Arizona-Nevada: U.S. Geological Survey Professional Paper 374-E, p. E1-E51.

Metcalf, R.V., Smith, E.I, Nall, K.E., and Reed, R.C., 1992, The Mt. Perkins pluton: Shallow-level magma mixing and mingling during Miocene extension: Geological Society of America Abstracts with Programs, v.24, no. 7, p. 87.

Metcalf, R.V., Smith, E.I., and Martin, M.W., 1993, Isotopic evidence of source variations in commingled magma systems: Colorado River extensional corridor, Arizona and Nevada: Geological Society of America Abstracts with Programs, Nevada, v. 25, no. 5, p. 120.

Mills, J.G., 1985, The geology and geochemistry of volcanic and plutonic rocks in the Hoover Dam 7 1/2 Quadrangle, Clark County, Nevada, and Mohave County, Arizona [M.S. thesis]: Las Vegas, Nevada, University of Nevada, 119 p.

Mills, J.G., 1991, The Timber Mountain Tuff, southwestern Nevada volcanic field: Geochemistry, mineralogy and petrogenesis [Ph.D. dissertation]: East Lansing, Michigan, Michigan State University, 332 p.

Mills, J.G., 1993, The production of intermediate magmas through magma mixing and commingling: Evidence from the Hoover Dam Volcanics, Mohave County, Arizona and Clark County, Nevada: Geological Society of America Abstracts with Programs, v. 25, no. 5, p. 123.

Naumann, T.R., 1987, Geology of the central Boulder Canyon quadrangle, Clark County, Nevada [M.S. thesis]: Las Vegas, Nevada, University of Nevada, 69 p.

Noorish, K., and Hutton, J.T., 1969, An accurate X-ray spectrographic method for the analysis of a wide range of geological samples: Geochimica et Cosmochimica Acta, v. 33, p. 431-453.

Rowland, S.M., Parolini, J.R., Eschner, E., and McAllister, A.J., 1990, Sedimentologic and stratigraphic constraints on the Neogene translation and rotation of the Frenchman Mountain structural block, Clark County, Nevada, *in* Wernicke, B.P., ed., Basin and Range extensional tectonics near the latitude of Las Vegas, Nevada: Geological Society of America Memoir 176, p. 99-121.

Schmidt, C.E., 1987, A mid-Miocene caldera in the central McCullough Mountains, Clark County, Nevada [M.S. thesis]: Las Vegas, Nevada, University of Nevada, 78 p.

Seaman, S.J., and Ramsey, P.C., 1992, Effects of magma mingling in the granites of Mount Desert Island, Maine: Journal of Geology, v. 100, p. 395-409.

Smith, E.I., 1982, Geology and geochemistry of the volcanic rocks in the River Mountains, Clark County, Nevada and comparisons with volcanic rocks in nearby areas, *in* Frost, E.G., and Martin, D.L., eds., Mesozoic-Cenozoic tectonic evolution of the Colorado River region, California, Arizona, and Nevada: San Diego, California, Cordilleran Publishers, p. 42-54.

Smith, E.I., Schmidt, C.S., and Mills, J.G., 1988, Mid-Tertiary Volcanoes in the Lake Mead area of southern Nevada and northwestern Arizona, *in* Weide, D.L., and Faber, M.L., eds., This extended land: Geological journeys in the southern Basin and Range; Geological Society of America Fieldtrip Guidebook, Cordilleran Section Meeting, Las Vegas, Nevada: University of Nevada at Las Vegas Department of Geoscience Special Publication 2, p. 107-122.

Smith, E.I., Feuerbach, D.L., Naumann, T.R., and Mills, J.E., 1990, Geochemistry and evolution of mid-Tertiary igneous rocks in the Lake Mead area of Nevada and Arizona, *in* Anderson, J.L., ed., Cordilleran Magmatism: Geological Society of America Memoir 176, p. 169-194.

Smith, R.L., 1960, Ash flows: Geological Society of America Bulletin, v. 71, p. 795-842.

Tuma-Switzer, T.E., and Smith, E.I., 1993, Geology of the Henderson Volcanic Complex, northern McCullough Mountains, Clark County, Nevada; Abstract: Journal of the Arizona-Nevada Academy of Science; Thirty-seventh annual meeting, Las Vegas, Nevada, April 17, 1993, p. 44-45.

Valentine, G.A, Wohletz, K.H., and Kieffer, S.W., 1992, Effects of topography on facies and compositional zonation in caldera-related ignimbrites: Geological Society of America Bulletin, v. 104, p. 154-165.

Internal Stratigraphy

Introduction

Determination of the internal stratigraphy of an ash-flow tuff is based upon recognition of vertical and lateral variation in geochemistry, lithology, mineralogy, and isotopic and paleomagnetic signatures (Hildreth and Mahood, 1985). These variations form by primary magmatic differentiation processes and syn- and post emplacement/secondary processes which act to modify the magmatic signatures of ash-flow tuffs. Primary variations in ash-flow tuffs reflect chemical gradients present in the parent magma chamber at the instant of their eruption. For this reason, ash-flow tuffs are commonly referred to as "snapshots" of syn-eruption magmatic conditions (Hildreth, 1985). If the primary characteristics of ash-flow tuffs are not altered by secondary processes, these internal variations are useful criteria for stratigraphic correlations.

Secondary modification processes can physically fractionate or chemically alter the magmatic signature of ash-flow tuffs during or after their emplacement. These processes include (1) elutriation of fine-grained material during pyroclastic flow; (2) concentration of lithic fragments and phenocrysts by either pyroclastic flow-associated ground surges or by post-emplacement compaction; and (3) devitrification and vapor phase crystallization of flows following emplacement (Hildreth and Mahood, 1985; Fisher and Schmincke, 1984). Devitrification and vapor phase processes are associated with specific horizons of the ash-flow tuff section (Cas and Wright, 1987). Devitrification typically occurs in the middle- to upper middle parts of the section. Vapor phase crystallization, which occurs in the moderately- to poorly-welded part of the section that overlies the zone of devitrification, may locally overprint devitrified tuff. These

Walker, J.D., Beaufait, M.S., and Zelt, F.B.,1981, Geology of the Devil Peak area, Spring Mountains, Nevada: Geological Society of America Abstracts with Programs, Cordilleran Section, v. 13, no. 2, p. 112.

Weber, M.E., and Smith, E.I., 1987, Structural and geochemial constraints on the reassembly of disrupted volcanoes in the Lake Mead-Eldorado Valley area of southern Nevada: Geology, v. 15, p. 553-556.

Wernicke, B.J., Axen, G.J., and Snow, J.K., 1988, Basin and Range extensional tectonics at the latitude of Las Vegas, Nevada: Geological Society of America Bulletin, v. 100, p. 1738-1757.

Wilson, B.M., 1989, Igneous petrogenesis: A global tectonic approach: London, United Kingdom, Unwin Hyman, p. 466.

Wooden, J.L., and Miller, D.M., 1990, Chronologic and isotopic framework for early Proterozoic crustal evolution in the eastern Mojave Desert region, southeastern California: Journal of Geophysical Research, v. 95, no. B12, pgs. 20,146-21,133.

Young, R.A., and Brennan, W.J., 1989, Peach Springs Tuff: Its bearing on structural evolution of the Colorado Plateau and development of Cenozoic drainage in Mohave County, Arizona: Geological Society of America Bulletin, v. 85, p. 83-90.

Appendix A: Major and Trace Element Analyses. Major element oxides in wt.% and trace elements in ppm.

Sample	92-BM1-2	92-BM1-1	92-BM1-4	92-BM1-3	93-DS7-1	93-DS7-2	93-DS7-3	92-E3-1	92-E3-2	92-E3-3
Position	7	8	9	10	10.5	10	3.5	1	2	3
SiO2	69.48	69.8	66.14	68.80	72.91	71.45	72.91	65.58	64.23	62.6
Al2O3	11.84	12.55	11.41	14.00	12.5	12.61	12.60	13.34	13.81	14.16
TiO2	0.24	0.26	0.29	0.32	0.18	0.23	0.23	0.43	0.57	0.60
FeO	1.30	1.33	1.54	1.89	1.18	1.60	1.56	2.18	3.00	3.13
CaO	2.12	2.24	4.05	1.22	1.05	2.13	2.50	3.03	2.99	3.2
K2O	5.95	6.23	5.78	6.33	5.24	4.49	5.20	3.56	4.08	4.53
MnO	0.03	0.04	0.04	0.04	0.04	0.05	0.06	0.06	0.07	0.07
P2O5	0.005	0.03	0.08	0.02	0.06	0.08	0.12	0.09	0.14	0.14
Na2O	1.57	1.57	1.57	4.02	2.79	3.15	2.85	0.14	0.14	0.14
MgO	0.21	0.31	0.24	0.14	0.51	0.745	0.46	1.05	1.36	1.66
LOI	N/A	1.90	N/A	4.30	N/A	N/A	N/A	10.57	N/A	N/A
Total	92.76	96.27	91.14	101.09	96.45	96.56	97.24	100.04	90.39	90.24
Cr	2.514	2.166	28.005	41.914	25.805	40.581	47.312	23.07	23.353	25.315
Nb	43.457	40.31	36.715	44.644	18.715	18.712	17.148	35.966	34.638	33.797
Ni	8.193	10.511	15.188	17.715	10.441	15.423	16.683	18.956	30.435	27.558
Rb	204	221	193	211	143	124	108	130	124	140
Sr	68	49	71	57	125	196	165	322	314	379
Th	37.154	39.242	34.225	29.946	15.913	14.037	13.225	31.512	32.182	27.408
Y	27.594	29.062	27.898	29.567	22.116	21.42	20.648	27.244	27.187	27.212
Zr	261	277	267	350	101	122	114	309	322	335
Ba	100	75	165	205	240	356	331	129	280	300

Appendix A, continued.

Sample	92-E3-4	92-E3-5	92-E3-6	92-E3-10	92-E3-9	92-E3-8	92-HS1-5	92-HS2-1	92-HS2-4	92-HS2-2
Position	4	5	6	7	8	9	1	5	6	7
SiO2	66.96	67.12	70.18	68.00	69.93	71.58	69.17	72.91	70.46	72.38
Al2O3	15.13	14.92	15.29	14.36	14.34	12.85	14.32	15.28	14.70	14.98
TiO2	0.57	0.52	0.46	0.44	0.41	0.41	0.35	0.39	0.35	0.38
FeO	3.02	2.84	2.49	2.16	2.11	2.36	2.24	2.01	1.89	2.03
CaO	1.66	1.62	1.17	1.72	0.97	1.15	0.84	1.06	0.91	0.92
K2O	6.65	5.40	5.57	5.34	5.37	4.62	5.57	5.71	5.44	5.66
MnO	0.07	0.06	0.08	0.07	0.07	0.05	0.07	0.07	0.07	0.07
P2O5	0.12	0.03	0.02	0.05	0.08	0.06	0.02	0.04	0	0
Na2O	3.15	4.31	3.026	2.30	3.90	3.35	4.05	5.15	3.76	4.31
MgO	1.0	0.84	0.66	0.61	0.48	0.52	0.50	0.42	0.2	0.42
LOI	1.72	N/A	N/A	N/A	N/A	N/A	0.64	N/A	N/A	N/A
Total	100.05	97.68	98.95	95.05	97.68	96.96	97.77	103.04	97.78	101.14
Cr	26.846	25.341	23.823	24.158	24.993	23.414	24.963	10.648	8.35	3.326
Nb	38.44	41.687	38.196	42.652	35.755	35.533	51.876	46.255	42.431	38.646
Ni	24.426	25.235	18.19	21.439	18.321	19.121	21.356	17.68	10.48	11.18
Rb	230	192	189	188	184	165	214	202	203	180
Sr	203	280	124	196	87	152	125	74	90	82
Th	35.418	33.658	39.683	38.783	35.602	29.093	44.631	34.12	29.254	29.744
Y	30.965	29.756	30.028	30.087	29.118	28.218	29.91	30.632	30.3	29.114
Zr	390	382	362	372	354	334	320	344	319	319
Ba	277	264	106	161	144	168	95	69	110	118

Appendix A, continued.

Sample	92-HS2-3	92-HS1-1	93-I151-1	93-I151-3	93-I151-4	93-I151-6	93-I151-5	92-LG1-1	92-LG1-2	92-M2-1
Position	9	9.5	1	3	4	5	6	8	9	5
SiO2	71.02	68.72	68.02	68.35	68.92	68.106	68.083	72.06	70.28	67.15
Al2O3	15.05	14.52	13.46	14.5	14.37	14.502	14.401	14.15	13.79	11.67
TiO2	0.41	0.44	0.32	0.45	0.41	0.422	0.407	0.28	0.29	0.41
FeO	2.23	2.34	1.44	2.11	2.17	2.079	2.316	1.77	1.7	2.12
CaO	1.68	1.43	2.85	2.66	2.31	2.741	2.288	0.86	0.69	3.3
K2O	5.44	5.29	4.82	6.01	5.66	5.747	5.696	5.24	5.73	2.39
MnO	0.07	0.07	0.07	0.08	0.08	0.074	0.082	0.06	0.06	0.06
P2O5	0.02	0.13	0.04	0.09	0.07	0.061	0.067	0.05	0.05	0.11
Na2O	3.16	4.25	4.35	4.40	4.55	4.485	3.883	4.07	4.25	2.02
MgO	0.87	0.71	0.44	0.9	0.72	0.862	0.607	0.34	0.2	1.94
LOI	N/A	1.03	N/A	1.45	N/A	N/A	0.17	0.4	0.23	N/A
Total	99.95	98.93	95.81	101	99.27	99.079	98	99.28	97.27	91.17
Cr	15.307	24.497	0	27.852	66.861	19.505	66.894	24.201	23.897	23.723
Nb	38.002	36.496	44.552	46.137	43.578	42.506	42.558	32.08	30.592	28.325
Ni	13.512	20.934	10.074	18.001	16.643	16.145	19.94	19.135	19.812	21.909
Rb	169	175	223	188	187	184	187	190	214	36
Sr	271	345	62	163	116	125	121	43	35	1083
Th	32.106	34.485	36.607	32.303	31.131	29.258	32.078	24.964	24.602	23.297
Y	27.937	27.483	30.314	29.909	29.971	30.003	29.702	30.36	30.824	22.859
Zr	329	325	285	325	342	334	325	261	258	301
Ba	511	477	63	188	185	207	192	28	102	530

Appendix A, continued.

Sample	91-M1-1	91-M1-2	92-M3-1	92-M2-2	91-M1-3	92-M3-4	91-M1-4	92-M3-5	91-SM1-1	92-SM2-1
Position	6	7	7.5	8	9	9.5	10	10.5	5	6
SiO2	62.55	62.84	62.16	65.17	66.39	66.56	64.94	66.076	63.84	65.69
Al2O3	16.1	16.05	16.08	14.61	15.34	15.09	15.92	15.92	13.09	13.71
TiO2	0.6	0.59	0.6	0.46	0.47	0.48	0.50	0.46	0.32	0.35
FeO	3.06	2.84	3.06	2.41	2.63	2.61	2.68	2.55	1.74	1.75
CaO	2.14	2.08	2.59	1.84	1.90	2.76	2.79	2.21	3.22	1.39
K2O	6.02	5.56	5.28	4.48	5.05	5.31	5.25	5.41	5.15	5.40
MnO	0.07	0.06	0.07	0.07	0.07	0.07	0.07	0.07	0.06	0.06
P2O5	0.13	0.04	0.03	0.11	0.03	0.08	0.09	0.05	0.05	0.04
Na2O	4.25	3.90	3.97	4.08	3.82	4.39	3.63	4.95	2.9	4.23
MgO	1.24	1.05	1.18	0.93	0.81	1.02	1.09	0.86	0.56	0.73
LOI	N/A	3.09	N/A	N/A	N/A	N/A	N/A	0.42	N/A	N/A
Total	96.16	98.1	95.04	94.16	96.51	98.37	96.96	98.96	90.94	93.35
Cr	27.782	25.311	24.458	24.145	26.007	23.897	26.081	25.056	18.674	50.649
Nb	23.97	29.001	24.024	35.784	35.355	33.844	30.014	33.317	43.663	45.952
Ni	15.52	24.275	16.686	21.56	21.312	16.368	22.267	9.412	10.778	13.621
Rb	143	134	139	180	129	146	132	143	199	202
Sr	524	420	506	331	330	387	434	428	100	74
Th	28.967	22.802	23.738	22.525	31.733	27.958	24.684	27.229	40.348	34.857
Y	26.381	26.579	25.49	27.881	25.397	25.98	24.26	25.242	29.284	29.633
Zr	584	552	638	352	398	381	374	401	306	326
Ba	1349	1280	1753	671	728	860	984	1048	69	89

Appendix A, continued.

Sample	92-SM3-3	92-SM3-2	92-SM3-4	92-SM2-3	92-SS2-1	92-SS2-2	92-TB3-1	92-TB3-3	92-TB2-1	92-TB3-2
Position	7	8	9	10	9	10	4	5	6	7
SiO2	67.05	66.95	67.94	66.56	71.267	66.52	65.86	65.40	64.045	66.565
Al2O3	13.86	13.86	13.89	13.94	11.17	14.38	15.53	14.96	15.179	14.489
TiO2	0.34	0.37	0.36	0.35	0.35	0.47	0.52	0.47	0.464	0.5
FeO	1.88	1.98	1.97	2.01	2.05	2.52	3.07	2.86	2.623	3.067
CaO	1.51	1.30	1.20	1.88	2.89	0.47	0.78	0.85	1.19	0.955
K2O	5.61	5.22	5.42	5.03	6.28	8.56	9.53	9.50	9.164	9.51
MnO	0.07	0.06	0.07	0.06	0.04	0.03	0.04	0.03	0.033	0.033
P2O5	0.06	0.04	0	0.03	0.11	0.02	0.06	0.05	0.059	0.072
Na2O	4.28	4.42	3.51	4.08	1.57	1.57	1.57	1.58	2.098	1.569
MgO	0.72	0.30	0.42	0.42	0.74	0.38	0.45	0.38	0.423	0.497
LOI	1.79	N/A	N/A	1.11	3.71	2.70	0.74	N/A	N/A	N/A
Total	97.16	94.50	94.77	95.46	100.16	97.62	98.14	96.06	95.278	97.257
Cr	44.718	36.464	111.62	65.748	13.505	23.022	76	77.729	27.072	60.012
Nb	43.445	44.908	45.805	44.761	23.522	32.208	32.291	27.412	27.142	27.769
Ni	14.677	14.081	25.915	17.93	12.868	14.241	24.894	25.833	17.167	23.57
Rb	200	203	184	191	130	196	314	308	295	309
Sr	74	70	61	65	112	56	200	214	191	186
Th	36.273	35.613	36.901	36.206	18.111	23.798	28.624	26.463	24.285	24.307
Y	29.707	30.298	29.561	30.068	23.178	27.605	30.544	30.178	29.839	30.117
Zr	320	334	329	346	226	340	378	360	375	345
Ba	85	76	81	78	388	392	1400	1260	1048	1298

Appendix A, continued.

Sample	92-TB3-4	92-TB3-5	92-WH2-2	92-WH2-4	92-WH2-3	92-WH2-1
Position	8	9.5	7	8	9	10
SiO2	64.809	60.571	62.059	59.204	56.115	61.821
Al2O3	14.162	14.438	15.937	15.622	16.969	15.713
TiO2	0.501	0.645	0.596	0.0604	0.68	0.665
FeO	2.796	3.574	3.14	3.202	3.436	3.786
CaO	2.016	4.103	2.48	4.127	5.127	3.42
K2O	9.435	6.132	6.232	5.823	7.45	5.519
MnO	0.029	0.062	0.07	0.065	0.073	0.093
P2O5	0.114	0.163	0.099	0.186	0.194	0.241
Na2O	1.569	2.835	3.769	3.525	3.362	3.815
MgO	0.428	1.243	0.718	1.009	0.892	1.782
LOI	1.63	N/A	N/A	N/A	3.35	1.53
Total	97.489	93.766	95.1	93.367	97.648	98.385
Cr	84.009	32.226	19.534	28.458	42.534	22.915
Nb	30.23	25.63	30.448	25.569	29.339	25.204
Ni	28.633	21.064	14.254	14.989	15.812	16.268
Rb	305	179	157	138	178	141
Sr	193	368	560	662	591	712
Th	24.174	21.921	22.101	16.726	22.154	18.154
Y	29.896	26.477	26.481	25.542	27.426	26.151
Zr	344	372	434	419	430	430
Ba	1341	1250	1330	1344	1524	1502

Appendix B: Point Counts. Part I: Whole Rock Modal Analyses. Counts normalized to 100%.

Position	7.0	8.0	9.0	10.0	6.0	1.0	2.5	4.5	4.7	5.0
Sample	92-BM1-2	92-BM1-1	92-BM1-4	92-BM1-3	92-BM1-6	92-E1-2	92-E1-3	92-E1-4	92-E1-5	92-E1-6
sanidine	5.4	5.2	7.8	17.2	6.6	5.7	6.8	7.6	8.4	9.6
plagioclase	0.8	2	1	0.4	3.4	2.6	3.2	2.2	3.6	2.8
matrix	92.2	91.8	87	80.2	61.6	83.3	68.3	82.6	65.5	71.8
pumice						2.4				
lithics			2.2	0.4	25.4	5.3	19.7	6.8	21.5	13.4
biotite	0.8	1	1.2	0.8	2	0.4	0.6	0.4	0.6	0.8
cpx					0.2		0.2			0.2
sphene					0.2	0.2	0.4	0.4	0.2	0.8
opaque	0.8		0.8	0.6	0.6				0.2	0.6
zircon				0.4						
hornblende										
hematite										
carbonate										
undiff. feldspar										
trace sphene										
trace zircon			y		y			y		y
trace apatite	y	y			y					
glass										
trace cpx									y	
secondary quartz										
trace opaque										
trace hornblende										

Appendix B: Part I, continued.

Position	6.0	7.0	8.0	9.0	10.0	5.5	7.5	3.0	2.0
Sample	92-E1-7	92-E3-10	92-E3-9	92-E3-8	92-E3-7	92-HS1-2	92-HS1-3	92-HS1-4	92-HS1-6
sanidine	8.4	9.6	9.8	9.2	5	6.6	3	9.8	7
plagioclase	4.6	4	5	5.1	8.9	88	77.8	83.6	85.6
matrix	76.4	76.8	76.4	62.4	80.7	2	4.6	2.6	2.1
pumice							6.8		
lithics	8.8	5.2	5.4	20.1	1.6	0.6	6.6	1	2.5
biotite	0.8	1.4	1.2	0.2	2.2	0.6	0.6	1.4	0.6
cpx	0.2	0.8	0.2		0.4	0.2	0.4	0.6	1
sphene	0.6	1.4	1.2	1	0.4	1.4		0.8	1
opaque	0.2	0.8	0.6	2	0.6	0.6	0.2	0.2	0.2
zircon			0.2		0.2				
hornblende									
hematite									
carbonate									
undiff. feldspar									
trace sphene									
trace zircon	y	y	y	y					
trace apatite		y	y	y					
glass									
trace cpx									
secondary quartz									
trace opaque									
trace hornblende									

Appendix B: Part I, continued.

Position	1.0	5.0	7.0	9.0	9.5	2.0	3.0	4.0	5.0
Sample	92-HS1-5	92-HS2-1	92-HS2-2	92-HS2-3	92-HS1-1	93-I151-2	93-I151-3	93-I151-4	93-I151-5
sanidine	7	9.4	4.8	4	6.7	5.3	5.8	7.8	9.9
plagioclase	5.4	3	2.6	4.6	4.6	1	4.6	6.2	4.2
matrix	81.2	84.8	89.2	85.6	82.9	82.9	81.8	80.8	80.7
pumice	0.2					3.6			
lithics	2.8		0.4	1.4	2.7	4	4.6	1	2.4
biotite	1.4	0.4	1.2	1.8	1.7	0.2	0.8	1.2	0.6
cpx	0.4	0.2		1.6	0.8	0.8	0.8	0.8	0.4
sphene	1.2	1.2	0.6			0.4	1.2	0.8	1.2
opaque	0.2	0.6	0.8	1	0.6	0.6	0.2	1.4	0.6
zircon	0.2	0.4	0.2			0.2	0.2		
hornblende									
hematite									
carbonate									
undiff. feldspar									
trace sphene									
trace zircon								y	y
trace apatite				y		y	y	y	y
glass									
trace cpx									
secondary quartz									
trace opaque									
trace hornblende									

Appendix B: Part I, continued.

Position	6.0	8.0	9.0	10.0	7.5	7.2	5.0	6.0	7.0
Sample	93-I151-6	92-LG1-1	92-LG1-2	92-LG1-3	91-M1-5	92-M2-3	92-M2-1	91-M1-1	91-M1-2
sanidine	12.6	9.8	12	9.2	14.3	10.2	6.4	17.4	14.3
plagioclase	3.6	1.8	1.6	1.2	10.2	7.2	3.7	10.2	9.4
matrix	77.6	65.4	81.6	86.4	59.7	64	79.8	47.1	55.8
pumice		0.6			10.8	13.4		13.9	6.6
lithics	2.2	20.8	1.6	1.6	1.8	2.6	7.9	8.6	8.6
biotite	1	0.8	0.4	0.2	1.8	1.4	0.2	1.2	1.6
cpx	0.4		1.2	0.6	0.6	0.4	0.6	0.4	2.2
sphene	1.4	0.6	0.8	0.6		0.4	0.6	0.2	0.8
opaque	1		0.6	0.2	0.8	0.4	0.8	0.6	0.4
zircon	0.2	0.2	0.2					0.2	
hornblende								0.2	
hematite									
carbonate									
undiff. feldspar									
trace sphene					y				
trace zircon				y	y				y
trace apatite	y								
glass									
trace cpx									
secondary quartz									
trace opaque		Y							
trace hornblende					y				

Appendix B: Part I, continued.

Position	8.0	9.0	9.5	10.0	10.5	5.0	6.0	7.0	8.0
Sample	92-M2-2	91-M1-3	92-M3-4	91-M1-4	92-M3-5	91-SM1-1	92-SM2-1	92-SM3-3	92-SM3-2
sanidine	3.8	10.4	10.5	17.5	22.2	4.2	10.2	8.4	12
plagioclase	74	13.4	8.6	12.7	9.6	0.6	3.6	2	1
matrix	74	66.5	69.3	59.7	62	80.4	78.4	80.8	71
pumice	9.8	5.4		2.1		11.2	1.2	4.4	12.2
lithics	2		4.2	2.8	0.6	1.2	4.4	1.8	1.4
biotite	1.6	2.2	3.4	2.8	2.2	0.8	0.4	0.6	0.6
cpx	0.6	1.1	2.2	1.6	1.4	0.4	0.2	0.2	0.4
sphene		0.4	0.2	0.6	0.2	0.8	0.8	0.8	0.6
opaque	6.2	0.6	1.4	0.2	1.2	0.2	0.8	1	0.6
zircon			0.2		0.6	0.2			
hornblende									
hematite									
carbonate									
undiff. feldspar									
trace sphene									
trace zircon		y	y		y		y	y	
trace apatite				y			y	y	y
glass									
trace cpx									
secondary quartz									
trace opaque									
trace hornblende									

Appendix B: Part I, continued.

Position	9.0	10.0	4.0	9.5	6.0	7.0	8.0	7.0	8.0
Sample	92-SM3-4	92-SM2-3	92-TB3-1	92-TB3-5	92-TB1-2	92-TB1-3	92-TB1-4	92-WH1-3	92-WH1-4
sanidine	7	10.4	19.8	10.4	20.7	10.3	23.1	11	11
plagioclase	2	5	0.6	12.5	1	0.6	0.6	4.6	11.2
matrix	73.8	80.4	60.4	61.9	60.2	54.7	53.7	70.6	67.4
pumice	10.4								
lithics	3.6	1.4	5.4	8.4	8	26	10.4	5	3.8
biotite	1	1.4	3	4.4	1.8	1.6	3.2	4.2	3.8
cpx	0.2	0.4						2.2	1.6
sphene	1.2	0.6					0.4	0.2	
opaque	0.6	0.4	1.2	1	0.8	1.4	0.8	1.6	0.8
zircon	0.2				0.2	0.4	0.4	0.2	
hornblende								.4	0.4
hematite			0.4						
carbonate									
undiff. feldspar			9.2	1.2	7.4	4.6	7.4		
trace sphene									
trace zircon								y	
trace apatite						y			
glass									
trace cpx									
secondary quartz				0.2	y				
trace opaque									
trace hornblende									

Appendix B: Part I, continued.

Position	9.0	10.0
Sample	92-WH1-2	92-WH1-1
sanidine	4.4	12.6
plagioclase	8	6.9
matrix	80	70
pumice		
lithics	3.8	6.3
biotite	2.6	3.2
cpx	0.6	
sphene	0.4	0.2
opaque	1	0.6
zircon		0.2
hornblende		
hematite		
carbonate		
undiff. feldspar		
trace sphene		
trace zircon		
trace apatite		
glass		
trace cpx		
secondary quartz		
trace opaque		
trace hornblende		

Appendix B: Point Counts. Part II: Phenocryst Modal Analyses. Counts normalized to 100%.

Position	7.0	8.0	9.0	10.0	6.0	1.0	2.5	4.5	4.7	5.0
Sample	92-BM1-2	92-BM1-1	92-BM1-4	92-BM1-3	92-BM1-6	92-E1-2	92-E1-3	92-E1-4	92-E1-5	92-E1-6
sanidine	69.2	63.4	72.2	88.7	50.8	64.0	60.7	71.7	64.6	64.9
plagioclase	10.3	24.4	9.3	2.1	26.2	29.2	28.6	20.8	27.7	18.9
biotite	10.3	12.2	11.1	4.1	15.4	4.5	5.4	3.8	4.6	5.4
cpx	0.0	0.0	0.0	0.0	1.5	0.0	1.8	0.0	0.0	1.4
sphene	0.0	0.0	0.0	0.0	1.5	2.2	3.6	3.8	1.5	5.4
opaque	10.3	0.0	7.4	3.1	4.6	0.0	0.0	0.0	1.5	4.1
zircon	0.0	0.0	0.0	2.1	0.0	0.0	0.0	0.0	0.0	0.0
hornblende	0.0	0.0	0.0	0.0	0.0	0.0	0.0	0.0	0.0	0.0
undiff. feldspar	0.0	0.0	0.0	0.0	0.0	0.0	0.0	0.0	0.0	0.0

Position	6.0	7.0	8.0	9.0	10.0	5.5	7.5	3.0	2.0
Sample	92-E1-7	92-E3-10	92-E3-9	92-E3-8	92-E3-7	92-HS1-2	92-HS1-3	92-HS1-4	92-HS1-6
sanidine	56.8	53.3	53.8	52.6	28.2	6.8	3.7	10.2	7.3
plagioclase	31.1	22.2	27.5	29.1	50.3	90.3	94.9	86.7	89.7
biotite	5.4	7.8	6.6	1.1	12.4	0.6	0.7	1.5	0.6
cpx	1.4	4.4	1.1	0.0	2.3	0.2	0.5	0.6	1.0
sphene	4.1	7.8	6.6	5.7	2.3	1.4	0.0	0.8	1.0
opaque	1.4	4.4	3.3	11.4	3.4	0.6	0.2	0.2	0.2
zircon	0.0	0.0	1.1	0.0	1.1	0.0	0.0	0.0	0.0
hornblende	0.0	0.0	0.0	0.0	0.0	0.0	0.0	0.0	0.0
undiff. feldspar	0.0	0.0	0.0	0.0	0.0	0.0	0.0	0.0	0.0

Appendix B: Part II, continued.

Position	1.0	5.0	7.0	9.0	9.5	2.0	3.0	4.0	5.0
Sample	92-HS1-5	92-HS2-1	92-HS2-2	92-HS2-3	92-HS1-1	93-I151-2	93-I151-3	93-I151-4	93-I151-5
sanidine	44.3	61.8	47.1	30.8	46.5	62.4	42.6	42.9	58.6
plagioclase	34.2	19.7	25.5	35.4	31.9	11.8	33.8	34.1	24.9
biotite	8.9	2.6	11.8	13.8	11.8	2.4	5.9	6.6	3.6
cpx	2.5	1.3	0.0	12.3	5.6	9.4	5.9	4.4	2.4
sphene	7.6	7.9	5.9	0.0	0.0	4.7	8.8	4.4	7.1
opaque	1.3	3.9	7.8	7.7	4.2	7.1	1.5	7.7	3.6
zircon	1.3	2.6	2.0	0.0	0.0	2.4	1.5	0.0	0.0
hornblende	0.0	0.0	0.0	0.0	0.0	0.0	0.0	0.0	0.0
undiff. feldspar	0.0	0.0	0.0	0.0	0.0	0.0	0.0	0.0	0.0

Position	6.0	8.0	9.0	10.0	7.5	7.2	5.0	6.0	7.0
Sample	93-I151-6	92-LG1-1	92-LG1-2	92-LG1-3	91-M1-5	92-M2-3	92-M2-1	91-M1-1	91-M1-2
sanidine	62.4	74.2	71.4	76.7	51.6	51.0	52.0	57.6	49.8
plagioclase	17.8	13.6	9.5	10.0	36.8	36.0	30.1	33.8	32.8
biotite	5.0	6.1	2.4	1.7	6.5	7.0	1.6	4.0	5.6
cpx	2.0	0.0	7.1	5.0	2.2	2.0	4.9	1.3	7.7
sphene	6.9	4.5	4.8	5.0	0.0	2.0	4.9	0.7	2.8
opaque	5.0	0.0	3.6	1.7	2.9	2.0	6.5	2.0	1.4
zircon	1.0	1.5	1.2	0.0	0.0	0.0	0.0	0.7	0.0
hornblende	0.0	0.0	0.0	0.0	0.0	0.0	0.0	0.0	0.0
undiff. feldspar	0.0	0.0	0.0	0.0	0.0	0.0	0.0	0.0	0.0

Appendix B: Part II, continued.

Position	8.0	9.0	9.5	10.0	10.5	5.0	6.0	7.0	8.0
Sample	92-M2-2	91-M1-3	92-M3-4	91-M1-4	92-M3-5	91-SM1-1	92-SM2-1	92-SM3-3	92-SM3-2
sanidine	4.4	37.0	39.6	49.4	59.4	58.3	63.8	64.6	78.9
plagioclase	85.8	47.7	32.5	35.9	25.7	8.3	22.5	15.4	6.6
biotite	1.9	7.8	12.8	7.9	5.9	11.1	2.5	4.6	3.9
cpx	0.7	3.9	8.3	4.5	3.7	5.6	1.3	1.5	2.6
sphene	0.0	1.4	0.8	1.7	0.5	11.1	5.0	6.2	3.9
opaque	7.2	2.1	5.3	0.6	3.2	2.8	5.0	7.7	3.9
zircon	0.0	0.0	0.8	0.0	1.6	2.8	0.0	0.0	0.0
hornblende	0.0	0.0	0.0	0.0	0.0	0.0	0.0	0.0	0.0
undiff. feldspar	0.0	0.0	0.0	0.0	0.0	0.0	0.0	0.0	0.0

Position	9.0	10.0	4.0	9.5	6.0	7.0	8.0	7.0	8.0
Sample	92-SM3-4	92-SM2-3	92-TB3-1	92-TB3-5	92-TB1-2	92-TB1-3	92-TB1-4	92-WH1-3	92-WH1-4
sanidine	57.4	57.1	58.6	35.3	64.9	54.5	64.3	45.8	38.2
plagioclase	16.4	27.5	1.8	42.4	3.1	3.2	1.7	19.2	38.9
biotite	8.2	7.7	8.9	14.9	5.6	8.5	8.9	17.5	13.2
cpx	1.6	2.2	0.0	0.0	0.0	0.0	0.0	9.2	5.6
sphene	9.8	3.3	0.0	0.0	0.0	0.0	1.1	0.8	0.0
opaque	4.9	2.2	3.6	3.4	2.5	7.4	2.2	6.7	2.8
zircon	1.6	0.0	0.0	0.0	0.6	2.1	1.1	0.8	0.0
hornblende	0.0	0.0	0.0	0.0	0.0	0.0	0.0	0.0	1.4
undiff. feldspar	0.0	0.0	27.2	4.1	23.2	24.3	20.6	0.0	0.0

Appendix B: Part II, continued.

Position	9.0	10.0
Sample	92-WH1-2	92-WH1-1
sanidine	25.9	53.2
plagioclase	47.1	29.1
biotite	15.3	13.5
cpx	3.5	0.0
sphene	2.4	0.8
opaque	5.9	2.5
zircon	0.0	0.8
hornblende	0.0	0.0
undiff. feldspar	0.0	0.0

Appendix C: Stratigraphic Section Descriptions

Sheep Mountain Section, Nevada
Location: SW 1/4, Sec. 17, T27N, R22W

top of section
Strongly welded, grayish red, devitrified crystal tuff containing sparse, mostly rounded lithophysal cavities which decrease in abundance upsection. Moderate carbonate alteration.

Pale brown, devitrified, spherulitic crystal tuff. Contains partially-flattened lithophysal cavities (to 4 cm) which decrease in abundance upsection. Moderate carbonate alteration.

Variably-welded, eutaxitic vitrophyre (eutaxia to 8 mm), consisting of a pale reddish brown, moderately-welded eutaxite that locally grades into lenses of medium dark gray, densely-welded eutaxite towards the base.

Poorly-welded, shard-rich, dark yellowish orange vitrophyre. Contains moderately flattened pumice (10%).

Poorly-welded, pale yellowish brown, pumiceous vitric tuff which contains slightly flattened, very pale orange, subrounded to subangular pumice (average size =1 cm, to maximum=7 cm; 17%).

Paleozoic carbonate rocks (undifferentiated)
bottom of section

Highland Spring Range Section, Nevada
Location: Sec. 26, T17N, R62E
References: Davis (1984)

top of section
Moderately-welded, grayish pink to pinkish gray crystal tuff

Poorly-welded, pinkish gray, pumiceous vitric tuff.

Lithophysal zone (lithophysal cavities to approximately 10 cm), which grades into a thick interval of devitified, gray orange pink to light gray, eutaxitic crystal tuff which contains abundant, extremely flattened, grayish pink eutaxia (to 9 cm).

Pale red, spherulite-rich crystal tuff. Spherulites are up to 9 cm in diameter.

Moderately welded, pale brown, partially-devitrified crystal tuff. Locally underlain by lensoidal intervals of perlitically-altered, moderately welded, dark gray vitrophyre or unwelded, very light gray ash locally underlie this unit.

Upper Volcanic and Sedimentary Assemblage of Davis (1984): debris flow deposits and fine-grained, moderate red volcaniclastic sediments.
bottom of section

McCullough Range Section, Nevada
Location: NE 1/4, Sec. 27, T25S, R61E
References: Schmidt (1987)

top of section
Moderately-welded, lithic-poor, devitrified, pinkish gray crystal tuff that has undergone extensive vapor phase crystallization. Tuff is pale lavender gray in outcrop. Weathers into shallow, flat cavities (<1 m wide). Abundance and size of lithic fragments varies upsection.

Densely-welded to moderately-welded, spherulitic, pale red, lithic-poor crystal tuff. Matrix contains irregular patches of dark gray, less-altered matrix. In outcrop, this unit

has a dark brownish gray color. Phenocrysts in this interval are larger (<4 mm) at the base. Lithics are very sparse (<5 %) but larger (<5 cm) with respect to the lower intervals.

Very poorly-welded, very pale orange, pumiceous vitrophyre.

Moderately-welded, moderate red crystal tuff with reddish brown fiamme (<1.0 cm), and sparse (<5%) lithics (<1.5 cm long).

Moderate reddish orange, eutaxitic crystal tuff. Devitrification increases upsection. Contains moderately to strongly flattened, pale reddish brown eutaxia (<1 cm long).

Medium dark gray lithic vitrophyre with strongly flattened, grayish black fiamme (<1.5 cm) and subangular lithic fragments (<1.0 cm).

Moderately-welded, eutaxitic crystal tuff with rounded to subrounded mafic lithic fragments (<1.2 cm) and strongly flattened, grayish black fiamme which vary between <1.5 cm (average) to <6.2 cm (maximum) in length. The matrix of this tuff is medium gray. Irregular, mottled patches of moderate reddish orange matrix occur about lithic fragments.

Dark gray, moderately-welded, eutaxitic lithic vitrophyre.

Poorly-welded, devitrified, pinkish gray lithic crystal tuff with subangular lithic fragments (generally < 0.7 cm, maximum to 12 cm) and angular, white, fibrous pumice (<5mm). Locally contains cobbles (< 13 cm) of the Eldorado Valley Volcanics incorporated within ash-flow tuff matrix. Rarely preserved: a thin interval of tuff enriched in lithic fragments and crystals (a possible pyroclastic surge or ground surge deposit).

Eldorado Valley Volcanics: volcaniclastic cobble breccia
bottom of section

White Hills Section, Arizona
Location: SW 1/4, Sec. 16, T29, R20W
Reference: Cascadden (1991)

top of section
Basaltic andesite flows (Basaltic Andesite of Squaw Peak? Cascadden, 1991).

Grayish pink, ridge-forming crystal tuff with partially-flatted pumice (<2 cm wide) and basaltic andesite lithic clasts (average size: 5.6 to 9.6 mm). Rare hornblende phenocrysts are present. Modal percent of biotite and clinopyroxene increase upsection. Basaltic andesite lithic clasts display crennulate margins. This texture may be indicative of magmatic mixing processes.

Poorly-welded, slope-forming, grayish orange pink crystal tuff.

Tertiary megabreccia (Cascadden, 1991)
bottom of section

Interstate-15 (I-15) Section, Nevada
Location: SE 1/4 of Sec. 35, SW 1/4 of Sec. 36, T23S, R60E
Reference: Bridwell (1991)

top of section
Pumice Mine Volcanics: basalt flows (Bridwell, 1990).

Massive, ridge-forming, densely-welded, pale red crystal tuff. Overall, phenocrysts in the I-15 section (in particular, sphene and clinopyroxene) increase in the upsection direction.

Eutaxitic crystal tuffs which become progressively less-welded and more crystal-rich upsection. Biotite phenocrysts and fiamme (<4.0 cm) increase in size noticeably upsection.

Very densely-welded, light gray, eutaxitic vitrophyre.

Very light gray vitrophyre.

Pale grayish orange, very-poorly to poorly-welded, pumiceous vitric tuff. Contains approximately 20% subrounded, fibrous pumice that varies in size from 0.3 to 6 cm wide, and < 5% predominantly subangular to subrounded, basaltic andesite clasts (0.4 cm wide). The matrix of this tuff is shard-rich.

Paleozoic carbonate rocks (undifferentiated).
bottom of section

Temple Bar Section, Arizona
Location: NW and NE 1/4, Sec.13, T22S, R20W
Reference: Cascadden (1991)

top of section
Light gray vitric tuff. Phenocrysts and pumice are smaller and less abundant in this unit in comparison to the underlying interval.

Grayish orange pink crystal tuff with pumice (15%; <2 cm in length) and angular to subrounded lithic clasts (6%; < 1 cm). A mafic enclave displaying a distinctive crennulate margin was found in float at the top of this ridge.

Crystal tuff with lithic clasts that are slightly less abundant and larger in size than the underlying unit (< 3cm). Abundance of pumice is also decreased (<5%) in this interval.

Vuggy zone of crystal tuff with large (<1m wide) flattened to rounded cavities. Lithic clasts in this unit are smaller (<1cm) and less numerous than the basal interval.

Blocky ledges of pale red crystal tuff that contains moderately-flattened, grayish pink pumice (<5 cm in length) and subangular to subrounded basalt and basaltic andesite lithic fragments.

Basaltic Andesite of Temple Bar.
bottom of section

Eldorado Mountains Section, Nevada
Location: SW 1/4, Sec. 27, T25S, R64E
Reference: Anderson, 1971

top of section
Mount Davis Volcanics: basalts (Anderson, 1971).

Pale red vitrophyre with platy outcrop habit produced by heatingby flows of Mt. Davis Volcanics basalts.

Very light gray to grayish orange pink vitric tuffs with strongly-flattened pumice (1 to 1.5 m) that increases in length upsection. Contacts between successive pyroclastic flow units are preserved in stratigraphically equivalent outcrops exposed at the Bridge Spring type section. These outcrops also contain banded pumice.

Pale red vitrophyre with flattened pumice (< 9 cm in length)

Pumice-rich, very pale red crystal tuff forming rounded to platy outcrops that contain large, elongated cavities (1m to approximately 12 m in width) which indicate vapor phase crystallization. Lithic fragments are increased in size (< 8 cm). Vapor phase amygdules
(< 9 cm) that are lined with pumice and/or contain lithic fragments are common. Phenocrysts are slightly less abundant in this interval but are coarser in comparison to underlying units.

Pale brown, very-densely welded, cliff-forming vitrophyre. Lithic fragments (subrounded, <5cm in length) are less abundant than underlying unit. Phenocrysts and pumice are larger (<2.5 mm and <5 cm, respectively).

Grayish orange pink, pumice- and lithic-rich tuff that exhibits a hackly, sheared outcrop surface. Phenocrysts in this interval are noticeably coarser (< 2.5 mm) than in underlying units (< 0.5 mm). Pumice is flattened and increased in size (< 5 cm) and abundance. Lithic clasts (length: <5 cm) are decreased in abundance.

Laterally-discontinuous outcrops of pinkish gray, ledge-forming, moderately-welded lithic tuffs interbedded with poorly-welded lithic tuffs that form rounded, exfoliated outcrops. Mafic inclusions with crennulate margins are found in this interval. Lithic fragments occur in slightly reduced amounts and are smaller (<3.5 cm), and pumice is slightly increased in abundance. A stratigraphically equivalent interval exposed at Bridge Spring contains a 1 m thick, laterally discontinuous ledge of pyroclastic breccia that is interpreted to be a coignimbrite lag deposit (Fisher and Schmincke, 1987). This outcrop consists of 50% angular to subangular mafic clasts (<2 cm) in a grayish orange pink crystal tuff matrix.

Grayish orange ilithic tuffs with irregularly shaped, elongated zones of concentrated lithics and coarse phenocrysts that are interpreted here to be gas escape pipes (max. length: 0.3 m, max. width: 1.5 cm).

Poorly- to moderately-welded, pinkish gray, lithic tuffs with angular to subangular, basalt and basaltic andesite lithic fragments (2.5 cm to 0.5 cm), and white to pale yellowish orange, partially-flattened, angular pumice fragments (<1.5 cm). This interval becomes progressively more densely-welded and enriched in both lithics and pumice in the upsection direction. A rare exposure of fine-grained, barely welded, lithic-poor ash occurs within this interval. This discontinuous interval is approximately 13 cm wide and 1.2 m long, and displays subtle cross-bedding, which suggests it was formed by a surge-related process (i.e., ash-cloud surge, pyroclastic surge, or pyroclastic flow related ground surge).

Patsy Mine Volcanics: basaltic andesites (Anderson, 1971)
bottom of section

Black Mountains Section, Arizona
Location: SE 1/4, Sec. 22, T27N, R22W
Reference: Faulds (1990)

top of section
Moderately welded, grayish pink devitrified tuff with fiamme (<7cm long) and lithic clasts (<1.4 cm). A cooling break lies beneath this unit.

Densely welded, pink, eutaxitic tuff.

Moderately welded, grayish orange pink, eutaxitic tuff with a shard rich matrix.

Thin discontinuous, light greenish gray, densely welded, lithic rich tuff with angular to subangular clasts of basaltic andesite (<3 cm in diameter). Contains flattened pumice in a shard rich matrix.

Pyroxene-olivine basaltic andesite.
bottom of section

Dolan Springs Section, Arizona
Location: Sec. 19, 20, 24, T26N, R19W

top of section
Regionally-extensive olivine basalt.

Poorly-welded to densely-welded, lithic-rich vitric tuff (lithics < 5 cm, pumice < 1.5 cm). Poorly-welded tuff is pale red and contains abundant (55 %) angular fragments of black glass and subrounded rhyolite lithic clasts (<3 cm). Densely-welded vitrophyre is light brown and eutaxitic (black eutaxia to 1.5 cm) and contains approximately 65% subrounded rhyolite clasts and black glass. This interval forms massive, ridge forming outcrops; crudely-formed columnar jointing is occassionally present.

Interbedded pyroclastic surge and ash-flow tuff. Lamination and cross-bedding in surge deposits is better developed upsection than in lower intervals. The uppermost part of the section is a very poorly-welded, grayish orange pink, pumice-rich vitric tuff with

pumice (< 1.5 to 8 cm) that decreases in abundance and is normally-graded upsection. Lithic fragments (predominantly rhyolite, <2.5 cm) increases in abundance and is reversely-graded upsection. Pumice varies from: (1) a dense, grayish pink, chalky textured pumice; (2) a very light gray pumice that varies in texture from granular and densely compacted to fibrous to bubbly; and (3) a compacted pumice with fibrous texture that displays alternately-colored bands of very light gray and pinkish gray. This banding suggests that a mixture of magmatic compositions has occurred.

Laterally discontinuous, highly vesiculated, brownish gray olivine basalt a'a flows. Basalt flows ramps onto and pinches out on the flanks of an adjacent rhyolite dome, but thickens considerably to the northwest of Dolan Springs. The top of the flow contains numerous elongated, ballistically-shaped volcanic bombs (to 1 m in length), which indicates a proximally-located source. Angular basalt fragments (< 10 cm in length) were caught up and incorporated into the overlying ash-flow tuff.

Interbedded lithic tuffs and thinly-laminated pyroclastic surge deposits. Surge deposits are poorly-welded, pinkish gray and are frequently rich in accretionary lapilli (< 1 mm in width). Cross-bedded surge laminations vary in width from 4 mm in basal deposits to 2 mm at the top of the section. Modal percent of lithic clasts and phenocrysts in surge deposits remain generally constant throughout the section. Modal percent of pumice increases slightly in the upsection direction from 2 to 5 %. Lithic clasts (approximately 12% of the whole rock) consists of < 2 mm wide, subrounded rhyolite (dominant fraction) and basaltic andesite.

Poorly-welded, hackly surfaced, pumice-rich, yellowish-gray lithic tuff which contains subrounded, white, fibrous pumice (<1 cm) and subangular rhyolite lithic fragments (<0.5 cm). Ash-flow tuffs exposed farther upsection are very pale orange, moderately-welded vitric tuffs with rhyolite and basaltic andesite lithic fragments. In general, the abundance and size of lithic fragments increase upsection. Lateral zones of concentrated mafic fragments occur periodically in the upper part of the section.

Rhyolite domes and associated breccia carapace aprons. Carapace deposits consist of angular to subangular clasts (< 1 m wide) of rhyolite glass and pumice in a very pale orange, sanidine and biotite-bearing, tuffaceous matrix. Rhyolite domes are massive, exhibit large-scale flow banding and ramping features.

Pyroxene-olivine basalts.
bottom of section

Salt Springs Wash Section, Arizona
Location: NE 1/4, Sec. 25, T30N, R19W
References: Cascadden (1991)

top of section
Tertiary megabreccia containing angular fragments of Precambrian crystalline basement.

Very light gray, swale-forming lithic tuff with a similar lithic content and abundance as the basal interval.

Stratified red brown sandstone.

Silicified, phenocryst-enriched, lithic fragment depleted zone of grayish pink tuff.

Ridge-forming, grayish pink lithic tuff with subangular lithic fragments of Precambrian basement (< 3 %; < 2.5 mm). Contains several vuggy zones with flattened cavities (possibly vapor phase zones).

Tertiary megabreccia containing angular fragments of Precambrian crystalline basement.
bottom of section